COUPLED ENGINEERED AND NATURAL DRAINAGE NETWORKS: DATA-MODEL SYNTHESIS IN URBANIZED RIVER BASINS

by

Soohyun Yang

A Dissertation

Submitted to the Faculty of Purdue University

In Partial Fulfillment of the Requirements for the degree of

Doctor of Philosophy

Lyles School of Civil Engineering

West Lafayette, Indiana

December 2019

THE PURDUE UNIVERSITY GRADUATE SCHOOL
STATEMENT OF COMMITTEE APPROVAL

Dr. P. Suresh C. Rao, Co-Chair
Lyles School of Civil Engineering and Agronomy

Dr. Dietrich Borchardt, Co-Chair
Department Aquatic Ecosystems Analysis and Management,
Helmholtz Centre for Environmental Research-UFZ, Germany

Dr. Amisha Shah
Lyles School of Civil Engineering and Environmental and Ecological Engineering

Dr. Antoine Aubeneau
Lyles School of Civil Engineering

Dr. Michael Mashtare
Agronomy and Environmental and Ecological Engineering

Dr. Enrico Bertuzzo
Department of Environmental Sciences, Informatics and Statistics,
Ca' Foscari University of Venice, Italy

Dr. Kyungrock Paik
School of Civil, Environmental, and Architectural Engineering, Korea University, South Korea

Approved by:
Dr. Dulcy M. Abraham
Dr. Linda S. Lee

To the LORD for directing every single step, and
to my parents for their steadfast support and trust.

ACKNOWLEDGMENTS

First and foremost, I would like to greatly and deeply acknowledge my co-advisors, Prof. P. Suresh C. Rao who guided me in the direction of critical thinking, transformative learning, and actively discussing with multidisciplinary perspectives, and Prof. Dietrich Borchardt who gave me wise advice, stimulating questions, and precious opportunities working in Germany every summer. I must say that, I would not have accomplished my PhD journey without their sincere encouragement, strong support, academic guidance and thorough discussions on my research topics.

I would also like to express the deepest gratitude to my committee members – Profs. Amisha Shah, Antoine Aubeneau, Michael Mashtare, Enrico Bertuzzo, and Kyungrock Paik, who were willing to provide intellectual inputs and share their experiences in research and career development. I was truly fortunate to have great interdisciplinary committee members.

I would like to extend the acknowledgement to Prof. James W. Jawitz, Dr. Gavan McGrath, and Dr. Olaf Buettner, who substantially contributed to my intellectual growth over the international network-synthesis workshops held during the last four years in Seoul, West Lafayette, Dresden, Gainesville, and Fort Collins.

Furthermore, I would like to thank Elisabeth Krueger, Christopher Klinkhamer, Leonardo Bertassello, and Anamika Shreevastava, who were more than colleagues within my Purdue research group. Whenever I faced obstacles in my research, they always became careful listener and helped me to get out of the frustration by sharing their clever insights and proactive characters.

Lastly, I wish to acknowledge the journals of *Water Resources Research* (Publisher: Wiley) and *Science of the Total Environment* (Publisher: Elsevier), which allowed me to retain the right to reproduce three published articles based on my PhD research in my PhD dissertation.

TABLE OF CONTENTS

LIST OF TABLES

LIST OF FIGURES

ABSTRACT

In urbanized river basins, sanitary wastewater and urban runoff (non-sanitary water) from urban agglomerations drain to complex engineered networks, are treated at centralized wastewater treatment plants (WWTPs) and discharged to river networks. Discharge from multiple WWTPs distributed in urbanized river basins contributes to impairments of river water-quality and aquatic ecosystem integrity. The size and location of WWTPs are determined by spatial patterns of population in urban agglomerations within a river basin. Economic and engineering constraints determine the combination of wastewater treatment technologies used to meet required environmental regulatory standards for treated wastewater discharged to river networks. Thus, it is necessary to understand the natural-human-engineered networks as coupled systems, to characterize their interrelations, and to understand emergent spatiotemporal patterns and scaling of geochemical and ecological responses.

My PhD research involved data-model synthesis, using publicly available data and application of well-established network analysis/modeling synthesis approaches. I present the scope and specific subjects of my PhD project by employing the *Drivers-Pressures-Status-Impacts-Responses* (*DPSIR*) framework. The defined research scope is organized as three main themes: (1) River network and urban drainage networks (*Foundation-Pathway of Pressures*); (2) River network, human population, and WWTPs (*Foundation-Drivers-Pathway of Pressures*); and (3) Nutrient loads and their impacts at reach- and basin-scales (*Pressures-Impacts*)

Three inter-related research topics are: (1) the similarities and differences in scaling and topology of engineered urban drainage networks (UDNs) in two cities, and UDN evolution over decades; (2) the scaling and spatial organization of three attributes: human population (POP), population equivalents (PE; the aggregated population served by each WWTP), and the number/sizes of WWTPs using geo-referenced data for WWTPs in three large urbanized basins in Germany; and (3) the scaling of nutrient loads (P and N) discharged from ~845 WWTPs (five class-sizes) in urbanized Weser River basin in Germany, and likely water-quality impacts from point- and diffuse- nutrient sources.

I investigate the UDN scaling using two power-law scaling characteristics widely employed for river networks: (1) Hack's law (length-area power-law relationship), and (2) exceedance probability distribution of upstream contributing area. For the smallest UDNs, length-

area scales linearly, but power-law scaling emerges as the UDNs grow. While area-exceedance plots for river networks are abruptly truncated, those for UDNs display exponential tempering. The tempering parameter decreases as the UDNs grow, implying that the distribution evolves in time to resemble those for river networks. However, the power-law exponent for mature UDNs tends to be larger than the range reported for river networks. Differences in generative processes and engineering design constraints contribute to observed differences in the evolution of UDNs and river networks, including subnet heterogeneity and non-random branching.

In this study, I also examine the spatial patterns of POP, PE, and WWTPs from two perspectives by employing fractal river networks as structural platforms: spatial hierarchy (stream order, ω) and patterns along longitudinal flow paths (width function). I propose three dimensionless scaling indices to quantify: (1) human settlement preferences by stream order, (2) non-sanitary flow contribution to total wastewater treated at WWTPs, and (3) degree of centralization in WWTPs locations. I select as case studies three large urbanized river basins (Weser, Elbe, and Rhine), home to about 70% of the population in Germany. Across the three river basins, the study shows scale-invariant distributions for each of the three attributes with stream order, quantified using extended Horton scaling ratios; a weak downstream clustering of POP in the three basins. Variations in PE clustering among different class-sizes of WWTPs reflect the size, number, and locations of urban agglomerations in these catchments.

WWTP effluents have impacts on hydrologic attributes and water quality of receiving river bodies at the reach- and basin-scales. I analyze the adverse impacts of WWTP discharges for the Weser River basin (Germany), at two steady river discharge conditions (median flow, Q_{R50}; low-flow, Q_{R90}). This study shows that significant variability in treated wastewater discharge within and among different five class-sizes WWTPs, and variability of river discharge within $\omega < 3$, contribute to large variations in capacity to dilute WWTP nutrient loads. For Q_{R50}, reach-scale water quality impairment assessed by nutrient concentration is likely at 136 (~16%) locations for P and 15 locations (~2%) for N. About 90% of the impaired locations are $\omega<3$. At basin-scale analysis, considering in stream uptake resulted 225 (~27%) P-impaired streams, which was ~5% reduction from considering only dilution. This result suggests the dominant role of dilution in the Weser River basin. Under Q_{R90} conditions [$(Q_{R50}/Q_{R90}) \sim 2.5$], water quality impaired locations are likely double than Q_{R50} status for the analyses. This study for the Weser River basin reveals that

the role of in-stream uptake diminishes along the flow paths, while dilution in larger streams ($4 \leq \omega \leq 7$) minimizes the impact of WWTP loads.

Furthermore, I investigate eutrophication risk from spatially heterogeneous diffuse- and point-source P loads in the Weser River basin, using the basin-scale network model with in-stream losses (nutrient uptake).Considering long-term shifts in P loads for three representative periods, my analysis shows that P loads from diffuse-sources, mainly from agricultural areas, played a dominant role in contributing to eutrophication risk since 2000s, because of ~87% reduction of point-source P loads compared to 1980s through the implementation of the EU WFD. Nevertheless, point-sources discharged to smaller streams ($\omega<3$) pose amplification effects on water quality impairment, consistent with the reach-scale analyses only for WWTPs effluents. Comparing to the long-term water quality monitoring data, I demonstrate that point-sources loads are the primary contributors for eutrophication in smaller streams, whereas diffuse-source loads mainly from agricultural areas address eutrophication in larger streams. The results are reflective of spatial patterns of WWTPs and land cover in the Weser River basin.

Through data-model synthesis, I identify the characteristics of the coupled natural (rivers) – humans – engineered (urban drainage infrastructure) systems (CNHES), inspired by analogy, coexistence, and causality across the coupled networks in urbanized river basins. The quantitative measures and the basin-scale network model presented in my PhD project could extend to other large urbanized basins for better understanding the spatial distribution patterns of the CNHES and the resultant impacts on river water-quality impairment.

1. INTRODUCTION

1.1 Research motivation and scope

River networks form the dominant continuous natural drainage pathways transporting water and substances from headwaters to the basin outlet in a river basin, which is the well-known as the *River Continuum Concept* (Vannote et al., 1980). In addition, self-organized structural patterns of river flow paths converging from all points in a river basin to the basin outlet is a popular example of fractals in nature (Mandelbrot, 1983; Feder, 1988). Rivers also act as spatial integrators and mediators of temporal dynamics of hydrological and biogeochemical processes occurring over a river basin, as manifested in the hydrologic responses (e.g., hydrograph) and biogeochemical responses (e.g., solute export, chemograph) (Gall et al., 2013; Kamjunke et al., 2013; Andres-Domenech et al., 2015; Musolff et al., 2017). Moreover, river networks provide the riverine ecosystems with diverse habitats across the entire riverine landscape (both the flood-scape and the river-scape), facilitating the biodiversity and integrity of the lentic and lotic ecosystems (Platts, 1979; Brown & Swan, 2010; Altermatt, 2013; Widder et al., 2014; Rinaldo et al., 2018), which is known as the *Riverine Ecosystem Synthesis* (Thorp et al., 2006).

Recognizing various attributes and roles of river networks encompassing multiple fields, well-established knowledge on globally consistent self-organized fractal river networks (Dodds & Rothman, 2000; Rodríguez-Iturbe & Rinaldo, 2001; Veneziano & Langousis, 2010) has been employed to generate a structural and functional framework for several modeling applications, including human migration along river networks (Campos et al., 2006; Bertuzzo et al., 2007), aquatic species dispersal and diversity (Muneepeerakul et al., 2008; Carrara et al., 2012; Peterson et al., 2013; Bertuzzo et al., 2015), and the spread of waterborne diseases (Bertuzzo et al., 2008; Bertuzzo et al., 2010; Mari et al., 2012). More recently, socio-hydrology studies of coupled human-water systems (Sivapalan et al., 2012; Hall, 2019) have used river networks to estimate the location and spatial pattern of human settlements in river basins (Kummu et al., 2011; Ceola et al., 2015; Fang et al., 2018; Fang & Jawitz, 2019). Researchers (referenced therein) commonly pointed out the diverse favorable roles of rivers to the human communities for explaining human settlement patterns they found, such as supply source of daily used water, receiving body of wastewater, transport pathways within/across nations, and provision of recreational spaces.

Simultaneously, humans have empirically recognized that people should maintain and conserve river systems for relying on the beneficial services of rivers (e.g., recreational, ecological), otherwise people inevitably encounter and suffer returning harms to ourselves. One representative example is the lethal cholera epidemics that erupted in Europe in the mid-1800s (Colwell, 1996; Davenport et al., 2019). In Germany, unprecedented growth of human population, propelled by urbanization and industrialization during that period, contributed to corresponding wastewater production. Poor sanitation systems at that time also accelerated the wastewater-driven cholera outbreak throughout the nation. Massive mortality from cholera in 1866 triggered the construction of sanitary sewer systems (Seeger, 1999). Despite the improvements in public hygiene, wastewater discharges from sanitary sewerages gradually increased severity of water-quality impairments in receiving rivers, prompting the initiative to construct wastewater treatments plants (WWTPs) in the late 1880s (Seeger, 1999). Increasing public awareness and expert knowledge about river and lake eutrophication prompted the development of a tertiary treatment (more advanced) for reducing nutrient loads. The first WWTP deploying the tertiary treatment technology began operations in 1978 (Seeger, 1999). The steady spread of the tertiary treatment technology and continuous expansion of the sewerage length in Germany (ATT et al., 2015; Berger et al., 2017) contributed to ~93% connectivity to WWTPs with tertiary treatment technology (EEA, 2017).

Indeed, Germany is among the top three EU countries in terms of establishing national-scale consistent sanitation systems and providing the wastewater collection and treatment services to most of residences across the nation. Thus, Germany has already met the goal for public access to adequate sanitation (goal 6.2) among the UN sustainable development goals (SDGs), which the UN member states agree to achieve by 2030 (BMUB/UBA, 2018). The evident achievements of Germany might depend on continued national investment around for the last century to construct sanitation systems and treatment technology development. However, as the global-scale agreement for SDGs shows, there are more countries requiring necessary sanitation systems. For example, even within EU countries, there are large variabilities in the percent of human population connected to urban wastewater collecting and treatment systems (from <50% to 100%) (EEA, 2017b). Although it cannot be argued that the current distribution patterns of the sanitation systems in Germany are ultimate exemplary archetype that other countries with lack of connectivity should pursue for accomplishing the given goal, understanding spatial patterns of river-humans-WWTPs

in a developed country with established wastewater treatment systems helps in characterizing the WWTPs-distribution of other countries and suggesting future development direction for ensuring public hygiene and riverine ecosystems integrity.

However, higher connectivity of people to sanitary sewer networks and WWTPs with advanced treatment technology cannot ensure the healthy status of receiving river bodies regarding nutrients, physio-chemical, and ecological perspectives. The European Union Water Framework Directive (EU WFD; 2000/62/EC) (European Commission, 2000) set the goal to achieve by 2027 at least "good status" for both surface water bodies (rivers; lakes; transitional and coastal waters) and groundwater. At the end of the first management cycle (2009-2015), Germany achieved the WFD objective for <10% of about total 9,800 surface water bodies. Major contributing factors were alteration of river morphology causing loss of habitat diversity, and continued diffuse nutrient loads (phosphorus P; nitrogen N) from intensively-managed lands (BMUB/UBA, 2016).

In Germany, relative contribution of point-sources N and P loads discharged from municipal WWTPs decreased continuously since 1983, through increased usage of phosphorus-free detergents, and introduction of stringent regulations for wastewater treatment (BMUB/UBA, 2014; Ibisch et al., 2016; Westphal et al., 2019). Similar reductions were achieved in several other EU countries (Ludwig et al., 2009; Passy et al., 2013; Meybeck et al., 2018). However, such remarkable reductions do not always guarantee mitigation of river water quality impairments and prevention of algal blooms. Nutrient loads from WWTPs could cause reach-scale (local) eutrophication, and may amplify the adverse impacts of diffuse sources (Jäger & Borchardt, 2018).

In smaller streams, nutrient loads discharged from WWTPs could degrade river water quality and habitat integrity if dilution of WWTP-effluents by river discharge is insufficient (Rice & Westerhoff, 2017). Even in larger river reaches, nutrient loads from WWTPs serving larger cities may also contribute to eutrophication when the dilution is insufficient (García-Galán et al., 2011). Such problems are exacerbated during extended periods of low-flow and drought conditions (Withers & Jarvie, 2008). Identifying and rehabilitating the impaired streams is a river basin management goal, especially for smaller streams and headwaters, which sustain diverse habitats and biodiversity (Meyer et al., 2007; Besemer et al., 2013; Baattrup-Pedersen et al., 2018) and are important for biogeochemical regulation of nutrient loads (Alexander et al., 2007). Thus, the impacts of WWTPs nutrient loads on water quality impairment need to be investigated both at the reach-scale (i.e., considering dilution of each WWTP discharge alone) and at the basin-scale (i.e.,

through cumulative nutrient loads attenuated by dilution and in-stream nutrient uptake) (Kuemmerlen et al., 2019).

In fact, spatial distributions of WWTPs discharges (treated effluents and nutrient loads) to a river network are determined by a combination of three main factors: (1) human population distribution within a river basin; (2) sizes of sanitary sewer-sheds connected to WWTPs, and (3) wastewater treatment regulations and the portfolio of technologies used at WWTPs (see Urban Waste Water Treatment Directive 91/271/EEC (EEC, 1991)). Thus, they can be represented as the multiple-layers of river network structures, human population settled, urban drainage networks (UDNs) and WWTPs for a given urbanized river basin. Furthermore, the influence of anthropogenic pressures from point- and diffuse-sources on river water-quality can be laid as the resultant layer for the inputs generated from multi-layers. The input multi-layers conceptualize the coupled natural-human-engineered (CNHE) systems in urbanized river basins, and the last output layer indicates their corresponding influence (Figure 1.1).

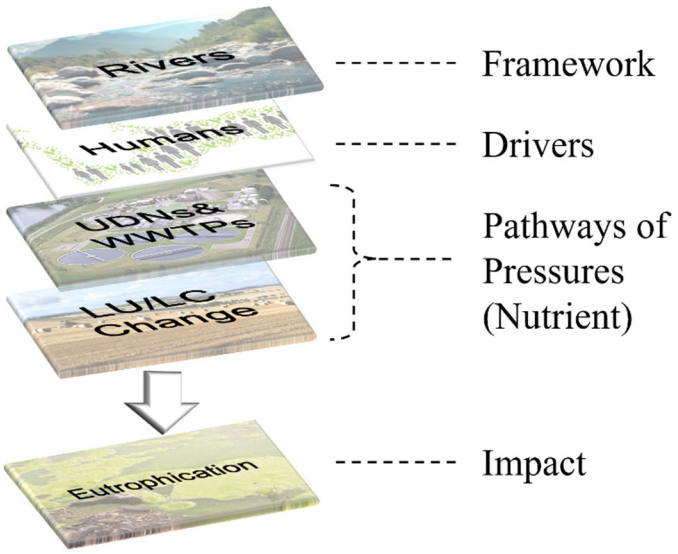

Figure 1.1 Schematic representation for the research subject and scope in this study

With the five layers of interest in this study, I present the scope and specific subjects by employing the *Drivers-Pressures-Status-Impacts-Responses* (*DPSIR*) framework (OECD, 1993; EEA, 1999), which has been employed to systematically understand and assess a system of interest (Whitall et al., 2007; Mattas et al., 2014; Elliott et al., 2017): People act as main *drivers* producing *pressures* (nutrients loads) on the water-quality, ecological and chemical *status* of receiving river

bodies through *pathways* (UDNs & WWTPs), thus *responses*, such as environmental regulations and relevant sanitation facilities, are applied to mitigate *impacts* of the anthropogenic pressures (hydrological alteration and eutrophication).

The defined research scope is organized as three main themes. In the next section, research background, questions and hypotheses are given for each theme:

1. River network and UDNs (*Foundation-Pathway*)
2. River network, human population, and WWTPs (*Foundation-Drivers-Pathway*)
3. Nutrient loads and their impacts at reach- and basin-scales (*Pressures-Impacts*)

1.2 Research background, questions, and hypotheses

1.2.1 Functional topological scaling of evolving urban drainage networks

Efficient drainage of urban landscapes is among the critical services provided to the citizens for avoiding flooding of streets and neighborhoods, and for maintaining flows to WWTPs. Early engineering studies on infrastructure networks focused on cost-optimal design solutions, maintaining efficient operations, and reliable (stable) provision of services to meet customer demands, guided by fail-safe engineering design principles within regional limitations such as demography, geology, and topography under budgetary and regulatory constraints (Froise & Burges, 1978; Loucks, 1979; Harremoës & Rauch, 1996; Cantarella & Vitetta, 2006; Ukkusuri et al., 2007; Türker, 2011). More recently, urban infrastructure has been examined from network theory perspectives, both as individual complex networks (Rosvall et al., 2005; Porta et al., 2006; Yazdani & Jeffrey, 2011, 2012; Diao et al., 2014; Masucci et al., 2014; Porse & Lund, 2015), and as interdependent complex networks (Chan & Dueñas-Osorio, 2014; Morris & Barthelemy, 2014). These studies have promoted a generalized understanding of structural and functional attributes of evolving engineered urban networks.

Of particular interest here are UDNs that include storm-water, sanitary sewers, and combined sanitary storm-water systems. UDNs are located below-ground at shallow depths and in close proximity to road networks (Blumensaat et al., 2012; Mair et al., 2012; Klinkhamer et al., 2017; Mair et al., 2017). The understanding about the network scaling characteristics of engineered UDNs is limited with surprisingly little literature (e.g., Oh (2010)). An intriguing question in this regard is how the topology of UDNs compares with their natural analogs, i.e., river networks. Like

rivers, UDNs involve gravity-driven and directed flows from all terminal points over the entire drainage area converging towards a WWTP. In river networks, terminal points are drainage areas for all first-order streams, whereas in UDNs households are the terminal points. Many large cities have multiple outlets (e.g., combined sewer overflow outlets; several WWTPs), forming multiple sewer-sheds, whose boundaries may overlap several natural watersheds. UDNs consist of junctions and conduits, which correspond to nodes and links, like confluences and reaches in river networks. Same as stream orders in river networks, UDNs exhibit hierarchy of pipe-diameters for a range of designed discharges. These structural and functional similarities prompted the application of river network hierarchical organization concepts to describe UDNs. Cantone & Schmidt (2011b, 2011a), Sitzenfrei et al. (2013), and Urich et al. (2010) classified the hierarchy of real/virtual sewer systems through Horton-Strahler ordering scheme (Strahler, 1957). However, they did not investigate sewer networks by using scaling relations for natural river networks.

Differences between rivers and UDNs are also informative. They differ in terms of generative processes, scale, growth direction, branching structure, and optimality (Table 1.1). While river networks evolve through natural processes, UDNs are engineered networks, designed to meet efficiently urban drainage requirements at the minimum cost. River networks drain large landscapes, up to the continental scales (~10^6 km^2; e.g., Amazon; Congo; Nile; de Plata; Mississippi). However, even the largest known UDNs drain much smaller urban sewer-sheds ($\leq$ 10^3 km^2) (USEPA, 2001). These differences are likely to contribute to differences in network topology of UDNs to those reported for river networks.

Table 1.1 Key differences between river networks and urban drainage networks

Factors	River Networks	Urban Drainage Networks
Generative Processes	River networks are formed by geomorphological processes, including erosion, deposition, weathering, tectonic uplift, and ecosystem functions over geologic time-scales.	UDNs are planned, designed, built, maintained, and operated by engineers to drain urban landscapes. Existing UDNs have evolved over several decades or centuries in some cases.
Network Size & Flow Direction	Large river networks drain continental-scale basins (~10^6 km^2), with nested sub-basins ranging from 10^2 to 10^5 km^2. Rivers carve out flow along the steepest downstream gradient.	Largest urban drainage networks are ~10^3 km^2, usually draining to a single outlet (a WWTP). Large cities (>10^6 population) have multiple WWTPs. Sewer lines are often laid out to follow roads rather than in the direction of steepest descent (Blumensaat et al., 2012; Haghighi, 2013).
Direction of Network Growth	For a given drainage area with an established outlet, starting with the main channel, river networks grow upstream, eventually occupying entire drainage area (Parker, 1977).	The drainage area grows in time as the city grows, and its maximum discharge increases. The initial UDN draining to a WWTP expands as new neighborhoods are added to the city.
Network Structure	Bifurcating, branching trees. Loops occur only under exceptional conditions such as river deltas and braided rivers (p. 231 in Knighton (1998)).	Imperfect branching trees, with 2 or more pipes connected to some junctions. Drainage areas can cross watershed boundaries. Loops exist although they usually represent less than 1% of the network. When loops represent a significant fraction of UDNs, methods have been proposed for defining equivalent binary-tree networks for looped configurations (Haghighi, 2013; Seo & Schmidt, 2014).
Optimality	Optimal channel network hypotheses, e.g., minimize total energy dissipation (Rodríguez-Iturbe, Rinaldo, et al., 1992; Paik & Kumar, 2010), given a fixed drainage area delineated by topography, under the assumption of uniform forcing (constant rainfall) over a heterogeneous landscape.	Maximum engineering efficiency for designed total discharge (at the outlet), and minimum costs. Most projects pursue local optimizations in time and space, often constrained by budgets. Expansion of the system after repeated local optimization may not result in optimality achieved over time.

Such analogies and differences lead me to compare topologies of UDNs and rivers. It is well-established that river networks are fractals with self-similarity revealed through quantitative scaling relationships (Horton, 1945; Hack, 1957; Tokunaga, 1978; Tarboton et al., 1991; Rodríguez-Iturbe, Ijjász-Vásquez, et al., 1992; Marani et al., 1994; Rigon et al., 1996). Here I examine whether UDNs and river networks share such scaling properties, given similarities in their functions (landscape drainage), and despite differences (engineered versus natural). In particular, I investigate the functional organization and scaling of UDNs in terms of their topological features, and examine how scaling patterns change as they grow over several decades. Here, I analyze UDN evolution towards some attractor ("mature" network) using time-stamped data. I begin with an explanation of scaling relationships for river networks underlying the study UDNs, to investigate their conformity with well-known and universal relationships established for river networks. Then, I explore the scaling relationships of the most recent UDNs, and compare the findings to those found from river networks. Further, I examine how the scaling of an engineered network has evolved over time by examining UDN topology during the preceding decades.

1.2.2 Spatial distribution patterns of wastewater treatment plants and human population

I selected as case studies three large urbanized river basins in Germany (Weser, Elbe, and Rhine; accounting for about 70% of total population in Germany], and examined the spatial organizations of three attributes: population (POP); aggregation of POP into sewer-sheds served by WWTPs (i.e., population equivalent, PE), and WWTPs distribution. I also characterized the inter-relationships in the spatial organizations of these three attributes. PE is the common measure of aggregated POP for a given WWTP and includes sanitary flows from households and non-sanitary flows (e.g., urban storm water runoff). Organic biodegradable load having a five-day biochemical oxygen demand (BOD5) of 60 g of oxygen per day is set as one PE (EEC, 1991). Note that (PE/POP) > 1 for each WWTP is indicative of the contribution of non-sanitary inflows. Urban storm water runoff is expected to be higher in larger cities with more impervious area, and the runoff coefficient is larger for bigger storm events (Shuster et al., 2005; Walsh et al., 2012; Yao et al., 2016).

I used a rich archive of national-scale, geo-referenced, high-resolution data for municipal WWTPs serving as spatially distributed point-sources of treated wastewater discharge and associated nutrient loads in German river basins. The following questions and corresponding

hypotheses guided the technical analyses in this study: (1) What are the spatial distributions of POP, PE served, and the number of WWTPs in urbanized river basins?; and (2) How can I quantify the spatial distributions of these three inter-related attributes (POP, PE, and WWTP) along river networks in urbanized catchments?

I used river networks, which exhibit universally consistent scaling patterns, as the structural platforms for investigating spatially organized patterns of anthropogenic pressures. Following Fang et al. (2018), I characterized the joint structure of the river networks and the population pressures based on stream order, width functions, and power spectra. Horton-Strahler (H-S) stream order (Horton, 1945; Strahler, 1957) allows systematic linkage of any spatial attribute embedded in river networks with the network hierarchy. The width function (WF) along the longitudinal flow path (Marani et al., 1994; Rodríguez-Iturbe & Rinaldo, 2001) is a one-dimensional representation of attributes distributed in a river basin along hydrological flow paths from upstream reaches to the basin outlet. I identified the similarities/differences in analyzed trends of spatial organization among the three river basins.

Motivated by previous findings for Horton scaling relationships of human-related variables (Miyamoto et al., 2011; Fang et al., 2018), I investigated whether POP distributions in German urbanized basins follow globally consistent patterns of human settlements (Fang et al., 2018). Knowing that sanitary sewer networks exhibit self-similar topology like river networks (Yang et al., 2017), I hypothesized that total PE, the aggregation of POP over multiple sanitary sewer networks, also involves scale-invariance over H-S orders. Spatial distribution of WWTPs by H-S orders reflects not only the total PE-size distribution over H-S orders, but also the aggregation of PE for multiple WWTPs discharging to a given H-S order. Thus, I hypothesized that the distribution of WWTPs also exhibits Horton scaling relationships.

I propose three dimensionless scaling indices to capture the functional relationships among river network hierarchy, and distributions of POP, PE, and WWTPs. I hypothesized that these scaling indices share consistent patterns across the three urbanized river basins, managed under similar environmental regulations and shared history of development.

1.2.3 Impact of point source nutrient loads on river water quality impairments

The primary motivation for this study was to determine the extent of water quality impairment from nutrient (N and P) loads discharged only from multiple WWTPs located along

the river network. Since Germany is one of three EU countries with >95% connectivity to WWTPs (EEA, 2017b), here as the case study, I selected the Weser River basin with the entire drainage area embedded in Germany (~46K km^2; ~13% of Germany's territory; ~8.4 million population; ~10% of Germany's population).

Analyses presented here are based on a synthesis of (1) empirical data for WWTPs discharges (treated effluents and nutrient loads); (2) total N and P loads from point- and diffuse-sources; (3) long-term water quality monitoring at multiple locations throughout the basin; (4) spatially explicit hydrologic model simulations (long-term hydrograph time series at all WWTP locations and basin outlet); and (5) estimation of likely N and P concentrations at reach- and basin-scales.

I estimated N and P concentrations from WWTPs loads alone at ~845 WWTP locations in the Weser River basin by considering: (1) at the *reach-scale*, dilution of treated wastewater discharge (Q_U) and nutrient loads (L_U) with river discharge (Q_R), and (2) at the *basin-scale*, the combined effects of dilution and in-stream uptake of the cumulative nutrient loads along downstream flow paths to the basin outlet. I considered two steady-state hydrologic conditions of river discharge: median flow (Q_{R50}) and low-flow (Q_{R90}). I estimated Q_{R50} and Q_{R90} values from the verified long-term (1960-2015) daily streamflow simulations generated by the mesoscale Hydrological Model simulations (mHM) (Samaniego et al., 2010; Kumar et al., 2013). To identify eutrophic risk, the estimated nutrient concentrations were compared to the ecological threshold concentrations (0.1 mg P/L and 2.8 mg N/L) regulated in Germany for achieving the EU WFD management objectives regarding nutrients (Heidecke et al., 2015).

In Germany, there are five class-sizes ($1 \leq k \leq 5$) of WWTP, based on population in the community served within the sewer-shed, expressed as the Population Equivalents (PE). Assuming a mean per capita water-use (q, [L^3/T/PE]), Q_U for each WWTP of given class-size k varies depending on total PE served. River discharge for a stream order (ω) at a given WWTP location j is approximated as $Q_{Rj} \sim (A_j\,(PR\text{-}ET)_j)$, where A_j is the contributing drainage area and $(PR\text{-}ET)_j$ is the *effective* rainfall, which contributes to mean stream discharge. It is well established that Q_R scales exponentially with ω, in proportion to increasing drainage area (Rodríguez-Iturbe, Ijjász-Vásquez, et al., 1992; Rodríguez-Iturbe & Rinaldo, 2001) For a given ω, the effective rainfall $(PR\text{-}ET)_j$ might be less variable across sub-basins, while variability in A_j for a given ω is much larger especially for smaller streams ($\omega \leq 3$). Thus, I hypothesize that two factors determining variability

in dilution and water quality impacts at the *reach-scale* are: (1) variability in PE *within* WWTPs class-size k, translated to variability of wastewater discharge (Q_U) and nutrient load (L_U); and (2) variability of drainage area, A_j, among sub-basins of a given stream order, ω, reflected in variability of river discharge (Q_R). Such variability would be most evident for WWTP locations on smaller streams (ω≤3).

Using river networks extracted from Digital Elevation Model (DEM), I estimated that Weser River basin has a total of ~1,700 stream reaches, of which most (~98%) are smaller streams (ω≤3), as expected. In larger streams (4≤ω≤7), converging river discharge from upstream drainage areas is larger and less variable. Thus, I hypothesize that dilution plays a dominant role in mitigating water quality degradation impacts from upstream WWTP nutrient loads. Variability in the efficiency of treatment of incoming nutrient loads in small WWTPs (1≤k≤ 3), which deploy a suit of primary and secondary treatment technologies, adds to the variability in N and P loads discharged. On this basis, I also hypothesize that any WWTP location with low dilution capacity (large Q_U/Q_R), resulting from combination of small ω (with small A_i) and large k (with large PE), has a greater likelihood of exceeding nutrient concentration thresholds. The analyses identify the WWTP locations in the Weser basin where such combination of ω and k exist.

1.3 Organization of the dissertation

The discussions of this dissertation consist of eight sections to follow. In **Section 2**, analyzed data and study areas are presented by matching with the order of research themes. **Section 3** focuses on the methodology used to demonstrate scaling relations, to identify longitudinal distribution pattern, and to quantify the impacts of point- and diffuse-sources pressures. Similarities in scaling relationships for naturally evolved river networks and engineered urban drainage networks are compared in **Section 4**, while scaling of several key attributes of three large urbanized river basins are presented in **Section 5**. Next, likely hydrologic and water-quality impacts are examined at reach-scale (**Section 6**) and basin-scale (**Section 7**). Overall conclusions and implications of my PhD research are presented in **Section 8**. I close my dissertation in **Section 9** with a research outlook through the perspectives of monitoring, modeling, and management. Sections 2 to 7 are derived from three papers published during my PhD research at Purdue University (USA) and Helmholtz Centre for Environmental Research-UFZ (Germany).

2. DATA & STUDY AREAS

The contents of this section are mainly based on the data & study areas sections of following published papers: **(1)** Soohyun Yang, Kyungrock Paik, Gavan S. McGrath, Christian Urich, Elisabeth Krueger, Praveen Kumar, and P. Suresh C. Rao, (2017). Functional Topology of Evolving Urban Drainage Networks. *Water Resources Research;* **(2)** Soohyun Yang, Olaf Buettner, James W. Jawitz, Rohini Kumar, P. Suresh C. Rao, and Dietrich Borchardt, (2019). Spatial organization of human population and wastewater treatment plants in urbanized river basins. *Water Resources Research;* **(3)** Soohyun Yang, Olaf Buettner, Rohini Kumar, Christoph Jaeger, James W. Jawitz, P. Suresh C. Rao, and Dietrich Borchardt, (2019). Spatial patterns of water quality impairments from point source nutrient loads in Germany's largest national River Basin (Weser River). *Science of the Total Environment.*

2.1 Sanitary sewer networks in Oahu Island and AAC

Detailed data of UDNs are difficult to obtain, and recent emphasis on security concerns and privatization of utilities have further limited data accessibility. Based on the availability of data recorded over decades, sanitary sewer networks (not combined with storm-water) from Oahu Island, Hawaii, USA (~1 million population), and a large anonymous Asian city (AAC) (~4 million population) (Figure 2.1) were examined. The two Oahu networks (Wahiawa and Honouliuli) are named after the WWTPs to which they discharge. These cities have contrasting socio-economic backgrounds, history, climate, and terrain. The Oahu data are publicly available while the AAC dataset was obtained under a confidentiality agreement from the city's water utility authority. Node-degree distribution and other topological metrics for AAC, based on dual mapping, were presented in Krueger et al. (2017). Here, the analyzed sewer-shed is the AAC's largest one (drainage area: ~126 km^2; population ~2.4 million) draining to a WWTP built around 1970. A summary of the characteristics of each network is provided in Table 2.1.

Table 2.1 Characteristics of the UDNs at the last year of record

	Wahiawa	Honouliuli	AAC
Data period	1929*-2009	1923**-2014	1968-2015
Drained area (km^2)	7.2	85.1	126.0
Number of pipes	1,364	17,255	49,355
Length of pipes (m)	77,725	929,205	1,895,459
Number of loops	8	23	252

* Wahiawa WWTP has been operating since 1928 (Owens, 2010).
** Website for Hawaii Water Environment Associate (http://www.hwea.org/) states that the Honouliuli WWTP was originally put into service in December 1984.

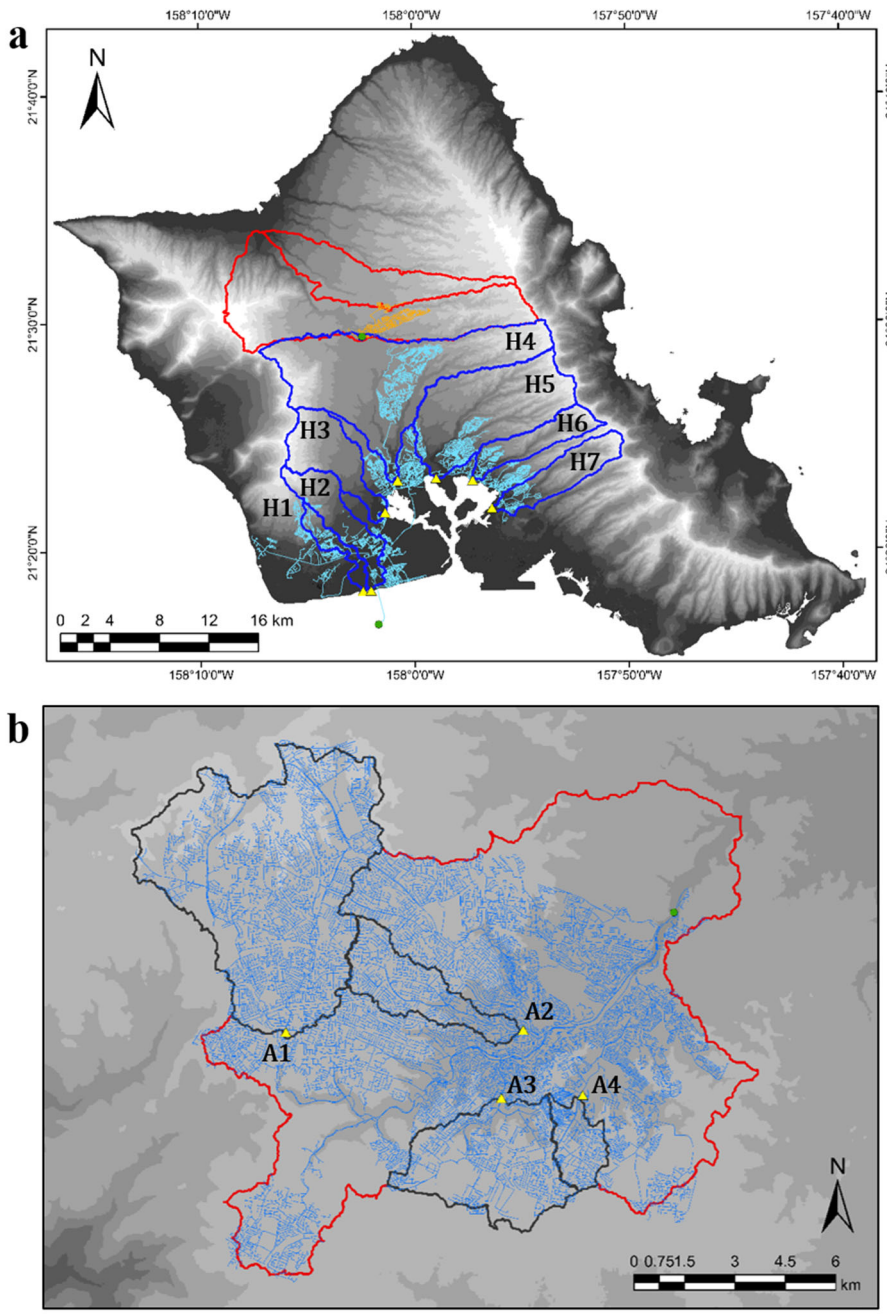

Figure 2.1 Geographic details of study UDNs and their underlying natural catchments. (a) Wahiawa (orange line) and Honouliuli (light blue line) sanitary sewer networks, residing over multiple independent catchments are shown. Catchment boundaries for Wahiawa and Honouliuli are colored with thick red and blue lines, respectively. (b) AAC sanitary sewer network (blue line). Black lines represent boundaries of five sub-catchments within the largest catchment embedding most of the AAC network (red line, 182.13 km²). Green circles are outlets of UDNs. Sub-catchments underlying the Honouliuli network and the AAC are indexed with initial H and A, respectively, and their outlets are marked as yellow triangles.

Catchment boundaries to which Wahiawa and Honouliuli belong (Figure 2.1a) are obtained from the State of Hawaii, Office of Planning. Catchment boundary of AAC is derived using SRTM (Shuttle Radar Topography Mission) 1 arc-second digital elevation model (DEM) provided by USGS (United States Geological Survey) (horizontal resolution ≈ 30 m) that has vertical resolution of 1 m (Figure 2.1b). Note that only a fraction of the obtained boundary forms the contributing area of each UDN or sewer-shed. The area within each boundary was discretized into raster grids with a size of 25×25 m^2 each. For each cell, a circular area of 100 m radius is drawn. Then, the open-source platform *DynaMind* (http://iut-ibk.github.io/DynaMind-ToolBox/) (Urich et al., 2012) was used to assign a nearest (direct distance) manhole (node) among those found within the circular area as the node to which the cell contributes. Then, upstream drainage area for every node in a network was calculated. The 100 m radius is empirically determined as a reasonable compromise between two requirements to minimize: (1) erroneous inclusion of rural cells in UDNs (which can happen as the threshold radius becomes too large); and (2) missing urban cells which are not assigned to any nearby manhole (which can happen if the threshold radius is too small). The sewer networks were found to contain only a small percentage (< 0.5 %) of pipes contributing to loops (Table 2.1), accounted for 16 pipe segments for Wahiawa, 86 pipe segments for Honouliuli, and 1218 pipe segments for AAC. Loops were manually removed by deleting selected pipes, ensuring connectivity and flow directions.

Sewer networks were retrieved at five-year intervals utilizing pipe installation date records. Beginning at a WWTP, from its construction date, a continuous pipe network was determined by incrementally sampling upslope pipes with the same or earlier installation date although not all pipes contained attribute data for installation date. For some pipes, their downslope or upslope pipes are older according to the records, indicating that they were replaced, and the new installation dates were retained in the dataset. In such incident, the newer pipe was incorporated into the older network to enforce flow connectivity.

2.2 Common data for three large rivers in Germany (Weser, Elbe, Rhine Rivers)

2.2.1 River network

Of the ten major rivers in Germany three large rivers (Weser, Elbe, and Rhine, with drainage areas in Germany of 46K, 98K, and 100K km^2, respectively; Figure 2.2) were selected

based on the following criteria. First, of the 14 German cities with population >500K, 13 (all except Munich) are located within one of the three selected basins (Table 2.2). Here, the size of German cities (Destatis, 2018) was categorized by following the United Nations (2016) classification. These three basins account for ~71% of the total population in Germany. Second, geo-referenced WWTP data for these three rivers are available with high accuracy and reliability. Lastly, for each of these river basins, more than half of the total basin area is embedded in Germany (Table 2.2). The Weser River basin is entirely within Germany, while only the downstream portion of the Elbe (~66% of total) and mid- and upstream portions of the Rhine (~54 % of total) are in Germany (Table 2.2). For the Elbe and Rhine, these analyses were limited to only the drainage areas within Germany. Thus, in this study, a basin outlet was designated as a location having the maximum accumulated drainage area within German territories. Analyses of the entire river basins spanning multiple countries are candidates for future research.

River networks were extracted from 100x100 m^2 resolution digital elevation model (DEM), scaled up from 50x50 m^2 DEM obtained from the State Institute for Environmental Protection Baden-Wuerttemberg (LUBW), Germany (Zink et al., 2017). Each depression cell was filled by raising its elevation to the lowest elevation among its eight neighboring cells. This process yielded some flat surfaces. The imposed gradients method (Garbrecht & Martz, 1997) was used to assign a flow direction over flat areas. For all pixels consisting of a river basin, accumulated drainage area was calculated, and H-S order (ω) was allocated. Then, I calculated the accumulated drainage area and H-S order only for the drainage areas within Germany; upstream drainage areas for the two international rivers (Elbe and Rhine) were not included. To extract river networks using the up-scaled 100x100 m^2 DEM, an average source area of 10 km^2 was applied as the minimum hillslope area to form a channel (Band, 1986; Montgomery & Dietrich, 1988; Tarboton et al., 1988). Note that the absolute values for H-S orders would vary depending on the river basin domain analyzed, but their scaling attributes are not affected. In this study, focusing point was the consistent conditions for one country.

Table 2.2 General information for the three German river basins

		River basin		
		Weser	**Elbe**	**Rhine**
Whole river basins	Total drainage area [km^2]	46,306	148,242	185,260
	Total population of the basin	8.4 M	25 M	58 M
	Number of countries	1	4	9
River basins in Germany	Portion of basin area in Germany (%)	100 %	66 %	54 %
	Part of the basin in Germany	Whole	Downstream	Mid-and up-streams
	Portion of population in Germany (%)	100 %	75 %	62 %
	Basin area in Germany over German territory area (%)	13 %	27 %	28 %
	Basin population in Germany over German total (%)	10 %	20 %	41 %
	Population density [people/km^2]	176	170	336
	Basin WWTPs over German total (%)	10 %	22 %	35 %
Cities in German river basins	Medium-sized cities* (1M - 5M inhabitants)	-	Berlin (1^{st}) Hamburg (2^{nd})	Cologne (4^{th})
	Cities* (500K - 1M inhabitants)	Bremen (11^{th}) Hannover (13^{th})	Leipzig (10^{th}) Dresden(12^{th})	Frankfurt (5^{th}) Stuttgart (6^{th}) Duesseldorf (7^{th}) Dortmund (8^{th}) Essen (9^{th}) Nuernberg (14^{th})
	Mean population density of the urban areas** [people/km^2]	2,112	2,894	2,713

Note. * I categorize here size of German cities by following classification of United Nations (2016); Megacity (more than 10M inhabitants); Large city (5M - 10M in habitants); Medium-sized city (1M - 5M inhabitants); and City (500K - 1M inhabitants). Values in parenthesis are rankings of cities in Germany based on the number of population in the dataset (Destatis, 2018). **I estimate the mean population density for each river basin by using the aforementioned dataset.

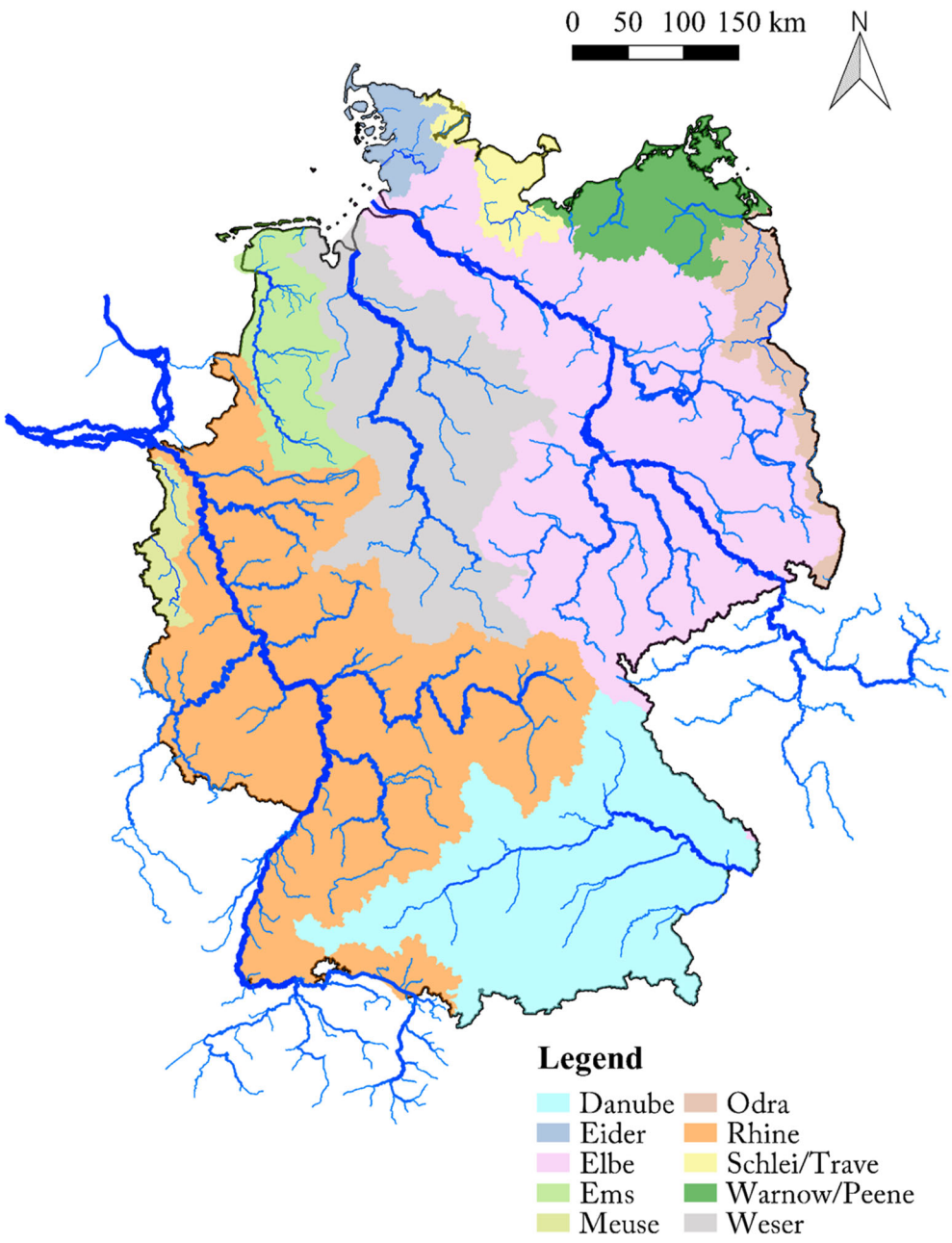

Figure 2.2 Ten German river basins shown with different background colors, and corresponding river networks. For the three study river basins (Weser, Elbe, Rhine), layouts of river networks show the entire river network (EU-Hydro River Network Dataset; https://land.copernicus.eu/imagery-in-situ/eu-hydro/eu-hydro-public-beta/eu-hydro-river-network). For the other seven river basins, river networks are shown only within German territory. Line thickness and color density of river networks vary over stream order (thicker and darker line represents higher stream order). Note that the basin outlets for the Weser and the Elbe in Germany are the same as those for the whole river basins, but not the Rhine.

2.2.2 Human population (Driver)

The spatial distribution of POP was determined from Gridded Population of the World, Version 4 (GPWv4) Adjusted Population Count (Center for International Earth Science Information Network - Columbia University, 2017), which is a global raster of human population (number of persons per pixel) at 30 arc-second (approximately 1 km at the equator) resolution. The German territory was extracted from the entire GPWv4 dataset (Figure 2.3). I checked the reliability of the data for total population in Germany, and then downscaled to 100x100 m^2 raster using ArcMAP (ver. 10.6). Spatial variability of population within one raster is not relevant to the scope of this study.

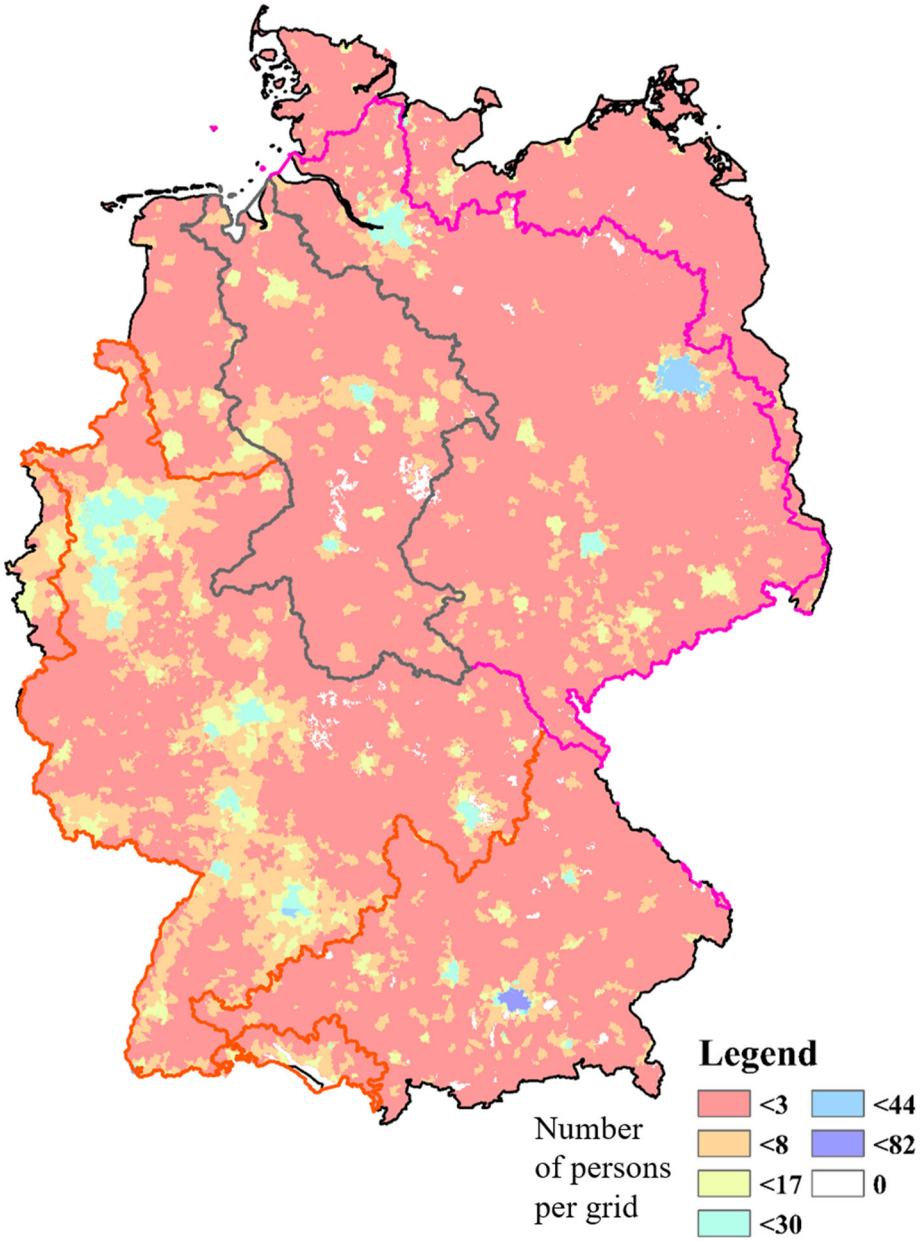

Figure 2.3 Map of total human population in Germany (~82 million). Blue regions represent German cities (≥ 500K inhabitants). Layouts of the three study river basins (Weser, Elbe, and Rhine) within Germany are shown as gray, magenta, and orange, respectively.

2.2.3 WWTPs (Pressure pathway)

I used country-scale data for ~8,900 WWTPs in Germany (Figure 2.4), collected from both the European Environment Agency (for WWTPs > 2,000 PE) and 13 Federal German States (including WWTPs < 2,000 PE) (except Hamburg, Bremen, and Berlin that have no WWTPs < 2,000 PE). German regulations divide WWTPs into five class-sizes based on PE served: Class-1 for PE < 10^3; Class-2 for $10^3 \leq$ PE < $5x10^3$; Class-3 for $5x10^3 \leq$ PE < 10^4; Class-4 for $10^4 \leq$ PE < 10^5; Class-5 for PE $\geq 10^5$ (https://www.gesetze-im-internet.de/abwv/anhang_1.html). In Germany, the total population of about 82 million translates to a total PE of 110 million, resulting a national-scale average, PE/POP = 1.34; however, variabilities in the contribution of non-sanitary flows are expected. On average, one German WWTP serves ~12K PE.

The original data for each German WWTP includes the magnitude of PE served, the annual discharged nutrient (N and P) loads [kg/yr], and the Federal State and catchment where it is located are included. However, layouts and boundaries of sanitary sewer networks connected to WWTPs are not available. The H-S order of the streams receiving discharged treated wastewaters was assigned based on the nearest stream to individual WWTPs within 2.5 km radius using ArcMAP (ver. 10.6). For <1% of total WWTPs which the rule was not reflected, its receiving stream was manually assigned.

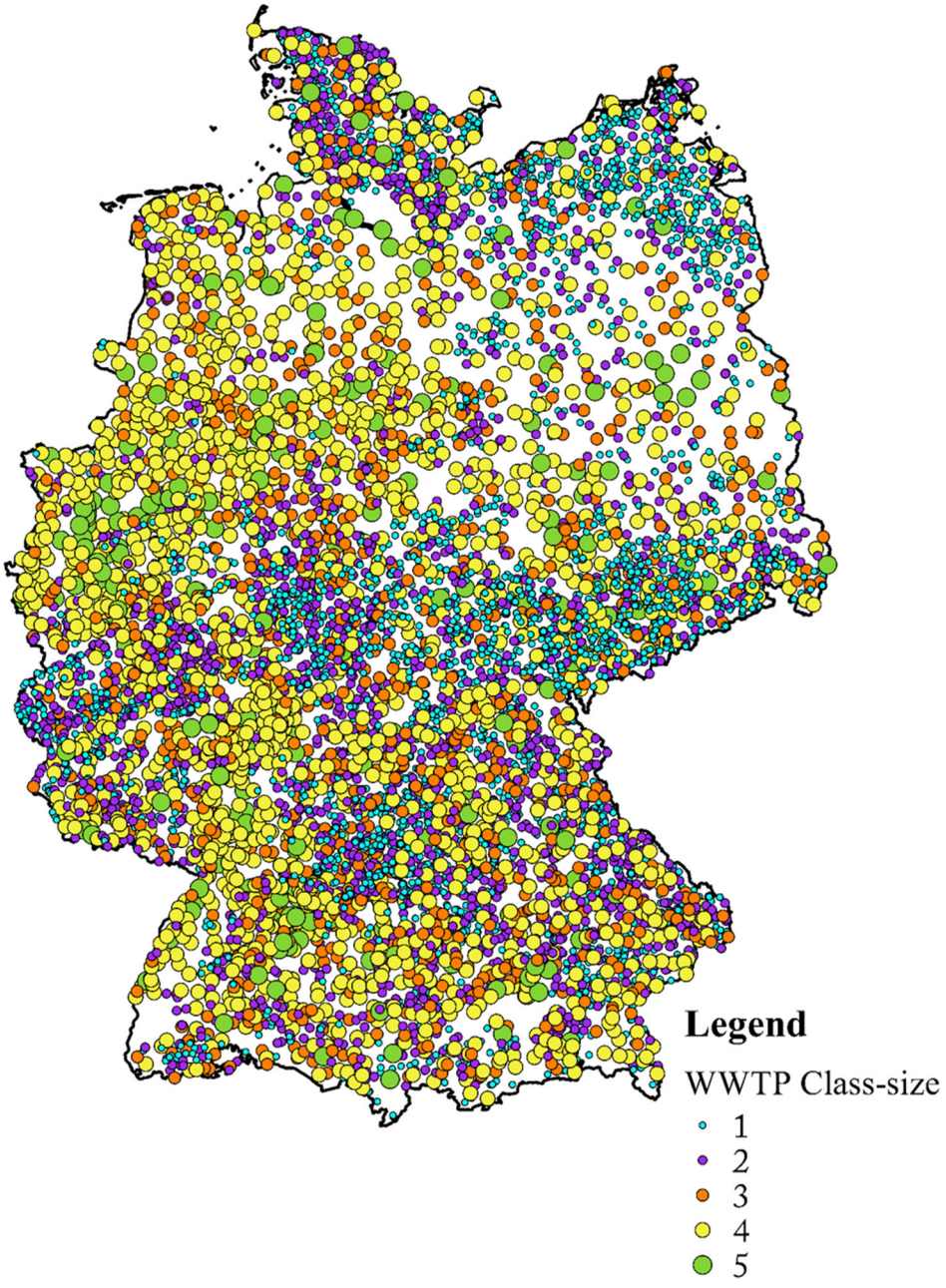

Figure 2.4 Spatial distribution of all WWTPs (~8,900) in Germany. Each WWTP is shown as a dot with distinguishing five class-sizes.

2.3 Specific data for the largest national river in Germany (Weser River)

2.3.1 River discharge

The Weser River basin is located in the humid-temperate climatic zone, with annual mean precipitation (*PR*) of ~780 mm/yr (range: 600-1,100 mm/yr), and evapotranspiration (*ET*) of 505 mm/yr. Mean aridity index (*PET*/*PR*, where *PET* is potential *ET*) for this basin is around 0.9 (IWRM-net, 2010; Zink et al., 2017). Using the long-term (56 years; 1960-2015) daily gridded (spatial resolution of 4 km) estimates of streamflow from well-established and verified mHM simulations (Samaniego et al., 2010; Kumar et al., 2013; Zink et al., 2017), volumetric discharge (Q_R, L^3T^{-1}) at the Weser River basin outlet for the median and low-flow conditions (Q_{R50} and Q_{R90}) were estimated as 311 m^3/s and 135 m^3/s, respectively. Temporal fluctuation in area-normalized discharge (Q^*, LT^{-1}) at the basin outlet was characterized by coefficient of variation (CV_{Q^*}) of 0.76, representing the "persistent" hydrologic regime ($CV_{Q^*} < 1$) as defined by Botter et al. (2013). Mean CV_{Q^*} values were <1 and decreased slightly with increasing stream order ω (~0.9 for ω =1 to 4; ~0.84 for ω = 5 and 6; ~0.8 for ω = 7). Variability in CV_{Q^*} values was the largest for ω =1 (*CV* of $CV_{Q^*} = 0.18$) and decreased continuously until ω =5 (*CV* of $CV_{Q^*} = 0.06$), while remarkably low diversity in CV_{Q^*} values was found in ω =6-7 (*CV* of $CV_{Q^*} = 0.01$). This trend suggests higher variations in hydro-climatic conditions among smaller streams.

2.3.2 Distributions of people and WWTPs discharges

Based on the United Nations (2016) definition of a city, among the top 14 German cities with > 500K inhabitants (Destatis, 2018) only two, Bremen and Hannover, are located within the Weser River basin. About 8.4 million inhabitants in the basin (~10.2% of Germany's population; Figure 2.5a) are served by ~845 WWTPs (~10% of total German WWTPs; Figure 2.5b) with one of top connectivity of people to WWTPs (~97%) in EU (EEA, 2017b). The number of WWTPs corresponds to a density of 2 point source entries per 100 km^2, and a mean separation distance between two successive WWTPs of ~11 km (*CV* = 0.9) based on a total river network length (~12K km). More than half of total WWTPs in the basin discharge the treated effluents to streams with the persistent hydrologic regime. The receiving streams consist of ~58% of total streams with ω≤3 and ~95% of total streams with 4≤ω≤7. About 700 WWTPs (~83% of total WWTPs in the Weser)

discharge to small streams (ω≤3), and ~26% of these receiving streams receive discharge from large WWTPs (k≥4). Thus, significant variability in WWTP discharges (treated effluents and nutrient loads) to small streams is expected, and the resulting variability in likely water quality impacts at the reach-scale.

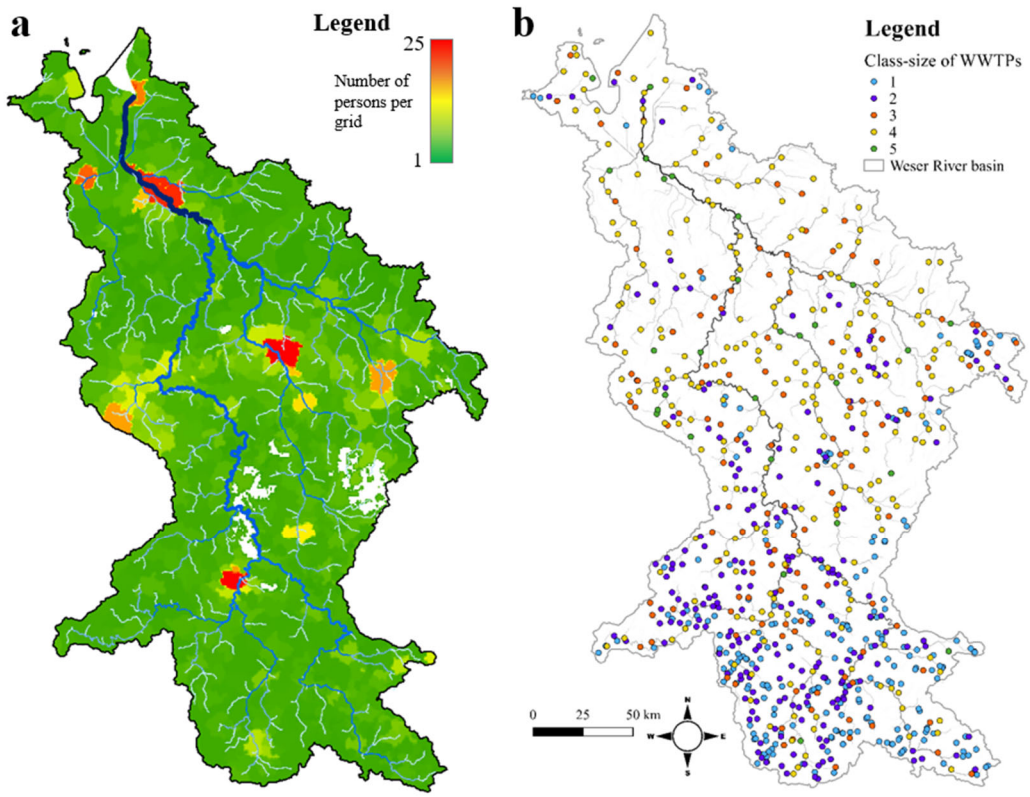

Figure 2.5 For the Weser River basin of ~46K km^2, (a) the distributions of ~8.4 million human population (background color of green to red scaled) and river network (darker blue color and thicker line width for higher H-S order). With the overlapped river network (gray-scaled color lines) (b) the location of ~845 WWTPs with classification for five class-sizes. Note that the original datasets are the same ones for Figures 2.3 and 2.4.

2.3.3 Land cover (Pressure pathway)

To reflect the temporal change of land cover over the Weser River basin, the CORINE Land Cover (CLC) 100 m grid data version 20 for three reference years (1990, 2000, and 2012) were used among five available ones (downloaded from https://land.copernicus.eu/pan-

european/corine-land-cover). The three time series were selected to be consistent with time-periods for available nutrient loads input data reported in literatures (see Section 2.3.4). Since the original CLC database provides land cover across Europe, national territory of Germany was extracted first, and then the extent of Weser River basin was clipped using the ArcGIS. The CLC datasets produced based on satellite imaginary are categorized as one of 44 classes in the hierarchical-order three class levels.

In this study, five main classes in the uppermost level 1 are used to distinguish different representative land cover (Class 1 = Artificial surfaces representing urban areas; Class 2 = Agricultural areas; Class 3 = Forest and semi-natural areas; Class 4 = Wetlands; and Class 5 = Water bodies). The CLC spatial maps over the Weser River basin for the three chosen years (Figure 2.6) obviously manifest the dominance of agricultural areas, the scattered urban areas, and upstream clustered formation of forest/semi-natural areas. A skewness index (Mineau et al., 2015) calculated for each land cover provide quantitative representation characterizing a spatial distribution of different land attributes within a river basin (Table 2.3). Distribution of forest/semi-natural land cover (skewness index >1) is skewed towards the headwaters. On the contrary, skewed distributions of artificial and agricultural areas are towards the basin outlet (skewness index ~0.9), and wetlands are distributed with stronger downward-skewness (skewness index ~ 0.5). For last few decades, agricultural areas consistently accounted for ~ 60% of total drainage area; land cover portions of artificial and forest/semi-natural areas slightly increased with a trade-off of decrease in wetlands proportion (Table 2.4).

In addition, to understand internal heterogeneity in land cover proportions within the entire Weser River basin (final stream order $\Omega = 7$), I delineated all possible 1681 sub-basins with final stream order ($\Omega^* = 1 – 6$) and examined the proportions of dominant land cover types within each sub-basin based on the latest 2012 land cover dataset. Since at least 50% of total drainage area for 99% of the 1681 sub-basins consists of artificial surface (CLC-Class 1), agricultural areas (CLC-Class 2), and forest / semi-natural areas (CLC-Class 3), I focused on the three dominant land cover types to compare variabilities in land cover composition within/across stream orders (Figure 2.7). As reflecting fractal structure of river network, lower-order sub-basins ($\Omega^* < 3$) are more dispersed from upstream to downstream regions over the entire basin area (Figures 2.7a-c), whereas higher-order sub-basins ($\Omega^* \geq 5$) are formed towards the basin outlet and spatially less variable located (Figures 2.7e-f). Within a given stream order, sub-basins located far from each basin outlet are

covered by more forest/semi-natural areas (>50%) than agricultural areas with a narrow range of artificial surface proportion (< 20%); on the contrary, sub-basins in more downstream are mainly dominated by agricultural than forest/semi-natural areas with a broader proportion of artificial surface area (0 to possibly 95%). It is also noteworthy that more aggregation of sub-basins for higher Ω* reduces variabilities in land cover proportion.

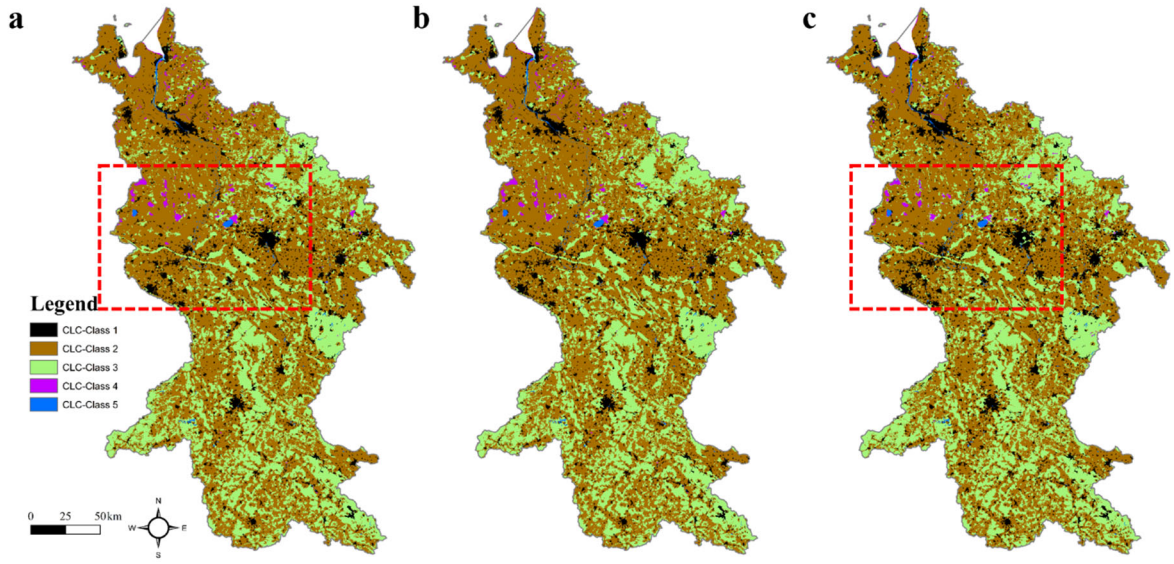

Figure 2.6 The CORINE Land Cover (CLC) map over the Weser River basin for three reference years: (a) 1990, (b) 2000, and (c) 2012. Five CLC-classes in the uppermost level 1 are consistently depicted: black-zone for CLC-Class 1 = Artificial surfaces representing urban areas; brown-zone for CLC-Class 2 = Agricultural areas; green-zone for CLC-Class 3 = Forest and semi-natural areas; purple zone for CLC-Class 4 = Wetlands; and blue-zone for Class 5 = Water bodies. Red-dashed rectangle represents the most visually distinct change over time, as an example.

Table 2.3 Skewness index of each land cover for a given year CLC data in the Weser River basin

CLC-class in level 1	Reference year		
	1990	2000	2012
Artificial surface	0.90	0.91	0.90
Agricultural areas	0.92	0.92	0.92
Forest & Semi-natural	1.20	1.20	1.18
Wetlands	0.50	0.50	0.51
Water bodies	0.65	0.66	0.66

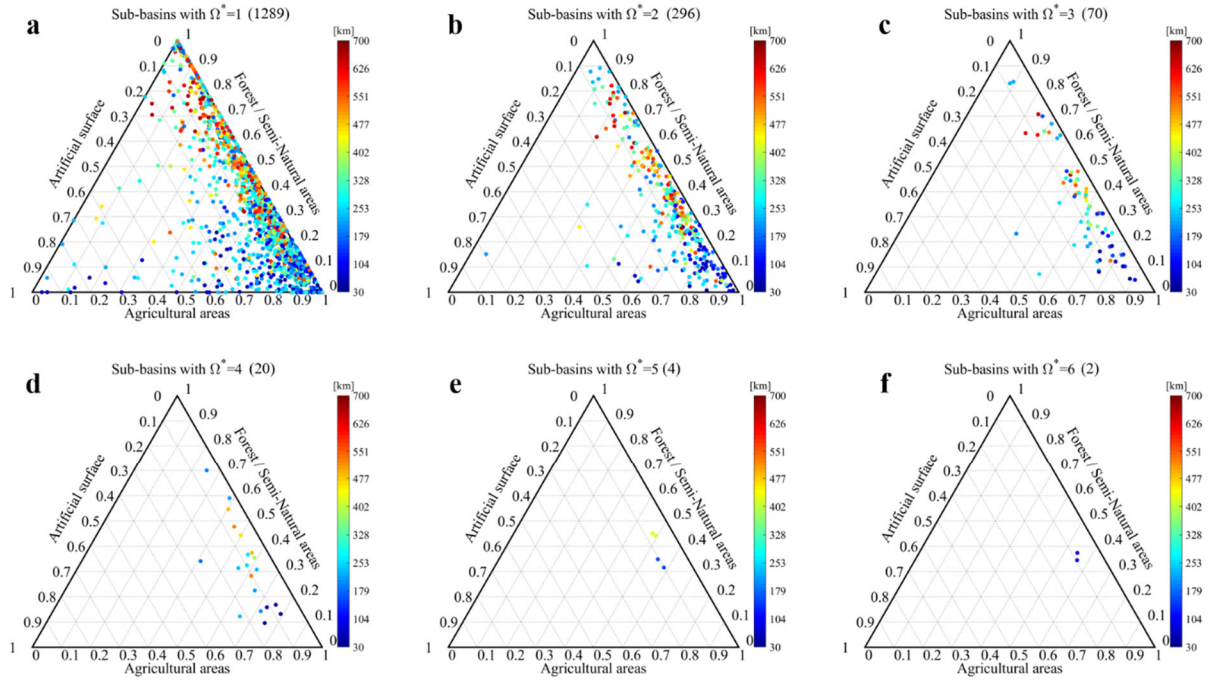

Figure 2.7 For all sub-basins in the Weser River basin, ternary diagrams for the portion of land cover within a sub-basin having its final stream order as Ω^*. From the 1st to 6th order sub-basins, results are shown in (a) to (f), sequentially. Among total five main classes of land cover, three dominant land cover types are used as the ternary axes (Class 1 = Artificial surface; Class 2 = Agricultural areas; Class 3 = Forest / Semi-natural areas). Number in the parenthesis in each sub-title is the total number of Ω^*th order sub-basins. Each dot represents each sub-basin. Color in each dot means the distance to the Weser River outlet from the outlet of each sub-basin.

Table 2.4 The percent (%) of each land cover for a given year CLC data in the Weser River basin

CLC-class in level 1	Reference year		
	1990	2000	2012
Artificial surface	7.0	7.5	9.0
Agricultural areas	61.8	61.3	58.9
Forest & Semi-natural	30.1	30.1	31.2
Wetlands	0.7	0.7	0.5
Water bodies	0.4	0.5	0.5

2.3.4 Nutrient loads (Pressures)

Nutrient loads given into river networks are distinguished between point-source and diffuse sources. There are a few or several sub-categorized sources and one type source can be transported through multiple pathways. Since this study scope is to consider relative impact from point- and diffuse-sources, sub-categorized sources being the most typical and compatible with available dataset in this study were selected as nutrient loads input sources. Thus, this study considers nutrient emissions from municipal WWTPs discharges as point-source, and those from urban areas, agricultural areas, and green areas (e.g., forests) as diffuse-sources.

To reflect temporal change in the magnitude and portion of nutrient emissions, three time periods were selected, 1983-1987, 1998-2002, and 2011-2014, which encompass environmental-political-social events such as water pollution, relevant regulations formation, and public practice. For a given period, nutrient emissions of each sub-categorized source in the Weser basin were estimated by employing its proportion to nutrient emissions for the entire Germany, based on the published values in reports of German Environment Agency (UBA, 2003; 2010; 2017). Note that this study deals with only Phosphorus loads (Table 2.5) which is preferred nutrient for algal growth. Municipal WWTPs P loads accounts for ~95% of total point-source P emissions. Each diffuse-source was categorized correspondingly to CLC-class 1 to 3, under the assumption to deal with terrestrial nutrient inputs mainly.

Table 2.5 Estimated P loads [tonP/yr] from different sources in the Weser River basin

	1983-1987	**1998-2002**	**2011-2014**
Municipal WWTPs	5391	861	694
Artificial surface	829	300	419
Agricultural areas	1300	1807	1576
Forest & Semi-natural	660	750	485

2.3.5 Water quality monitoring (State)

During 1979-2015, nutrient concentrations ($C_{means(i)}$, i = total inorganic N and P) were monitored at a total of 361 locations in river reaches of the Weser River basin (Figure 2.8), at approximately monthly intervals. The reaches were sampled at different times of the year, and at varying intervals, under diverse range of hydrologic conditions. Archived data (total: ~57K data recorded) were obtained from the official EIONET (European Environmental Information and Observation Network) and WFD sample sites. Only ~35% of the total archived data concurrently included the measured river discharge (Q_{Rmeas}) at the same location.

Given the major shifts in governance, wastewater treatment technology, and environmental regulations over the past few decades in Germany, the monitoring data were pooled into two time periods: (1) $C_{meas,pre(i)}$ for 1979-1999 (T_{pre}), which includes the period prior to German Reunification in 1990, and subsequent changes in regulatory and technological regimes; and (2) $C_{meas,post(i)}$ for 2000-2015 (T_{post}), during which Germany initiated monitoring for the implementation of the EU WFD (EEA, 2017b). For total inorganic N, the C_{meas} ranges for T_{pre} and T_{post} were similar, and ranged from 0.08 (and 0.06) to 45 mg N/L. For total inorganic P, the range of C_{meas} values for T_{post} was smaller (0.006 to 6 mg P/L) than that for T_{pre} (0.005 to 7.9 mg P/L). The monitoring records were also analyzed to examine spatial patterns in the measured concentrations for inorganic nutrients over H-S stream orders.

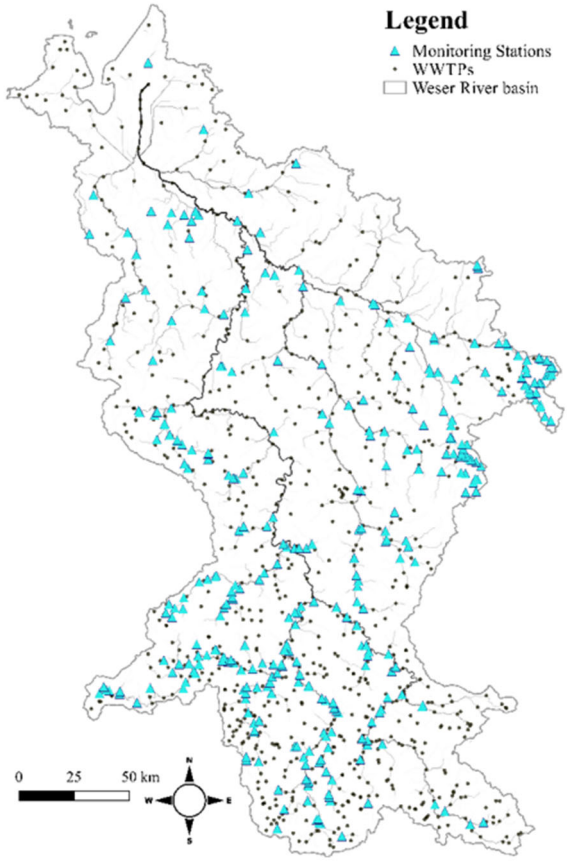

Figure 2.8 The distribution of ~360 monitoring stations (cyan colored triangular) in the Weser River basin. For comparing locations, WWTPs are depicted as dots without class-size category.

3. DATA ANALYSIS & MODELING

The contents of this section are mainly based on the analyses methods sections of following published papers: (1) Soohyun Yang, Kyungrock Paik, Gavan S. McGrath, Christian Urich, Elisabeth Krueger, Praveen Kumar, and P. Suresh C. Rao, (2017). Functional Topology of Evolving Urban Drainage Networks. *Water Resources Research;* **(2)** Soohyun Yang, Olaf Buettner, James W. Jawitz, Rohini Kumar, P. Suresh C. Rao, and Dietrich Borchardt, (2019). Spatial organization of human population and wastewater treatment plants in urbanized river basins. *Water Resources Research;* **(3)** Soohyun Yang, Olaf Buettner, Rohini Kumar, Christoph Jaeger, James W. Jawitz, P. Suresh C. Rao, and Dietrich Borchardt, (2019). Spatial patterns of water quality impairments from point source nutrient loads in Germany's largest national River Basin (Weser River). *Science of the Total Environment.*

3.1 Power law scaling relationships

To address whether UDNs exhibit scaling behavior comparable to that of rivers, two relationships widely found in river networks, were used in this study. The first, Hack's law, is a power-law relationship between the main channel length, *L,* and its corresponding drainage area *A*:

$$L \propto A^h \tag{3.1}$$

with the exponent *h* for rivers found to be universally in a small range, $h = 0.6 \pm 0.1$ (Hack, 1957; Robert & Roy, 1990; Crave & Davy, 1997; Paik & Kumar, 2011). For UDNs, I take 'the length along main sewer line' as *L*. The other scaling relationship is the exceedance probability distribution of the upstream drainage area (Rodríguez-Iturbe, Ijjász-Vásquez, et al., 1992) within catchments retrieved from DEMs. The exceedance probability that the upstream drainage area is equal to or greater than a value δ is reported to follow a power-law. For UDNs, this can be expressed as an exponentially tempered Pareto distribution (Aban et al., 2006),

$$P(A \geq \delta) = a\delta^{-\varepsilon} \exp(-c\delta);\ \delta \geq \delta_{min}\,. \tag{3.2}$$

The exponent ε for most river networks is 0.43 ± 0.03 (and $c = 0$, representing truncation) suggesting universality of this scaling relationship (Rodríguez-Iturbe, Ijjász-Vásquez, et al., 1992; Maritan et al., 1996; Crave & Davy, 1997; Rinaldo et al., 2014).

3.2 Hierarchical scaling relationships

3.2.1 Horton scaling ratios framework

Self-similar structures of natural river networks exhibit nearly consistent ratios, known as *Horton scaling ratios*, for geometric variables between two successive H-S orders. I investigated whether the studied German rivers conform to well-established scale-invariant structure found universally for river networks. I used four well-known Horton scaling ratios of stream number, R_B (Horton, 1945), stream length, R_L (Horton, 1945), drainage area, R_A (Schumm, 1956), and eigen-area (i.e., order-specific area variable), R_E (Beer & Borgas, 1993), expressed as:

$$R_B = N_\omega / N_{\omega+1} \tag{3.3}$$

$$R_L = \overline{L}_{\omega+1} / \overline{L}_\omega \tag{3.4}$$

$$R_A = \overline{A}_{\omega+1} / \overline{A}_\omega \tag{3.5}$$

$$R_E = \overline{E}_{\omega+1} / \overline{E}_\omega \tag{3.6}$$

where N_ω, $\overline{L}_\omega$, and $\overline{A}_\omega$ (for $\omega \geq 1$) are the number, the mean length, and the mean drainage area of ω-order streams, respectively. $\overline{E}_\omega$ (for $\omega \geq 2$) are the mean eigen-area of ω-order streams. The first three ratios have typical ranges observed from natural river networks, $3<R_B<5$, $1.5<R_L<3$, and $3<R_A<6$ (Smart, 1972; Kirchner, 1993). Horton scaling ratios are inter-related through fractal dimensions. For example, the fractal dimension for network branching, D_b ($1 \leq D_b \leq 2$; mean ~1.8), links R_B and R_L as $R_B = R_L^{D_b}$ (La Barbera & Rosso, 1989). I infer $R_A = R_E^{D_b}$ based on the finding of cross-relationships among the four ratios $R_E (\approx R_L) < R_A (\approx R_B)$ (Yang & Paik, 2017).

In this study, I propose three *extended* Horton scaling ratios to examine scale-invariant distributions of population (R_{POP}), PE (R_{PE}), and the number of WWTPs (R_{WWTP}) over H-S orders in the three case study river networks, evident in consistently increasing or decreasing rate of change between any two successive H-S orders. The extended ratios are defined as:

$$R_{POP} = \overline{POP}_{\omega+1} / \overline{POP}_\omega \tag{3.7}$$

$$R_{PE} = \overline{PE}_{\omega+1} / \overline{PE}_\omega \tag{3.8}$$

$$R_{WWTP} = N_\omega^{WWTP} / N_{\omega+1}^{WWTP} \tag{3.9}$$

where $\overline{POP}_\omega$ (for $\omega \geq 1$) are the mean population living in ω-th order eigen-areas (i.e.,

$\overline{POP}_\omega = \sum POP_\omega / N_\omega$), $\overline{PE}_\omega$ (for $\omega \geq 1$) are mean PE served by WWTPs discharging to ω-th order streams per ω-th order stream (i.e., $\overline{PE}_\omega = \sum PE_\omega / N_\omega$), and N_ω^{WWTP} (for $\omega \geq 1$) are number of WWTPs regardless of class-sizes discharging to ω-th order streams.

I used an eigen-area-based perspective (i.e., order-specific drainage area) to examine scaling of both POP and PE, while previous researchers employed cumulative drainage area to estimate the Horton scaling ratios for surrogate variables for population (Miyamoto et al., 2011; Fang et al., 2018). Both the order-specific and cumulative-area perspectives allow for evaluating the scale-invariance of the spatial distribution of POP based on census data (as in this study) or surrogate variables (Miyamoto et al., 2011; Fang et al., 2018). However, PE for each WWTP is an aggregated representation of POP and corresponding pressures (wastewater and nutrient loads) for its contributing sewer-shed. Thus, I used the spatially more distinct eigen-area-based approach in this study to represent the underlying attribute of PE indicating the point-source pressures for all non-overlapping regions.

3.2.2 Proposed scaling indices

As measures for quantifying the spatial distributions of three attributes (POP, PE, and WWTP) across river networks, I propose three new scaling indices, γ, ε, and δ, defined as:

$$\gamma = R_{POP} / R_E \,, \tag{3.10}$$

$$\varepsilon = R_{PE} / R_{POP} \,, \tag{3.11}$$

$$\delta = (R_{PE} \cdot R_{WWTP}) / R_B \,. \tag{3.12}$$

The index, γ, identifies the preferred eigen-area for population settlement by H-S order, with preferences either for higher orders ($\gamma > 1$), lower orders ($\gamma < 1$), or neutral ($\gamma \simeq 1$). A similar index used by Fang et al. (2018) is based on cumulative area and surrogate population variable. Two approaches are related based on the relationship between R_A and R_E, $\gamma = R_{POP} / (R_A)^{1/D_b}$ ($1 \leq D_b \leq 2$; mean $D_b \sim 1.8$).

The index, ε, estimates the contribution of non-sanitary inflow to wastewaters treated at the WWTPs. A value of $\varepsilon > 1$ suggests that WWTPs discharging to higher H-S orders have a larger contribution of non-sanitary wastewaters, while $\varepsilon < 1$ represents that lower orders receive

more non-sanitary wastewaters collected into WWTPs. Uniform or zero contribution of non-sanitary wastewaters yields $\varepsilon = 1$.

The third index, δ, indicates the degree of centralization in WWTP locations. Here, higher centralization means fewer WWTPs, but of higher class-size, whereas lower centralization means more number of lower class-size WWTPs, to treat a given amount of wastewaters. For $\delta > 1$, the increase in PE by H-S order is greater than the corresponding increase in the number of WWTPs, and thus higher (lower) centralization of WWTPs in eigen-areas of higher (lower) stream orders. On the other hand, $\delta < 1$ represents lower (higher) centralization of WWTPs in eigen-areas of higher (lower) stream orders. A value of $\delta = 1$ can reflect either the construction of same class-size WWTPs for all H-S orders (idealized case) or the absence of a tendency for the degree of centralization in WWTPs construction across H-S orders.

3.3 Longitudinal distribution pattern characterization

3.3.1 Width function and spatial clustering indices

The geomorphological width function (G-WF, $W_G(x_G)$) is an operator to examine the structural character of drainage network along a hydrological path in a one-dimensional domain (Marani et al., 1994; Rodríguez-Iturbe & Rinaldo, 2001). The G-WF relates the drainage areas at a flow distance from the basin outlet, thus the integral of G-WF along flow distances represents the total drainage area :

$$\int_0^{x_{\max}} W_G(x_G)dx_G = A_\Omega \tag{3.13}$$

where x_{max} is the longest distance from the basin outlet, x_G is a distance variable for the G-WF, and A_Ω is the total drainage area of the basin with the final H-S order Ω.

Applying human-related width function (Fang et al., 2018), I investigated the population width function (POP-WF, $W_{POP}(x_{POP})$) and the directionality of population clustering (Ψ_{POP}) with one-dimensional perspective as:

$$\int_0^{x_{\max}} W_{POP}(x_{POP})dx_{POP} = POP_\Omega \tag{3.14}$$

$$\Psi_{POP} = \hat{x}^{POP,50} \big/ \hat{x}^{G,50} \tag{3.15}$$

where x_{POP} is a distance variable for the POP-WF, POP_Ω is the total population in the river basin.

I used a distance interval of $dx_{POP} \approx \overline{L}_1 + x_e$ (where x_e is a distance yielding rectangular area equivalent to a given source area). $\hat{x}^{POP,50}$ is normalized flow length from the basin outlet for half of the population in the river basin. $\hat{x}^{G,50}$ is normalized flow length for half of total drainage area of the river basin.

Furthermore, I extended these metrics for the PE width function (PE-WF, $W_{PE}^{k}(x_{PE})$, where $1 \leq k \leq 5$ is a class-size of WWTPs, and the directionality of PE clustering for each k-th class-size ($\Psi_{PE(k)}$). Their mathematical expressions are given as:

$$\int_0^{x_{\max}} W_{PE}^{k}(x_{PE})dx_{PE} = PE^{k} \tag{3.16}$$

$$\Psi_{PE(k)} = x_k^{PE,50} \Big/ x_k^{PE,100} \tag{3.17}$$

where x_{PE} is distance for PE-WF, and PE^k is the total PE of class-k. I employed a distance interval of $dx_{PE} \approx \overline{L}_1$. For each class k, $x_k^{PE,50}$ is a hydrological distance from the basin outlet to take 50% of total PE and $x_k^{PE,100}$ is the longest flow distance.

For all three basins, I normalized POP-WFs by each maximum POP of $W_{POP}(x_{POP})$ to facilitate cross-basin comparison. To differentiate the population in cities, here I introduced the concept of the *urban zone*, considered as regions where the normalized $W_{POP}(x_{POP})$ is above a particular threshold (POP*; 0 <POP*< 1). I then estimated the interval distance for each urban zone as a distance between upstream and downstream crossing points for the threshold of POP* = 0.5, which determined based on the national-scale portion of population in the cities. I estimated the inter-urban separation distance (σ_i) for cities, and normalized separation distances (τ_i) as the ratio σ_i/L_{max}, and reported the mean ($\overline{\tau}$; $0 < \overline{\tau} < 1$).

3.3.2 Power spectral analysis

The power spectra, $S(f)$, of G-WF as a function of frequency, f [L^{-1}], reveals the spatial auto-correlations. A power-law relationship, $S(f) \propto f^{-\beta^G}$, has been found for river networks, with exponent β^G between 1.2 and 2.1 (Marani et al., 1994; Fang et al., 2018). This implies that scale-invariance of river network structures is reflected in the G-WF. To explore how the spatial clustering for populations is different from that of river network structures, I compared the power-

law exponents for POP-WF and G-WF (β^{POP} / β^{G}) for the three river basins. Moreover, I investigated power-law exponent for PE-WFs for each class-size k (β_k^{PE}), to examine how the degree of spatial clustering for PE is different among WWTP class-sizes. Each power-law exponent β was estimated through Matlab *fitlm* function referring to a linear relationship of $S(f)$ and f on a log-log paper. The significance of the power-law exponent was determined by the *p*-value for *t*-statistic of the null hypothesis test that the estimated coefficient is zero.

3.4 Impacts of point-source pressure

3.4.1 Reach-scale perspective

3.4.1.1 Urban wastewater discharge fraction (Hydrological impact)

I used the concept of Urban Wastewater Discharge Fraction (Φ) to estimate the likely reach-scale dilution of WWTP treated effluents with river discharge. I calculated Φ as:

$$\Phi = \frac{Q_U}{Q_R + Q_U} \quad (0 \le \Phi \le 1) \tag{3.18}$$

where Q_R is the steady volumetric discharge [L^3T^{-1}] of receiving stream, and Q_U is the (mean annual) steady volumetric discharge [L^3T^{-1}] of treated wastewater from a WWTP. Note that Φ~0 for $Q_R >> Q_U$, Φ=0.5 for $Q_R = Q_U$, and Φ~1 for $Q_R << Q_U$.

In this study, I considered two conditions for river discharge (Q_R): (1) median river discharge (Q_{R50}), and (2) low-flow condition, which is exceeded 90% of the time (Q_{R90}). These values were derived based on the long-term, daily (56 years, 1960-2015) hydrographs simulated using the grid-based mHM (Samaniego et al., (2010); Kumar et al., (2013) for model details/parameterizations, and Zink et al. (2017) for a detailed model set-up including verification of modeled fluxes and states across Germany). Location of each WWTP was matched with its nearest mHM grid (spatial resolution of 4 km x 4 km) using the ArcGIS, and the simulated hydrograph was allocated to each WWTP. Using feature scaling, for about 11% of all WWTP locations, I modified hydrographs showing inconsistency compared to hydrographs for the same H-S order from other locations. I calculated Q_U for each WWTP based on PE served and the annual per capita water-use in Germany (q= 46.3 m^3/yr/PE) (Eurostat, 2013).

3.4.2.2 In-stream nutrient concentration (Water quality impact)

I examined reach-scale water quality impairments using N and P concentrations ($C_{reach(i)}$, i = N or P) estimated using only the point source nutrient loads from each WWTP discharge alone. The estimation for $C_{reach(i)}$ was based on the mass-balance equation for nutrient loads at the point of WWTP discharge:

$$L_{reach(i)} = L_{R(i)} + L_{U(i)} \tag{3.19}$$

where L [MT^{-1}] variable means nutrient loads, and the subscripts of R, U, and *reach* denote the representation of *river before* receiving WWTP discharge, *WWTP* discharge, and *reach* received WWTP discharge, respectively. Given that L is the product of concentration C [ML^{-3}] and discharge Q [L^3T^{-1}], Eq. (3.19) is expressed as:

$$C_{reach(i)}Q_{reach} = C_{R(i)}Q_R + C_{U(i)}Q_U \tag{3.20}$$

where Q_{reach} denotes the mass balance at the reach-scale for combined streamflow within a receiving stream reach ($Q_{reach} = Q_R + Q_U$). To investigate the sole influence of the WWTP point source nutrient loads on water quality impairment, here I considered zero nutrient concentrations in receiving rivers (i.e., $C_{R(i)} = 0$), resulting in the following expression of $C_{reach(i)}$:

$$C_{reach(i)} = \frac{L_{U(i)}}{Q_R + Q_U}. \tag{3.21}$$

To interpret $C_{reach(i)}$ values estimated at the reach-scale, I applied the following conservative assumptions, similar to a US EPA study for estimation of wastewater impacts on surface waters through US (Rice & Westerhoff, 2015) : (1) complete and instantaneous mixing of WWTP effluents and river flow at the point of discharge; (2) neglecting diurnal and seasonal patterns in WWTP effluents; (3) no loss of nutrient loads from WWTPs through in-stream processes within the reach; (4) no loss of WWTP effluents to groundwater; and (5) no temporal evolution of PE served by each WWTP.

3.4.2 Basin-scale perspective

3.4.2.1 In-stream nutrient uptake process

At basin-scale considering downstream cumulative nutrient loads with in-stream uptake, total loads of nutrient i at the location of the j-th WWTP ($L_{i,tot(j)}$) consist of two types of nutrient

loads: (1) constant nutrient loads discharged from the j-th WWTP ($L_{i,in(j)}$) and (2) sum of attenuated nutrient loads discharged from all upstream WWTPs along flow paths, expressed as:

$$L_{i,tot(j)} = L_{i,in(j)} + \sum_{\gamma=1}^{\Gamma} L_{i,in(\gamma)} \cdot \exp\left(\sum_{m=1}^{M} \int_{l_{\min(m)}}^{l_{\max(m)}} -k_x(l)dl \right) \quad (3.22)$$

where Γ is the total number of upstream WWTPs of the j-th WWTP, and M is the total number of stream segments along a flow path from upstream γ-th WWTP to the j-th WWTP.

In-stream nutrient uptake rate constant k_x [L^{-1}] scales inversely with river discharge (or stage) (Ensign & Doyle, 2006; Basu et al., 2011). Thus, in this study, I estimated k_x, as a function of a flow length l to a given location along the longest flow path from the basin divide. I derived $k_x(l)$ based on a scaling of k_x with hydraulic and geomorphologic properties of a river network (Basu et al., 2011; Hall Jr. et al., 2013; Bertuzzo et al., 2017) as:

$$k_x = v_f/(h \cdot v) = v_f/(Q_{Rmean}/w) \quad (3.23)$$

where v_f is nutrient uptake velocity [m/yr] in the hyporheic zone. Here, I assumed spatially uniform v_f over the entire river network (Alexander et al., 2000; Wollheim et al., 2006; Basu et al., 2011). Note that the product of river depth (h) and velocity (v) corresponds to specific discharge (Q_{Rmean}/w, where Q_{Rmean} is the mean annual river discharge and w is the river width).

At the same frequency of occurrence, power-law relation between Q_{Rmean} [$m^3\ s^{-1}$] and w [m] is well-known (Leopold and Maddock, 1953) as:

$$w = \pi_1\ Q_{Rmean}^{\ b} \quad (3.24)$$

where π_1 and b are river width scaling coefficient and scaling exponent. I used reference values of π_1 = 7.2 [$m^{1-3b}\ s^b$] and b = 0.5 [-] found by Moody & Troutman (2002) who analyzed the synthesized data including Leopold and Maddock (1953). For mean annual frequency, steady-state Q_{Rmean} can be estimated based on mass balance with spatially homogeneous precipitation (PR) and evapotranspiration (ET) [mm/yr] as:

$$Q_{Rmean} = A(PR\text{-}ET) \quad (3.25)$$

where A is accumulated drainage area at a given location within a river basin. Last scaling I used for $k_x(l)$ derivation is a power-law relation between A [m^2] and l [m] along a mainstream, known as Hack's law (Hack, 1957):

$$l = \pi_2\ A^h \quad (3.26)$$

where π_2 and h are coefficient and the power-law exponent in Hack's law. Analysis for the Weser river network yielded π_2 = 0.37 [m^{1-2h}] and h = 0.59 [-] of which value is within a narrow h range

(0.5 – 0.7) universally found in natural rivers (Hack, 1957; Crave & Davy, 1997; Paik & Kumar, 2011). Substituting Eqs. (3.24) to (3.26) into Eq. (3.23) yields the power relation with the exponent of (b-1)/h (< 0) as:

$$k_x(l) = \tau \cdot v_f \cdot \pi_1 \cdot (\pi_2)^{(1-b)/h} \cdot (PR - ET)^{b-1} \cdot (l)^{(b-1)/h} \quad (3.27)$$

where τ is an unit conversion coefficient set as $10^{3(1-b)} \cdot (365 \cdot 24 \cdot 3600)^{-b}$ to result k_x [m^{-1}] from the predetermined units of dependent variables in this study.

For each nutrient, mean uptake velocity at the basin-scale ($v_{f(i)}$, i = N or P) was estimated through the inverse calculation of Eq. (3.22), Eq. (3.24), and the nutrient delivery ratio (NDR) near the basin outlet ($NDR_{i(out)}$), expressed as:

$$NDR_{i(out)} = \frac{L_{i,tot(out)}}{L_{i,tot(in)}} \ (0 \le NDR_{i(out)} \le 1) \quad (3.28)$$

where $L_{i,tot(in)}$ is the total input of nutrient loads from both point- and diffuse-sources, and $L_{i,tot(out)}$ is the current nutrient loads nearby the basin outlet. Note that $NDR_{i(out)}$ is related to the fraction of nutrient loads removed (Ψ_i) over the entire Weser basin as:

$$\Psi_i = 1 - NDR_{i(out)} \quad (0 \le \Psi_i \le 1). \quad (3.29)$$

Thus, $NDR_{i(out)}$ = 1 (Ψ_i = 0) means no nutrient losses through in-stream nutrient uptake, whereas $NDR_{i(out)}$ = 0 (Ψ_i = 1) represents complete loss of input nutrient loads over the entire basin.

I used the latest value for $L_{i,tot(in)}$ during 1998-2000, 655,530 ton N/yr and 3,576 ton P/yr as the total input nutrient loads to Weser River basin (Behrendt et al., 2003). The value of $L_{i,tot(out)}$ was determined as the mean of Q_{Rmeas} x $C_{Rmeas(i, \omega=7)}$ for the same period at the only one monitoring station located in the 7-th order stream (total 34 data points were available for both Q_{Rmeas} and $C_{Rmeas(i, \omega=7)}$). This estimation resulted Ψ_N = 0.3 and Ψ_P = 0.4, and sequentially, $v_{f(N)}$ = 43 and $v_{f(P)}$ = 62 m/yr.

3.4.2.2 In-stream nutrient concentration (Water quality impact)

At each of WWTP locations along converging flow paths, I evaluated the impact of the spatially heterogeneous distribution of point sources (five different class-sizes of WWTPs with constant nutrient loads) on the eutrophication risk in the Weser basin. Nutrient concentration at the basin-scale $C_{cum(i)}$ (i = N or P) is estimated by considering cumulative discharge and nutrient loads from all upstream WWTPs. For a given ω-th H-S order, the estimated values of $C_{cum(i)}$ were

compared with measured nutrient concentration at monitoring stations ($C_{meas(i)}$) to identify the contribution of the point source nutrient loads from WWTPs to the water quality impairment. The value of $C_{cum(i)}$ at the location of j-th WWTP was calculated as:

$$C_{cum(i)} = \frac{L_{i,tot(j)}}{Q_{R(j)} + Q_{U(j)} + \sum_{\gamma=1}^{\Gamma} Q_{U(\gamma)}} \tag{3.30}$$

where $L_{i,tot(j)}$ is total loads of nutrient i at the location of the j-th WWTP, and Γ is the total number of upstream WWTPs of the j-th WWTP.

3.4.3 Assessment thresholds for nutrient concentrations

The status of water quality impairment is one of quality elements for ecological status assessment (BMUB/UBA, 2014). In-stream nutrient concentrations lower than specific thresholds (C_N^* and C_P^*) contribute to the achievement for *Good* ecological status. However, the water quality assessment satisfaction does not always guarantee better than *Good* ecological status because of comprehensive assessment for other quality elements (e.g., river channel alteration, biota). In this study, to evaluate water quality impact (eutrophication), I referred to C_N^* = 2.8 mg/L and C_P^* = 0.1 mg/L, which are set as the management objectives for the EU WFD to be achieved by 2021 in Germany (Heidecke et al., 2015).

3.5 Impacts of point- and diffuse-sources pressures

3.5.1 Basin-scale network model

The Eulerian perspective model at the basin-scale (described in Section 3.4.2.1) was originally designed to evaluate the sole contribution of point-source nutrient loads pressure to river eutrophication threat at the WWTP discharge points. The approach was appropriate with the primary interest for point source, but its limitation that diffuse sources were not included drove the need for an extended model dealing with both sources in a river basin. The necessity came up with a basin-scale spatially explicit model. The model presented here follows the essential framework of elemental removal based network model of Bertuzzo et al. (2017) which demonstrate scaling pattern of terrestrial dissolved organic carbon removal with drainage area. Compared to the original model application to conceptual diffuse-source input over synthetic optimal channel

networks, this study model covers practical nutrient loads from both point- and diffuse sources in real river network.

In this model, incoming loads of nutrient *i* to reach *z* ($L_{in(i),z}$) is estimated with the sum of three components: (1) point-source loads from WWTP discharges into reach *z* ($L_{U(i),z}$), (2) diffuse-source loads from directly draining area (i.e., eigen-area) into reach *z* ($K_{L(i),Y}E_{Y,z}$), and (3) cumulative loads from direct upstream reaches of reach *z* ($W_{nz}L_{d(i),n}$), expressed as:

$$L_{in(i),z} = L_{U(i),z} + K_{L(i),Y}E_{Y,z} + \sum_{n} W_{nz}L_{d(i),n} \tag{3.31}$$

where $K_{L(i),Y}$ is the nutrient *i* loads per unit area for land cover of a certain *Y*-category following CORINE level 1 data ($Y = 1\sim5$), $E_{Y,z}$ is the eigen-area of reach *z* with *Y*-category land cover, W_{nz} is the connectivity indicator between upstream reach *n* and reach *z*, and $L_{d(i),n}$ is the nutrient *i* loads at downstream end of reach *n*.

Following the original model approach, a reach *z* is considered as a channel segment between two connected pixels, and the nutrient loads within every reach is removed with first-order reaction. Thus, nutrient loads delivered at the end of reach *z* ($L_{d(i),z}$) can be estimated through the uptake velocity (v_f), the specific river discharge(Q_R/w), and the reach length (l), as:

$$L_{d(i),z} = L_{in(i),z} \cdot \exp\left(-\frac{v_{f(i)}}{Q_{R,z}/w_z} l_z\right) = L_{in(i),z}NDR_{(i),z} \tag{3.32}$$

where $NDR_{(i),z}$ is the nutrient delivery ratio of reach *z*.

Concentration of nutrient *i* from both point- and diffuse-sources loads in reach *z* ($C_{Total(i),z}$) is calculated as:

$$C_{Total(i),z} = \frac{L_{in(i),z}}{Q_{R,z} + Q_{U,z} + \sum_{n} W_{nz}Q_{TotU,n}} \tag{3.33}$$

where $Q_{TotU,z}$ is the total (mean steady) volumetric treated wastewater discharged to reach *z* from all upstream WWTPs. Thus $Q_{TotU,z} = 0$ if there are no WWTPs in upstream area of reach *z*. $Q_{U,z}$ is the treated wastewater discharge directly from a WWTP at reach *z*.

For a river discharge at a reach *z* ($Q_{R,z}$), to reflect more diverse conditions of river discharge that can potentially happen, I considered six additional conditions for river discharge based on percentiles (10th, 25th, 50th, 75th, and 90th percentiles) as well as the annual mean river discharge (Q_{Rmean}). Note that the resolution of the mHM simulation domain (4 km grid) is too coarse to

indicate river discharges of individual reaches (100 m grid) in the basin-scale model described in this dissertation. Thus, as an alternative way, I estimated a relative proportion of each percentile river flow to Q_{Rmean} (e.g., κ_{90} = low-flow 10th percentile Q_R / Q_{Rmean}) based on the mHM time-series at the Weser River basin outlet. Each relative proportion for a given Q_R percentile was applied to all river reaches homogeneously (κ_{90} = 0.34; κ_{75} = 0.49; κ_{50} = 0.78; κ_{25} = 1.26; and κ_{10} = 1.94), representing the steady-state river discharge with the same frequency over the entire river network.

4. SCALE-INVARIANCE IN RIVER & URBAN DRAINAGE NETWORKS

The contents of this section are mainly based on the results & discussions sections of following published paper: Soohyun Yang, Kyungrock Paik, Gavan S. McGrath, Christian Urich, Elisabeth Krueger, Praveen Kumar, and P. Suresh C. Rao, (2017). Functional Topology of Evolving Urban Drainage Networks. *Water Resources Research.*

4.1 Scaling in river networks

I investigated the underlying river networks of the study area. I extracted and analyzed river networks using SRTM 1 arc-second DEM provided by USGS (Figure 2.1a for Honouliuli; Figure 2.1b for AAC). Various river networks located within the same catchment boundary show an overlapping straight trunk in the exceedance probability distribution of the upstream area (Figure 4.1a for Honouliuli; Figure 4.1b for AAC). With the lower threshold area $\delta_{min} = 0.01$ km^2, I fitted the exceedance probability (Eq.(3.2)) without exponential tempering, i.e., $P(A \geq \delta) = a\delta^{-\varepsilon}$ as widely done for river networks. Each ε value was found using Matlab's *nlinfit* function of which the objective function is to minimize the sum of the squares of the residuals for the fitted model. The estimated range for a parameter was calculated with 95% confidence intervals. Averaged ε values are 0.4 for Honouliuli and 0.45 for AAC, which is in the range reported for other river networks (Rodríguez-Iturbe, Ijjász-Vásquez, et al., 1992; Maritan et al., 1996; Crave & Davy, 1997; Rinaldo et al., 2014). The length-area relationships of the underlying river networks also exhibit power-law scaling typical of a natural river network (Figure 4.1c for Honouliuli; Figure 4.1d for AAC). Breaking points starting the power-law length-area relationships with slope $h \sim 0.6$ are close to δ_{min} in area-exceedance probability distributions.

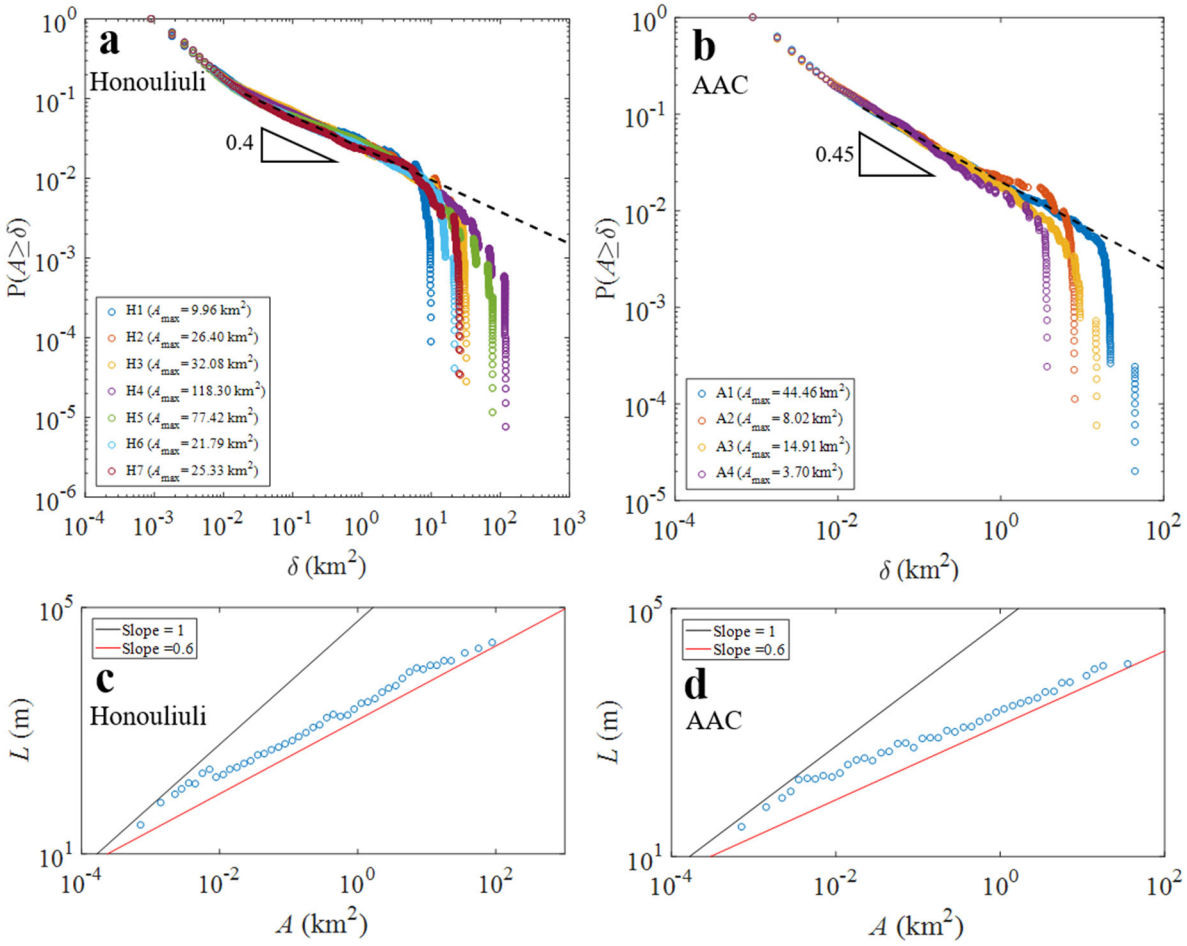

Figure 4.1 Scaling relationships of multiple catchments within the boundaries of Honouliuli and AAC catchments. (a, b) Area-exceedance probability distribution plots. Black dashed lines represent the fitted equation $P(A \geq \delta) = \alpha \delta^{-\epsilon}$ ($\delta \geq \delta_{min}$) with each averaged power-law slope of 0.4 for Honouliuli and of 0.45 for AAC. Each catchment index is compatible to those shown in Figure 2.1. (c, d) Log-binned power-law relationships between the main channel length (L) and its corresponding drainage area (A). To obtain this figure, the range of A is divided into equal interval (0.1) on log scale (log-binning size of 0.1) and then the average L for each class interval is obtained. The two lines are displayed as the 'ideal slope' for comparison with the data (linearity h=1; Hack's exponent h = 0.6).

4.2 Scale-invariant topology of UDNs

4.2.1 Scaling patterns for "Quasi-mature" UDNs

$P(A \geq \delta)$ plots for the most recent UDNs show similar patterns (Figure 4.2a): a straight middle part, here called "trunk," and the tempered "tail" resulting from the finite-size effect. The trunk section becomes evident for larger UDNs (e.g., AAC). Drainage areas for these UDNs (< 130 km^2) are much smaller than typical river networks. These are constrained by the city size and economy-of-scale constraints on the size of the WWTPs; thus, large cities are often drained by multiple UDNs. Notably for UDNs, finite-size constraints are shown as the smooth exponential tempering of $P(A \geq \delta)$. In contrast, finite-size effects for river networks are evident as abrupt power-law truncation of $P(A \geq \delta)$ (i.e., c in Eq.(3.2) is close to 0) at all spatial scales (Rinaldo et al., 2014) (Figure 4.1).

Fitting Eq.(3.2) involves three degrees of freedom: (1) the lower threshold $\delta_{\min}$ where the power-law begins; (2) the upper threshold (parameterized as c) where the power-law diminishes; and (3) the power-law exponent ε. For river networks, the lower area threshold (δ_{min}) has often been interpreted as where "hillslope" ends and the "channel" begins (Maritan et al., 1996). For UDNs, I still observe the lower threshold, although there is no hillslope in this case. I interpret the area below the lower threshold as the area inside a city block (with terminal nodes, cul-de-sacs, etc.) draining to local sewer lines along streets. Such terminal branches organize differently than most other branches; their topology differs from that of the entire network. I measured drainage areas of several such branches for the given networks and estimated the lower threshold to be 0.02 km^2. This corresponds well to the reported size of a medium-size city block (Siksna, 1997). For a typical river network, $P(A \geq \delta)$ distribution for $\delta < \delta_{min}$ (hillslope) shows an upward concave trend on log-log plots (Figures 4.1a and 4.1b). In contrast, the UDNs show a concave downward trend of $P(A \geq \delta)$ for $\delta < \delta_{min}$ on a log-log plot (Figure 4.2), indicating the disparate organization between hillslope rill and sub-block scale pipe networks.

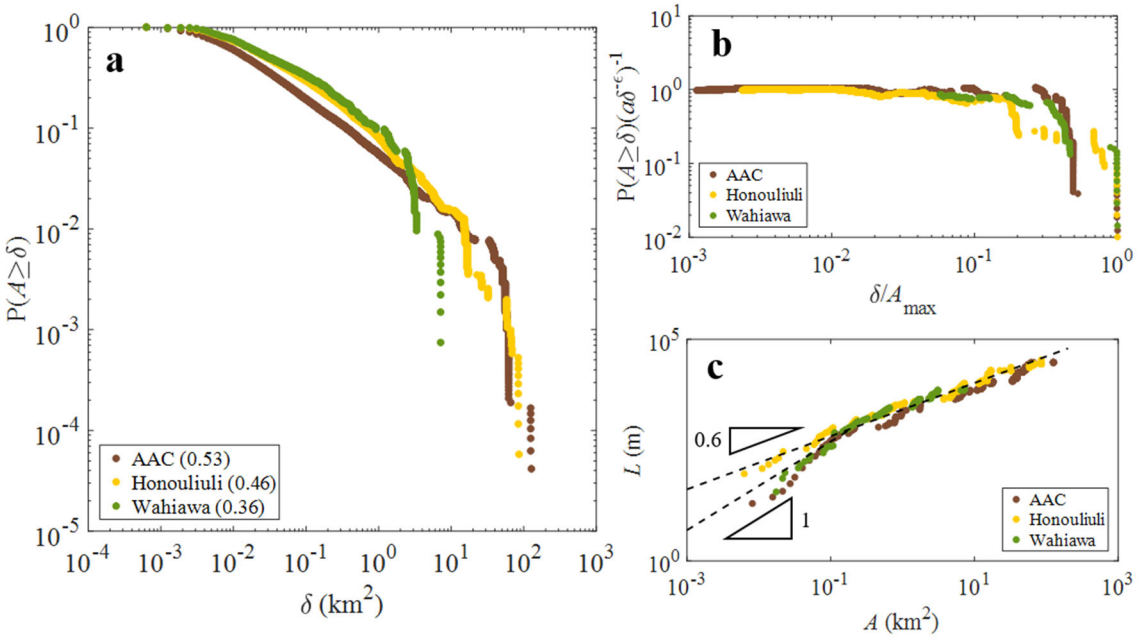

Figure 4.2 Scaling relationships of three UDNs of the most recent data. (a) Area-exceedance probability distributions for AAC, Honouliuli, and Wahiawa networks (total drainage area A_{max} are 126.0 km^2, 85.1 km^2, and 7.2 km^2, respectively). Numbers inside the parentheses in the legend are the mean fitted ε value in Eq. (3.2). Standard errors with 95% confidence interval are: for the ε value, 0.001 (AAC), 0.002 (Honouliuli), and 0.005 (Wahiawa); for the c value, 0.001 (AAC), 0.006 (Honouliuli), and 0.021 (Wahiawa). Mean squared error values for the fitted model are: 3.3×10^{-6} (AAC), 3.1×10^{-5} (Honouliuli), and 7.0×10^{-5} (Wahiawa). (b) Normalized area-exceedance probability distribution with power-law fit. (c) Length-area relationships for the three UDNs. L is the length along main sewer line and A is the drainage areas corresponding to L. The two dotted black lines are displayed as the "ideal slopes" for comparison with the data (linearity h=1; Hack's law exponent h=0.6).

For contributing area ≥ 0.02 km^2, the two parameters of ε and c in Eq. (3.2) were found using the same method mentioned in Section 4.1. Overall, the fitted ε and c of UDNs depend on the UDN size. I find ε values of 0.36, 0.46, and 0.53, and c values of 0.43, 0.20, and 0.03, respectively, for Wahiawa (year 2009), Honouliuli (year 2014), and AAC (year 2015). A small UDN of Wahiawa shows a strong exponential tempering with a short power-law range fitted with a small ε value. A large UDN of AAC, on the other hand, exhibits a long power-law range with sharp tail truncation, comparable with river networks. This implies that a UDN tends to exhibit a more robust power-law, as its drainage area expands (subject to size constraints as discussed above). For such a large UDN, ε (0.53), is greater than that reported for rivers. This can be partly

due to the fact that UDNs are not strict binary trees, unlike river networks, and can have more than two upstream pipes draining into some junctions.

From Eq. (3.2), $P(A \geq \delta)$ can be normalized as $P(A \geq \delta)(a\delta^{-\varepsilon})^{-1}$ (Rinaldo et al., 2014). The trunk portions of the normalized exceedance probability distributions collapse onto the single value of unity (Figure 4.2b). This suggests comparable topologies among the UDNs regardless of diverse (e.g., climatic, demographic, economic, engineering, and geographic) constraints underpinning the evolution of these UDNs. Normalized exceedance probability distributions deviate from unity for the tail of the distribution due to the finite size effect and difference in the tempering parameter *c* among UDNs.

The relationship between main sewer line length and corresponding drainage area also follows a power-law (Figure 4.2c), like Hack's law for rivers, which describes a power-law relationship between the main channel length and its corresponding drainage area with exponent $h = 0.6 \pm 0.1$. To be specific, length-area relationships for UDNs are often dissected into two segments, i.e., upstream segment which shows the convergence to $h \approx 1$ and the downstream segment with $h \approx 0.6$. I postulate the following scenario for the emergence of power-law scaling with the growth of UDNs. Given an initial single sewer line, the length-area relationship of such a simple system is linear and thus $h \approx 1$. As the system starts growing, repeated additions of other pipes along its length from adjoining branches lead to a self-repetitive tree, still far from self-similarity and having a linear length-area relationship. Nevertheless, with continuous network growth, some random factors such as the size of added subnets and junction locations are introduced, which is sufficient to drive the transition from this deterministic, repetitive structure, to that approaching a self-similar tree (Paik & Kumar, 2007).

The threshold between upstream and downstream segments is about 0.2 km^2, much greater than δ_{min} in Figure 4.2a. This implies that the topological reasoning for the threshold in length-area relationship differs from the reasoning for δ_{min}. The downstream segment is considered as the 'mature' section of a UDN where enough number of branches have been connected. The upstream segment is the terminal section, corresponding to the new development area at the outskirt where early settlements form only along the single major line which is connected to the main body of the network, without the development of background blocks. As cities expand such areas can be densified but another new development forms further away from the city core (e.g. Figures 4.3 and 4.4). Hence, such a break point in the length-area relationship can be found at any stage of a

growing city. The break point, however, is invisible in Figure 4.2a because $P(A \geq \delta)$ is for the entire network rather than a single path.

It has been suggested that the scaling constants, ε and h, are related as $\varepsilon+h \approx 1$ for natural river networks (Rigon et al., 1996). Given estimated values of ε and h in Figure 4.2, such constraint is not obeyed for UDNs. This is because the space-filling constraint in river networks is not necessarily applied for UDNs. For example, a single sewer-line which connects a sub-sewershed to the main network (e.g., a pipeline Ψ in Figure 4.4) can be lengthy but has a little lateral contributing area. Therefore, unlike river networks, decoupling between ε and h can be expected.

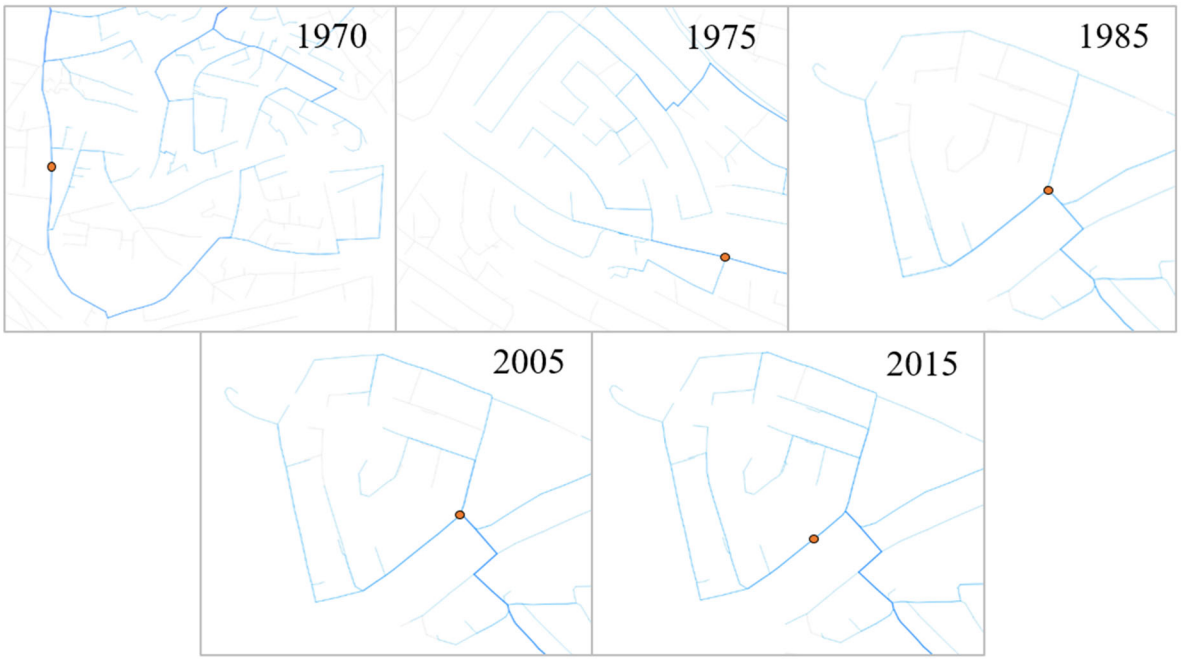

Figure 4.3 For the UDN in AAC (1970-2015), detailed upstream network of the break point (marked as an orange dot) in a length-area relationship (the accumulated drainage area is about 0.2 km^2). Poorly developed tree topology is clearly shown. Blue-colored lines show the pipe-layout existed in each year. Grey-colored background lines are the latest networks (2015). Full network configuration for each year is given in Figure 4.4, facilitating the observation for relative location of the orange dot.

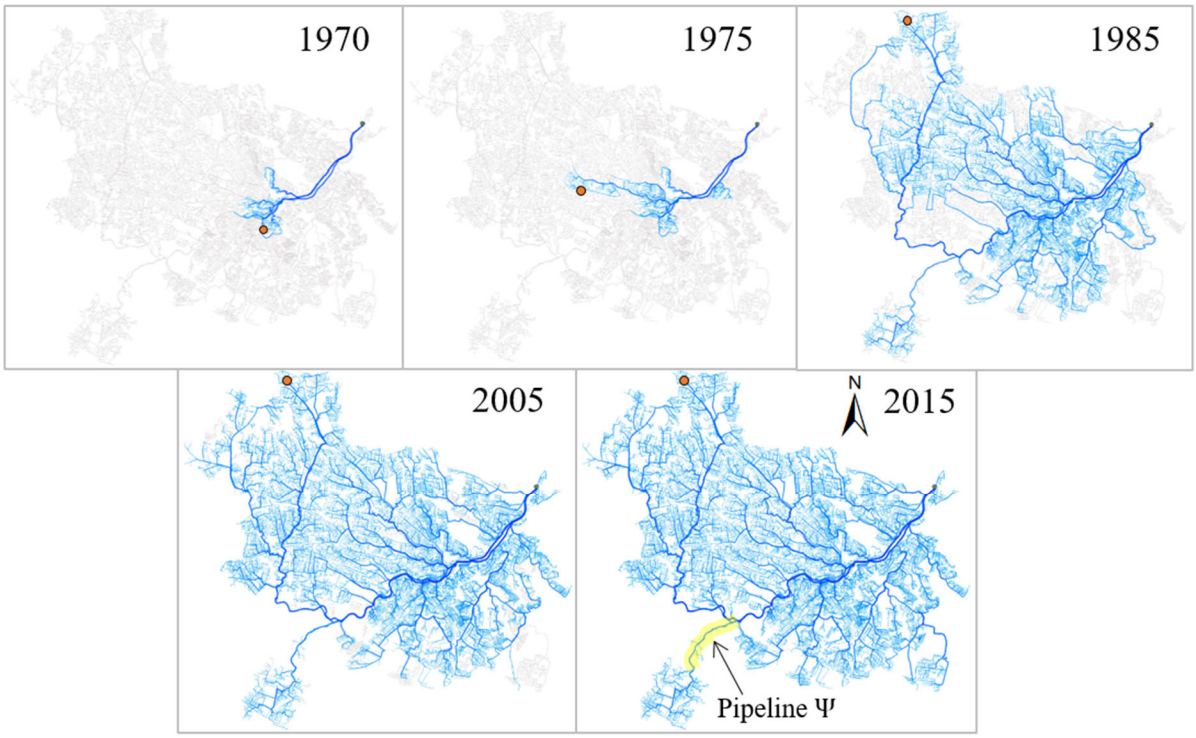

Figure 4.4 Evolution of the pipe layout (blue lines) for the UDN in AAC over decades (1970-2015). Line thickness is proportional to the Horton-Strahler order of each pipe branch. The latest UDN is shown in the background with grey color. An orange dot represents the node of which upslope area is 0.2 km^2, on the main branch (the visible break point in Hack's law of Figure 4.2c).

4.2.2 Scaling of evolving UDNs

Water infrastructure networks in cities evolve over time with increasing population and economic development. Network growth involves two processes: (1) *expansion* in area with the addition of new suburbs; and (2) *densification* as older neighborhoods are filled in or vertically expanded. These processes can occur in sequence or in parallel (Gudmundsson & Mohajeri, 2013; Mohajeri et al., 2015). Both processes contribute to an increase in total pipe length and number of network nodes in proportion to population (Krueger et al., 2017; Zischg et al., 2017). Water infrastructure also changes with retrofitting over time to accommodate growth, and changing design principles, regulatory requirements, financial constraints, etc.

I investigated the evolution of the pipe layout for the UDN (AAC shown in Figure 4.4; the other UDNs shown in Figure 4.5) and the associated scaling relationships over several decades

(Figures 4.6a-f). Specific ε and c values estimated for evolving UDNs are given in Figures 4.6a, 4.6c, and 4.6e. The power-law exponent ε in Eq. (3.2) increases as the total drainage area, A_{max}, increases over time (Figure 4.6g). On the other hand, the exponential tempering parameter, c, scales inversely with increasing A_{max} (Figure 4.6h), with an apparent log c versus log A_{max} slope of 0.73. These results suggest that as UDNs grow to drain larger urban areas, the exponential tempering diminishes, with $P(A \geq \delta)$ tending to be more abruptly truncated, thus increasingly resembling river networks.

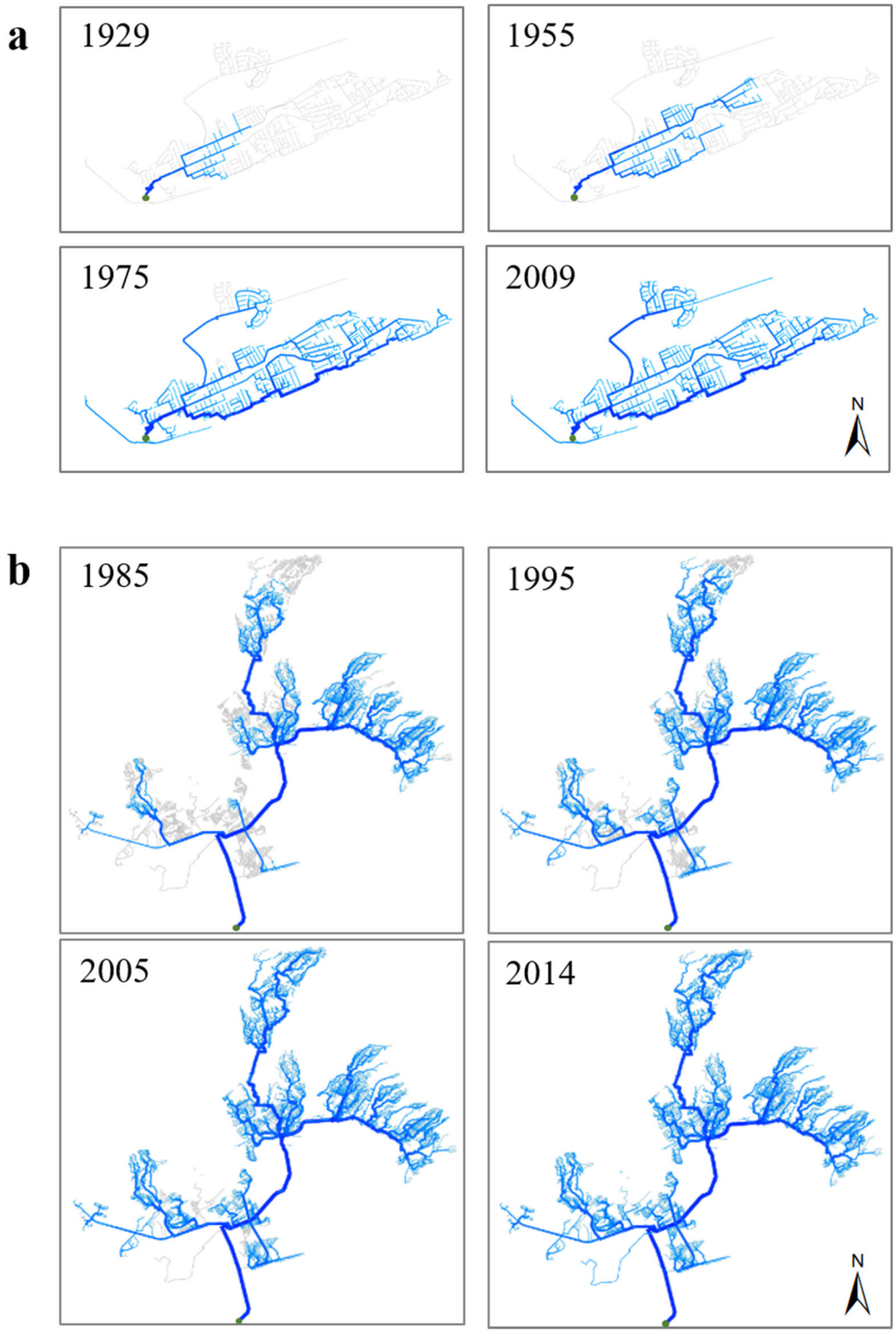

Figure 4.5 Evolution of the pipe layout for two UDNs in Oahu Island. (a) Wahiawa network. (b) Honouliuli network. The latest networks are drawn in grey line. Blue-colored line thickness is proportional to the Horton-Strahler order of each pipe branch.

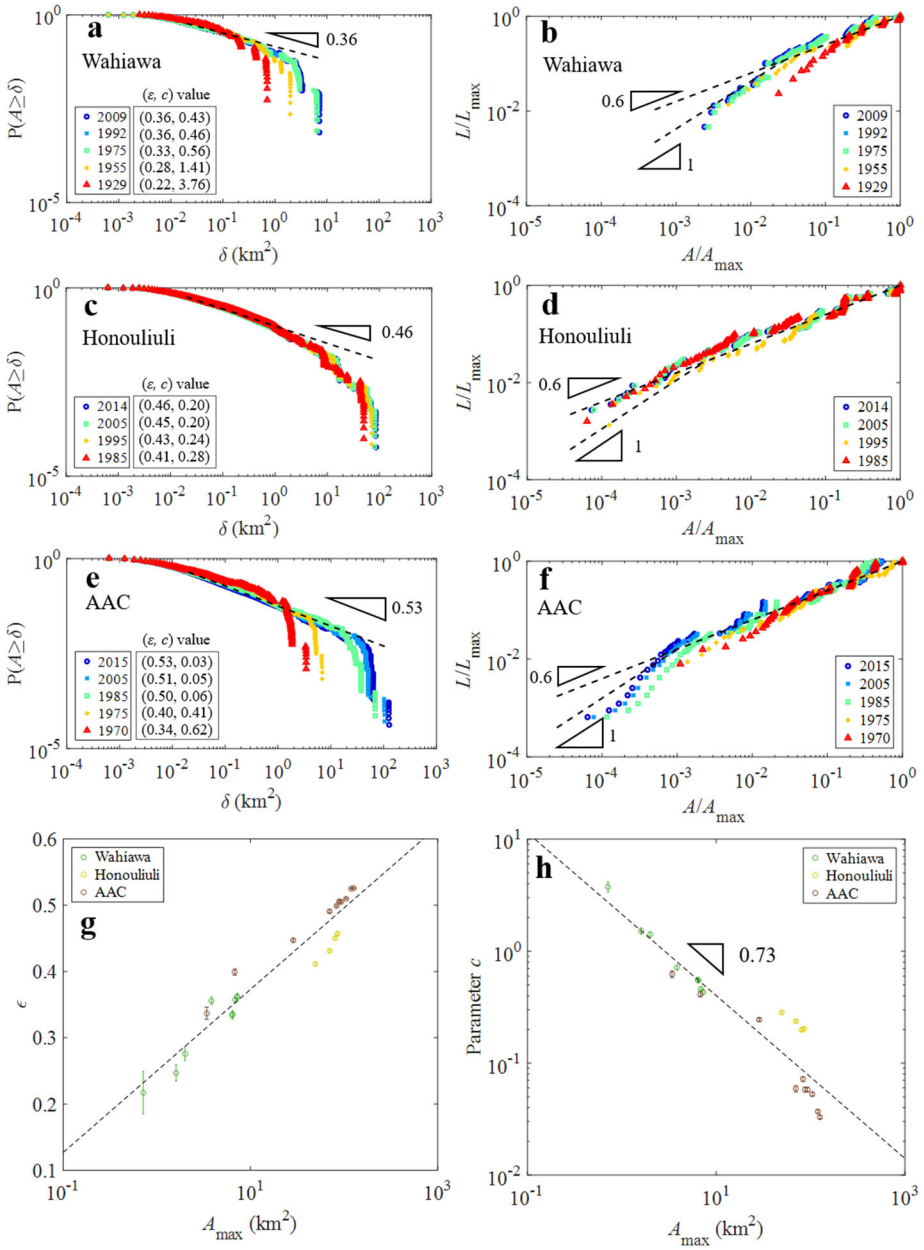

Figure 4.6 Scaling relationships of three evolving UDNs: Wahiawa (1929-2009); Honouliuli (1985-2014); and AAC (1970-2015). (a, c, e) Area-exceedance probability distribution plots. Black dashed lines represent the fitted straight power-law lines with each ε of the most recent UDNs. (b, d, f) Power-law relationship between normalized length (L/L_{max}, where L_{max} is a maximum length of main sewer line in each year) - normalized area (A/A_{max}). The two dashed black lines are shown as the "ideal slope" (linearity h=1 and Hack's law exponent h=0.6) for comparison. (g) Trend of the exponent ε in Eq. (3.2) over varying maximum sewer-shed drainage area (black dashed line is fitted as $\varepsilon = 0.053\ln A_{max}+0.25$). (h) Power-law relationship between the maximum sewer-shed drainage area and the exponential tempering parameter c (fitted power-law exponent -0.73 with standard error 0.13 for 95% confidence interval).

The long-term expansion of sewer networks occurs in an episodic fashion, with short periods of quick growth, either to accommodate anticipated growth in demand or to connect new neighborhoods with increasing population, or because of retrofitting catalyzed by technological advancements. Such spurts in UDN growth are largely reflected in the extension of trunks of the area exceedance plots and steps in tails (Figures 4.6a, c, e). In river networks, similar dynamic shifts have been shown to occur, but at rates orders-of-magnitude less frequent over geologic time scale, as revealed in stream piracy or migration of drainage divides (Bonnet, 2009; Willett et al., 2014) resulting from tectonic activities or non-stationary climate forcing. UDN expansion can also involve pipe networks crossing topographic watershed divides of naturally drained catchments.

As the population of a city grows, drainage density tends to increase in a given area of a city. Figure 4.7a shows an example of growing UDN sub-nets within a 53 km^2 boundary area of AAC. The growing UDN within the bounded region shows well-collapsed $P(A \geq \delta)$ curves (Figure 4.7b). The repeated analysis for a total of four sub-networks in AAC (the other three shown in Figure 4.8a) shows similar evolving patterns, with elongation of the trunk and more abrupt truncation over time (Figures 4.8b, c, d). Increasing drainage density with population pressure (increasing sanitary sewer discharge) is also analogous with a river basin where the drainage density tends to increase with increasing precipitation (wetter climate) (Wang & Wu, 2013).

The total length of pipes within each clipped area of the UDN increases rapidly during the initial decade or two, representing the period of expansion, followed by much slower increase over the next decades (Figure 4.7c), consistent with empirical analyses of city growth (Gudmundsson & Mohajeri, 2013; Mohajeri et al., 2015). Exponential tempering of $P(A \geq \delta)$ diminishes as the sub-networks grow within the clipped area, with c decreasing inversely with increasing total pipe length (Figure 4.7d). Thus, c is a measure of the stages of expansion and densification. The rate at which c decreases varies among different subnets in the city (drainage areas ranging from 7 to 46 km^2), revealing the heterogeneity of UDN growth processes within subnets of AAC.

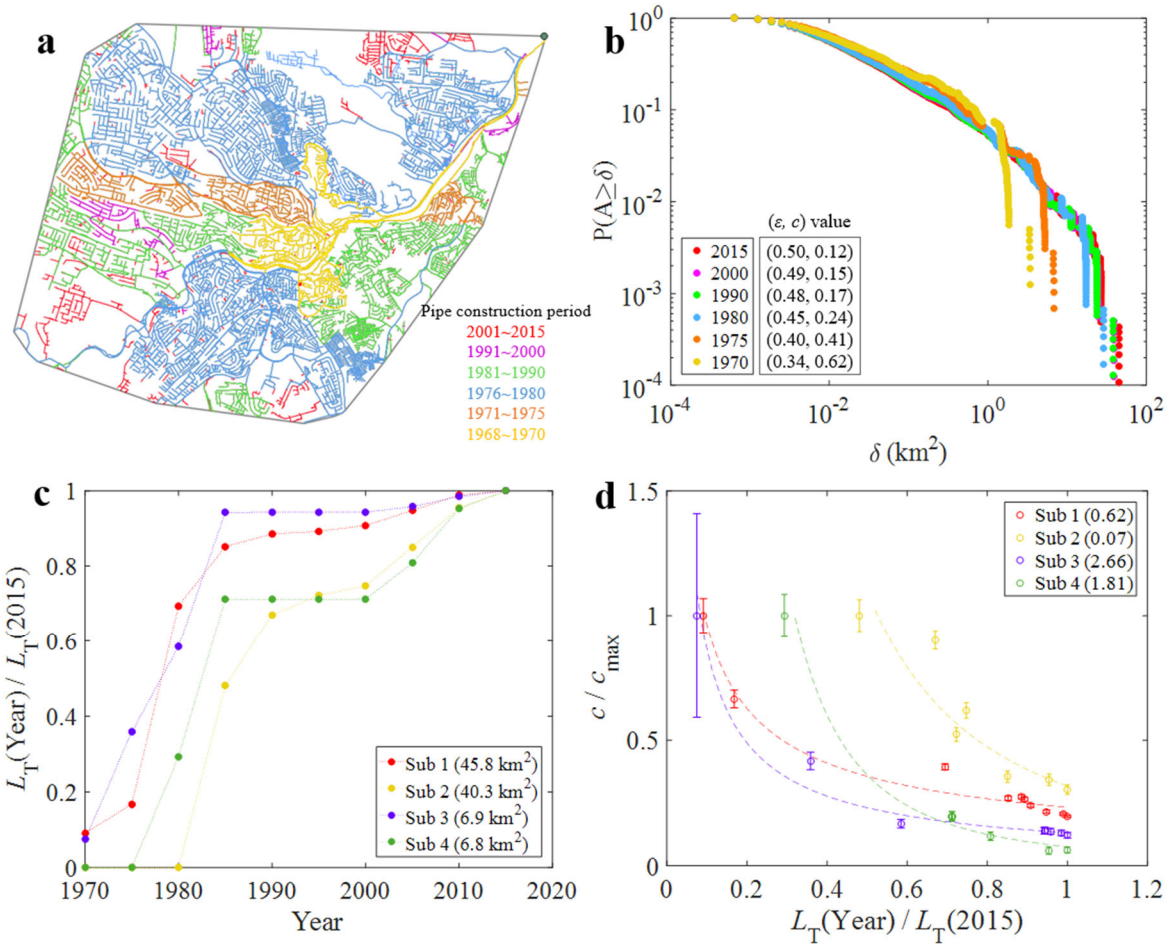

Figure 4.7 Evolution of sub-networks in AAC. (a) Map of the sub-network 1, which is within a clipped area (53 km^2) of AAC. (b) Area-exceedance probability distribution of growing pipe networks shown in Figure 4.7a. (c) Growing total pipe length over time. Total pipe length in a certain year L_T (Year) is normalized by the longest total pipe length in the latest L_T(2015). Numbers inside the parentheses in the legend are the maximum drainage area in 2015. Sub 1 indicates the sub-network shown in Figure 4.7a. Other sub-networks are shown in Figure 4.8a. (d) Variation of exponential tempering parameter c, normalized to the maximum c value at the earliest time c_{max}. Numbers inside the parentheses in the legend are c_{max} values. 95% confidence intervals are also shown as the bars.

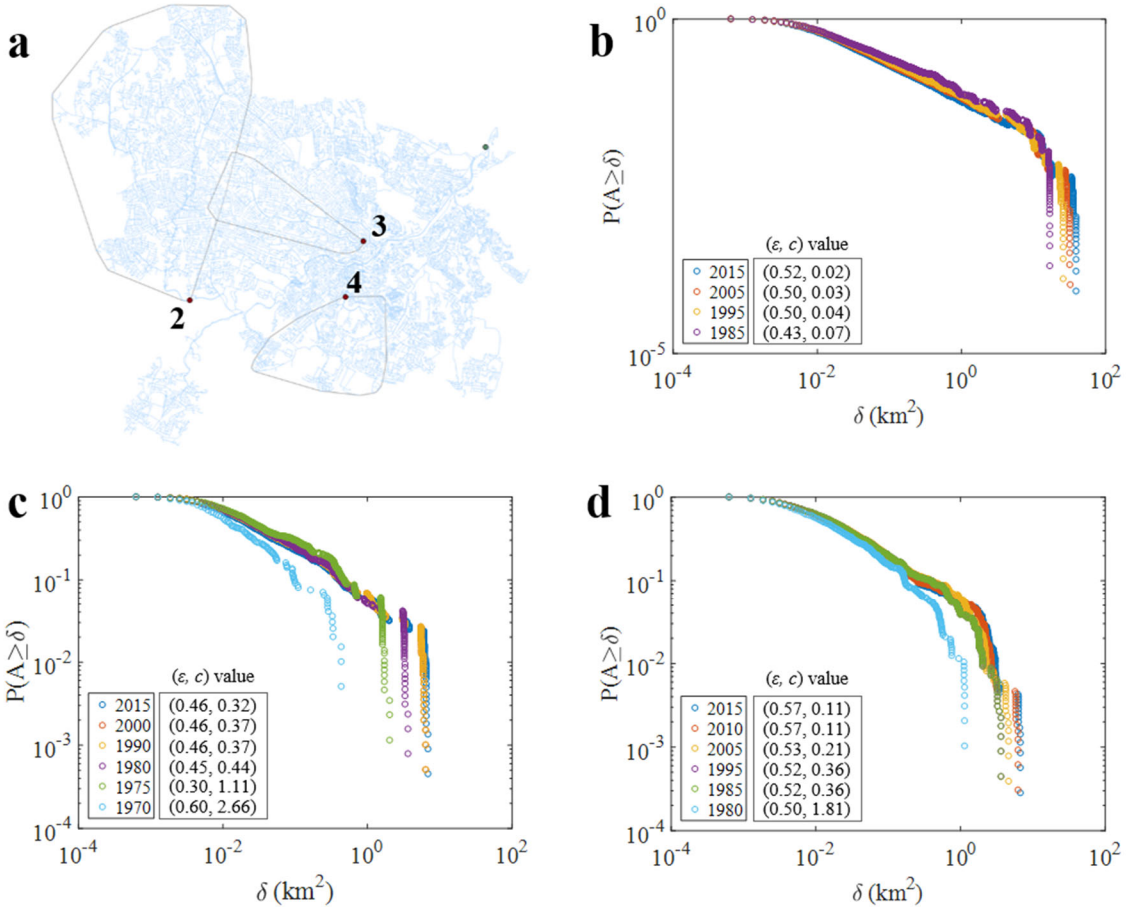

Figure 4.8 Map of subnet 2, 3, and 4 in AAC and their area-exceedance probability distributions. (a) Light blue lines represent the latest UDN layout. Grey lines display boundaries of subnets (subnet numbers are printed next to outlets marked as brown dots). The boundary lines were extracted using *Convexhull* function in Qgis (http://www.qgis.org/en/site/); (b, c, d) Area-exceedance probability distributions of the subnets 2, 3, and 4 over time, respectively. Evolving values of ε and c in Eq. (3.2) are shown.

5. SCALING AND SPATIAL ORGANIZATION OF THE CNHE SYSTEMS

The contents of this section are mainly based on the results & discussions sections of following published paper: Soohyun Yang, Olaf Buettner, James W. Jawitz, Rohini Kumar, P. Suresh C. Rao, and Dietrich Borchardt, (2019). Spatial organization of human population and wastewater treatment plants in urbanized river basins. *Water Resources Research.*

5.1 River network and human population

5.1.1 Scaling in hierarchical structures

Horton scaling ratios for stream number, length, drainage area, and eigen-area for the Weser, Elbe, and Rhine River networks were within the reported range from global river networks analyses (Table 5.1), although the analyzed drainage areas for the Elbe and Rhine were only within Germany. This result is consistent with universal scale-invariance of river network structures.

Mean population in a given eigen-area increased at a consistent rate over H-S orders in the three river basins, with $R_{POP} = 2.1 \pm 0.2$ (Figure 5.1; Table 5.1), suggesting similar hierarchical scale-invariance of POP distribution in the three river basins. In addition, POP distributions similarly indicate weak or neutral preference for settlements in eigen-areas of higher H-S orders (γ= 1.10 for Weser; 1.05 for Elbe; and 1.12 for Rhine, Table 5.1). These results are consistent with Fang et al. (2018), who also found mostly neutral preference for settlement by stream orders in the global basins they examined.

Table 5.1 Metrics used for hierarchical structure (Horton scaling ratios and scaling indices)

	Metrics	River basin		
		Weser	**Elbe**	**Rhine**
Fraction of non-sanitary flows contribution	$\Theta = \frac{\text{Total PE - Total POP}}{\text{Total PE}}$	0.3	0.1	0.3
Hierarchical structure	R_B	3.4	3.7	3.8
	R_L	1.8	2.0	2.1
	R_A	3.7	4.0	4.0
	R_E	1.7	2.0	2.0
	R_{POP}	1.9	2.1	2.3
	R_{PE}	3.1	2.6	3.3
	R_{WWTP}	1.7	2.0	1.8
	$\gamma (= R_{POP}/R_E)$	1.10	1.05	1.12
	$\varepsilon (= R_{PE}/R_{POP})$	1.63	1.23	1.46
	$\delta (= R_{PE}R_{WWTP}/R_B)$	1.59	1.35	1.54

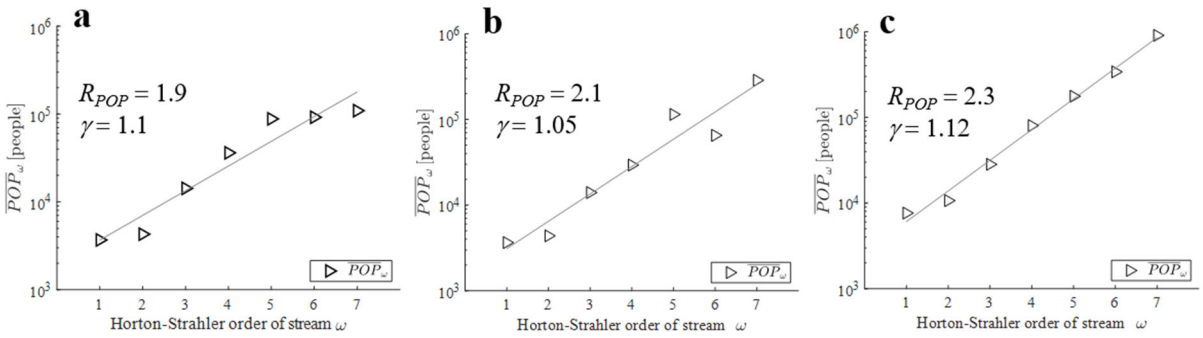

Figure 5.1 (a-c) For Weser, Elbe, and Rhine River basins, variations of the mean population living in eigen-area (triangle) across H-S stream orders ω on a semi-log scale. Values of the population ratio (R_{POP}) and scaling index $\gamma (= R_{POP} / R_E)$ indicating the preferred settlement eigen-area are inset.

5.1.2 Longitudinal distribution patterns

Along longitudinal flow directions, population patterns in the three river basins were similar, with weak downstream clustering (Ψ_{POP} = 0.84 to 0.92 in Table 5.2). Nevertheless, the patterns of urban zones in each of POP-WFs (with similar dx_{POP} values of 8.3-8.6 km) were heterogeneous among the three river basins, manifesting different number, size, and location of cities in each river basins (gray-shaded regions in Figure 5.2). The heterogeneous distribution patterns of urban zones among river basins depend on the long-term political and historical legacy in Germany. For example, in the Holy Roman Empire, hundreds of politically independent territorial states were governed by each of the medieval lords, related to the locations of modern cities (Johnson, 2002).

Estimated values of β^G (1.8 - 1.9) ($R^2 > 0.95$, $p < 0.05$) were within the reported range from natural rivers (Marani et al., 1994; Fang et al., 2018), revealing again the consistency in scale-invariance of river network structures (Table 5.2). The degree of population clustering, β^{POP} ($R^2 >$ 0.90, $p < 0.05$), was not significantly greater than β^G ($p < 0.05$) for the three river basins, consistent with the lack of large cities (> 5M inhabitants) in these basins, and a smaller percentage of the population living in cities of >500K inhabitants (about 17%) compared to the global average (about 28%) (United Nations, 2016).

Table 5.2 Metrics used longitudinal patterns along flow path (directionality of clustering and power-law exponent from power spectral analysis with standard error (SE) estimated from the 95% confidence interval)

	Metrics	River basin		
		Weser	**Elbe**	**Rhine**
Longitudinal patterns along flow path	Ψ_{POP}	0.91	0.92	0.84
	$\Psi_{PE(1)}$	0.76	0.73	0.63
	$\Psi_{PE(2)}$	0.71	0.73	0.55
	$\Psi_{PE(3)}$	0.46	0.67	0.60
	$\Psi_{PE(4)}$	0.40	0.66	0.46
	$\Psi_{PE(5)}$	0.30	0.54	0.22
	$\beta^{G} \pm$SE	1.90 ± 0.03	1.90 ± 0.04	1.80 ± 0.05
	$\beta^{POP} \pm$SE	1.50 ± 0.14	1.60 ± 0.12	1.70 ± 0.14
	$\beta_{k=1}^{PE} \pm$SE	1.24 ± 0.21 [a]	1.44 ± 0.12 [c]	1.05 ± 0.16 [f]
	$\beta_{k=2}^{PE} \pm$SE	1.04 ± 0.16 [a]	1.29 ± 0.11 [c]	0.73 ± 0.19 [f]
	$\beta_{k=3}^{PE} \pm$SE	0.74 ± 0.14 [a]	0.58 ± 0.21 [d]	0.71 ± 0.16 [f]
	$\beta_{k=4}^{PE} \pm$SE	0.98 ± 0.21 [a,]	0.83 ± 0.20 [d]	0.84 ± 0.22 [f]
	$\beta_{k=5}^{PE} \pm$SE	0.23 ± 0.19 [b]	0.18 ± 0.12 [e]	0.64 ± 0.15 [f]

Note. Superscripts a ~ f : For each river basin, individual alphabets characterize a group with statistically significant difference from others at the 95% confidence level (Knezevic, 2008).

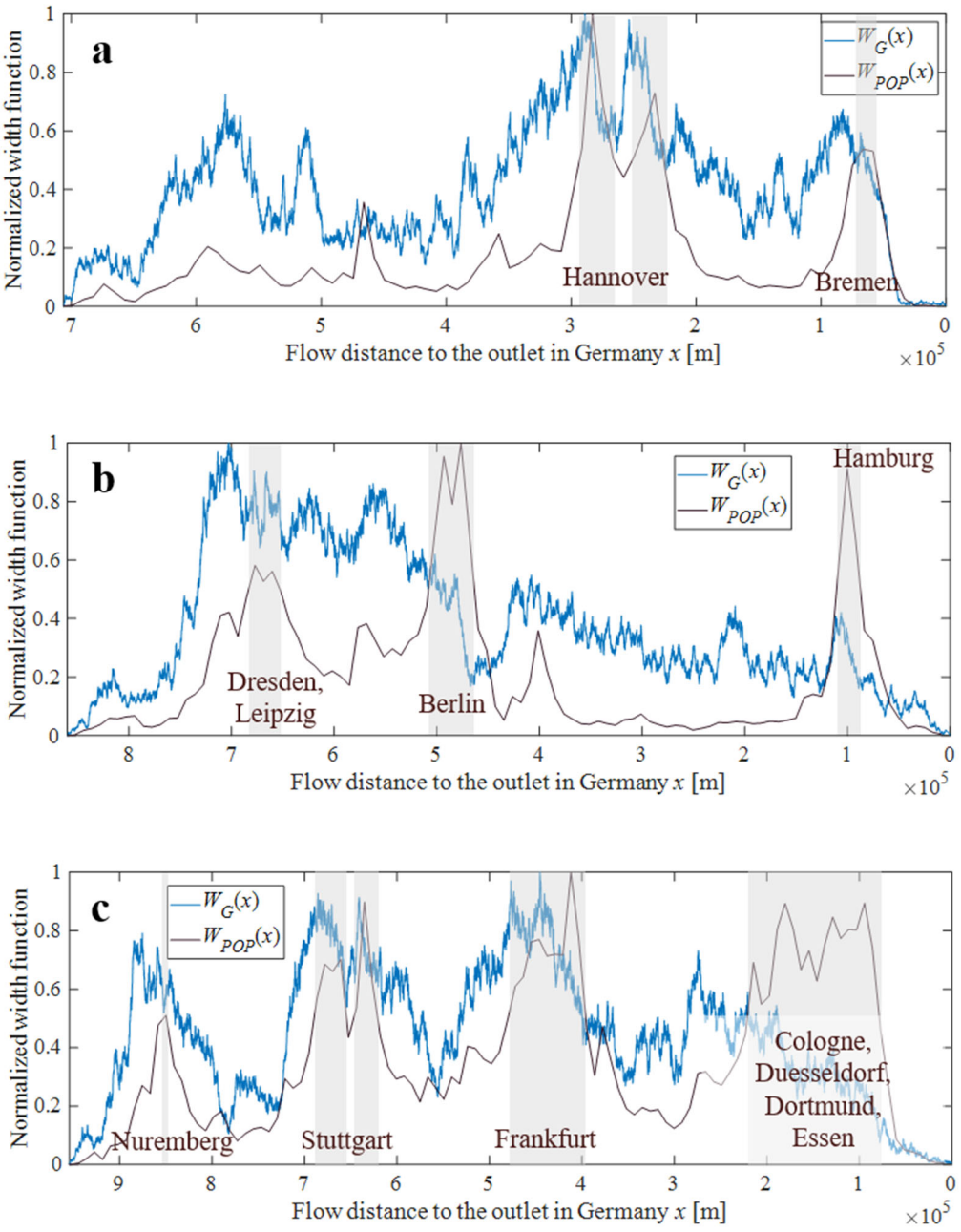

Figure 5.2 (a-c) For Weser, Elbe, and Rhine River basins, the geomorphological width functions (G-WF, $W_G(x)$) with dx_G = 100 m (blue line) and the population width functions (POP-WF, $W_{POP}(x)$) with dx_{POP} = 8.3 km for Weser; 8.4 km for Elbe; and 8.6 km for Rhine (black line). Variables on y-axes were normalized by the maximum value of each dataset. The x-axis indicates hydrological flow distance from the outlet in Germany. Note that the flow direction from the left to the right-hand side is toward the outlet in Germany. Names of German cities (with more than 500K inhabitants) in each river basin are given at their corresponding location points along hydrological flow paths. Gray-shaded regions show urban zones where the each POP-WF is above a threshold of 0.5.

5.2 PE and WWTPs

5.2.1 Scaling in hierarchical structures

PE spatial patterns in the three river basins followed Horton scaling (Figure 5.3), indicating scale-invariance of the aggregated POP through sewer networks over H-S orders. In addition, I found similar values of R_{PE} for the three basins (3.0±0.3, Table 5.1), suggesting consistent basis for POP aggregation as PE served by WWTPs. Non-sanitary wastewaters accounted for 10-30 % of total wastewater within the three river basins (Θ in Table 5.1). The scaling index ε suggested that for all three German basins, more non-sanitary wastewater is collected and treated at WWTPs discharging to higher H-S orders (1.63 for Weser; 1.23 for Elbe; and 1.46 for Rhine, Table 5.1).

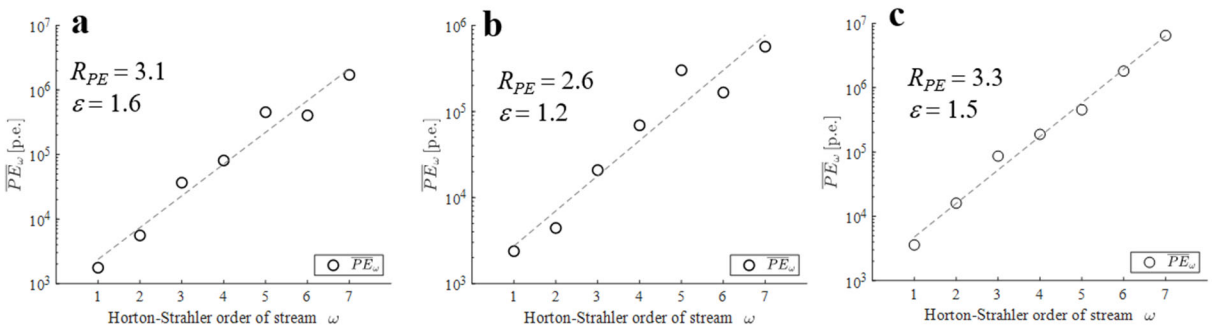

Figure 5.3 (a) For Weser, (b)Elbe, and (c)Rhine River basins, variations of the mean PE served by WWTPs discharging across H-S stream orders ω on a semi-log scale. Values of the PE ratio (R_{PE}) and ε (= R_{PE} / R_{POP}) indicating the contribution of non-sanitary inflows to wastewater collected into a WWTP are inserted.

The total number of WWTPs decreased exponentially with H-S order in all the three basins (Figure 5.4), resulting in similar values of R_{WWTP} = 1.8±0.1 (Table 5.1). These findings support the hypothesis of scale-invariance of WWTPs distribution when not categorizing by class-sizes. Given the five class-sizes of WWTPs based on PE ranges, I found that for all three basins, WWTP locations were highly centralized as H-S order increased (with δ = 1.59 for Weser; 1.35 for Elbe; 1.54 for Rhine, Table 5.1), indicating that a smaller number of WWTPs but with higher class-size were located in eigen-areas of higher H-S orders. The lower δ value for the Elbe basin captures the higher proportion of class-1 WWTPs and smaller fraction of class-5 WWTPs over 5^{th} ~ 7^{th} stream orders in the Elbe than either the Weser or the Rhine basins (Table 5.3)

.

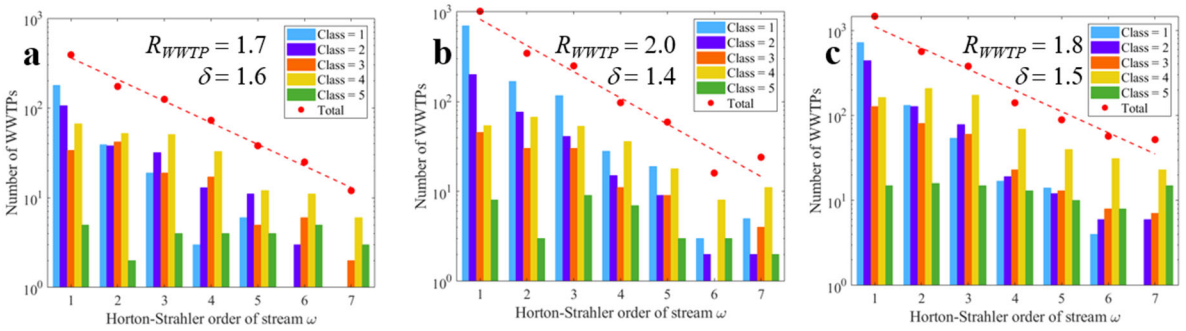

Figure 5.4 (a) For Weser, (b) Elbe, and (c) Rhine River basins, variations of the total number of WWTPs discharging to streams of a given stream order (red circle) across H-S stream orders ω on a semi-log scale. Bars represent the number of WWTPs by class-size. Values of the WWTP ratio (R_{WWTP}) and a scaling index of δ (=$R_{PE}R_{WWTP}$ / R_B) indicating the degree of centralization in WWTPs locations are inserted

Table 5.3 Percent (%) of the number of wastewater treatment plants (WWTPs) for each class-size over stream orders

River basin	WWTP class-size	Stream order (ω)						
		ω = 1	ω = 2	ω = 3	ω = 4	ω = 5	ω = 6	ω = 7
Weser	1	46	23	15	4	16	0	0
	2	27	22	26	19	29	12	8
	3	9	24	15	24	13	24	17
	4	17	30	41	47	32	44	50
	5	1	1	3	6	11	20	25
Elbe	1	69	49	47	29	**33**	**19**	**21**
	2	20	22	16	15	16	13	8
	3	4	9	12	11	16	0	17
	4	5	19	21	37	31	50	46
	5	1	1	4	7	**5**	**19**	**8**
Rhine	1	49	23	14	12	16	7	2
	2	30	23	21	13	13	11	12
	3	9	14	16	16	15	14	13
	4	11	37	46	49	45	54	44
	5	1	3	4	9	11	14	29

5.2.2 Longitudinal distribution patterns

Patterns of PE-WFs with all WWTP class-sizes in the three river basins were mostly equivalent with those of POP-WFs (e.g., compare Figure 5.2a with Figure 5.5a for Weser). On the other hand, the patterns of class-merged PE-WFs were generally the inverse longitudinal distributions of the number of WWTPs (see upper and lower panels in Figures 5.5a, 5.6a, and 5.7a). This suggests the need for differentiating among the five class-sizes of WWTPs. Larger urban zones were served by higher class-sizes (k = 4 and 5) WWTPs which deploy mandatory tertiary treatment technologies (EEC, 1991) (Figures 5.5e-f, 5.6e-f, and 5.7e-f). In contrast, smaller communities were served by lower class-size (k = 1 to 3) WWTPs deploying primary and secondary treatment (combination of physical and biological technologies) (EEC, 1991) (Figures 5.5b-d, 5.6b-d, and 5.7b-d). Given no regulatory requirements for nutrient loads discharges by lower class-size WWTPs, the operators customize cost-effective combinations of primary and secondary treatment technologies.

These analyses showed that PE-clustering is downstream for higher WWTP class-sizes, while upstream for lower WWTP class-sizes (Figure 5.8). The metric $\Psi_{PE(k)}$ decreased as class-size k increased (Table 5.2). The Weser basin provided a representative example for PE-clustering for the five class-sizes (Figure 5.8a). On the other hand, the Elbe and Rhine basins showed less variability among the five class-sizes (Figures 5.8b-c), because of the exclusion of the other basin regions outside Germany. I anticipate that if WWTPs in the portions of the Elbe and Rhine basins outside Germany exhibit similar scale-invariance distributions to those in the German portion of the basins, Figures 5.8b and 5.8c will shift to become similar to Figure 5.8a, by adding WWTPs outside Germany. Demonstrating this argument for the whole of Elbe and Rhine basins will be the focus for future research.

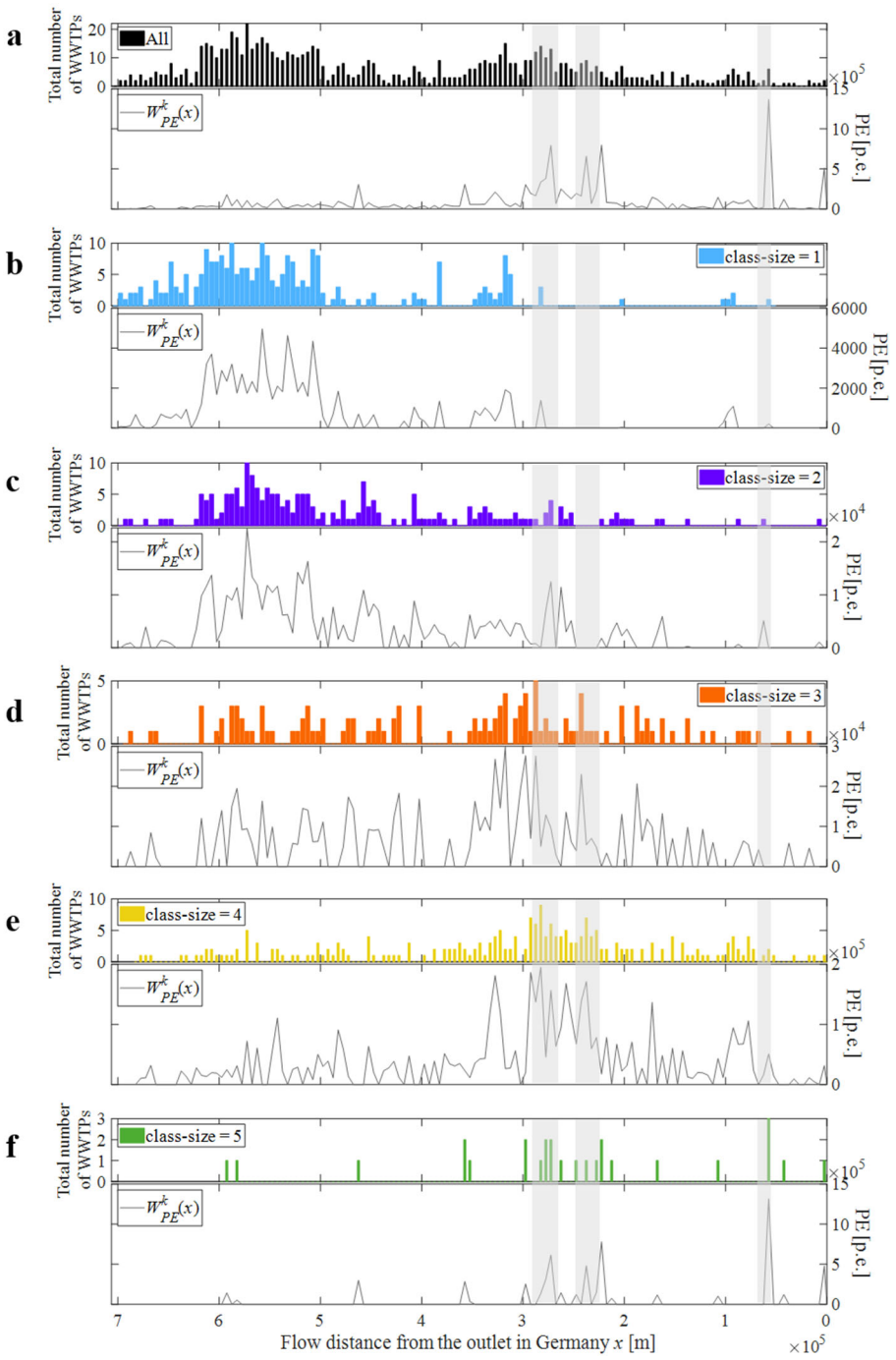

Figure 5.5 For Weser River basin, width functions for the number of WWTPs (upper panels) and for population equivalent (PE-WFs, $W_{PE}(x)$) (lower panels) for (a) all classes and for (b-f) each class-size k = 1-5 in sequence along hydrological flow distance from the outlet in Germany. Note that the flow direction from the left to the right-had side is toward the outlet in Germany. Gray-shaded regions show urban zones where the normalized width function for population (Figure 5.2a) is above a threshold of 0.5

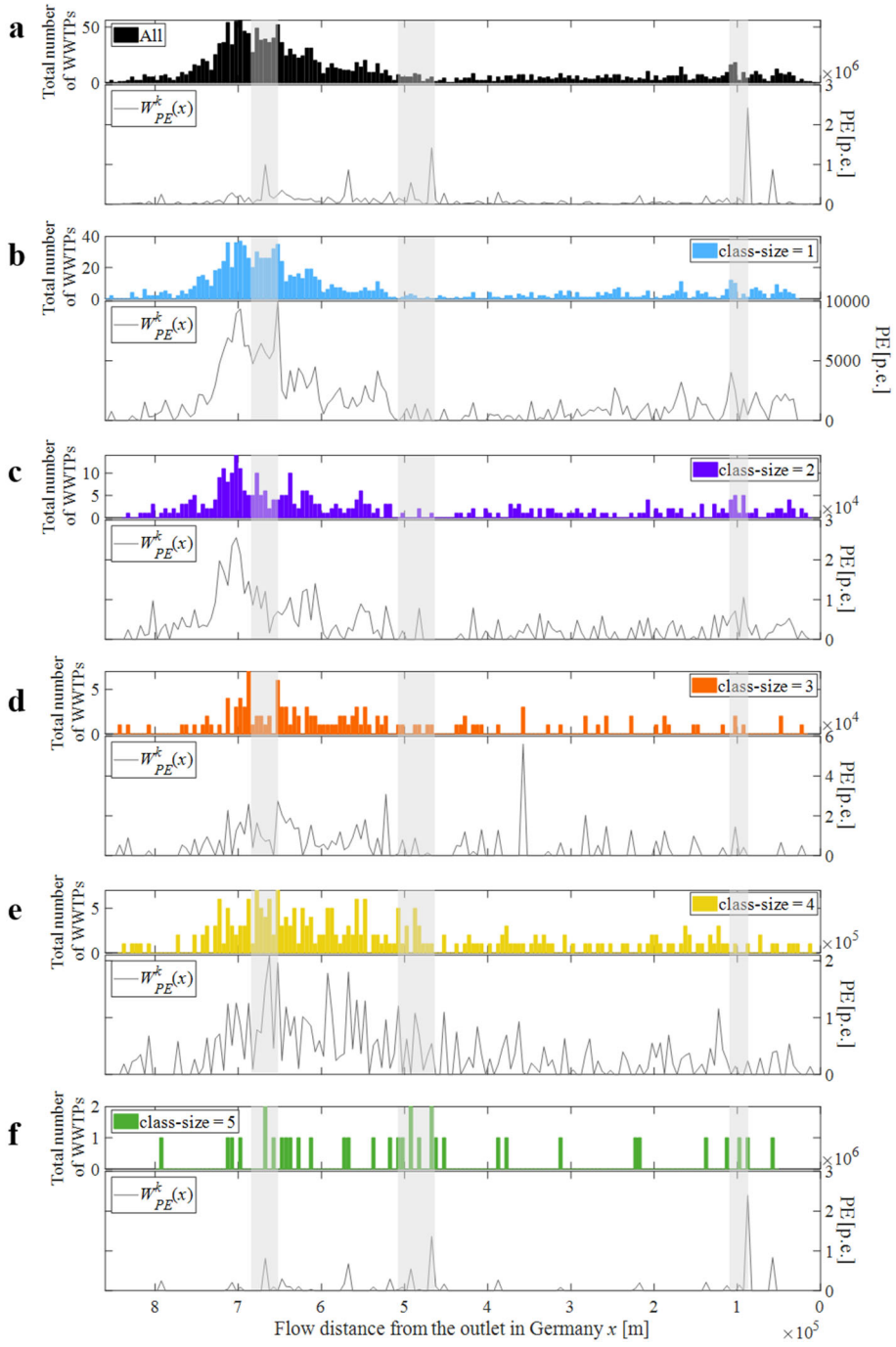

Figure 5.6 For Elbe River basin, width functions for the number of WWTPs (upper panels) and for population equivalent (PE-WFs, $W_{PE}(x)$) (lower panels) for (a) all classes and for (b-f) each class-size k = 1-5 in sequence along hydrological flow distance from the outlet in Germany. Note that the flow direction from the left to the right-had side is toward the outlet in Germany. Gray-shaded regions show urban zones where the normalized width function for population (Figure 5.2b) is above a threshold of 0.5

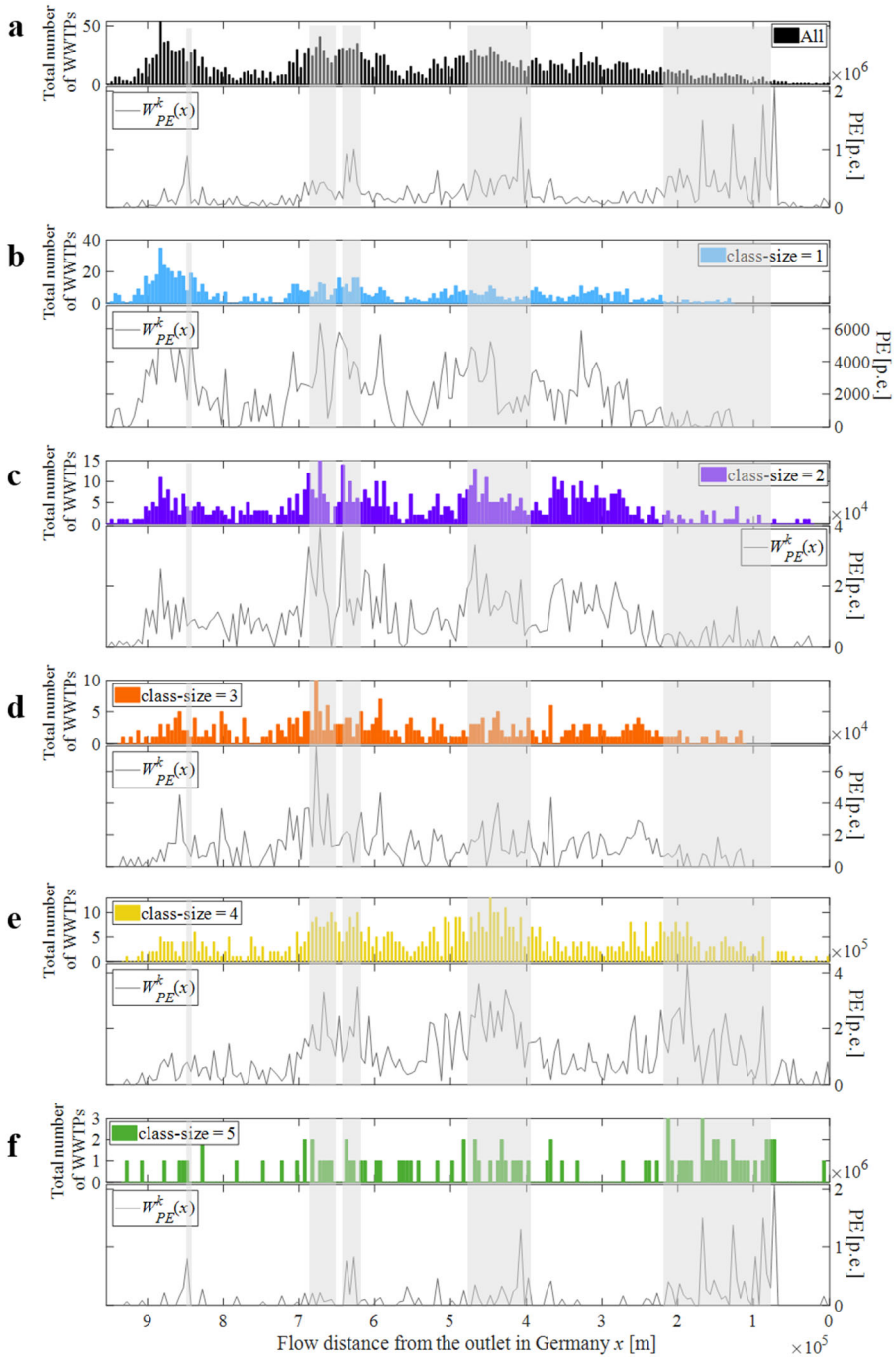

Figure 5.7 For Rhine River basin, width functions for the number of WWTPs (upper panels) and for population equivalent (PE-WFs, $W_{PE}(x)$) (lower panels) for (a) all classes and for (b-f) each class-size k = 1-5 in sequence along hydrological flow distance from the outlet in Germany. Note that the flow direction from the left to the right-had side is toward the outlet in Germany. Gray-shaded regions show urban zones where the normalized width function for population (Figure 5.2c) is above a threshold of 0.5

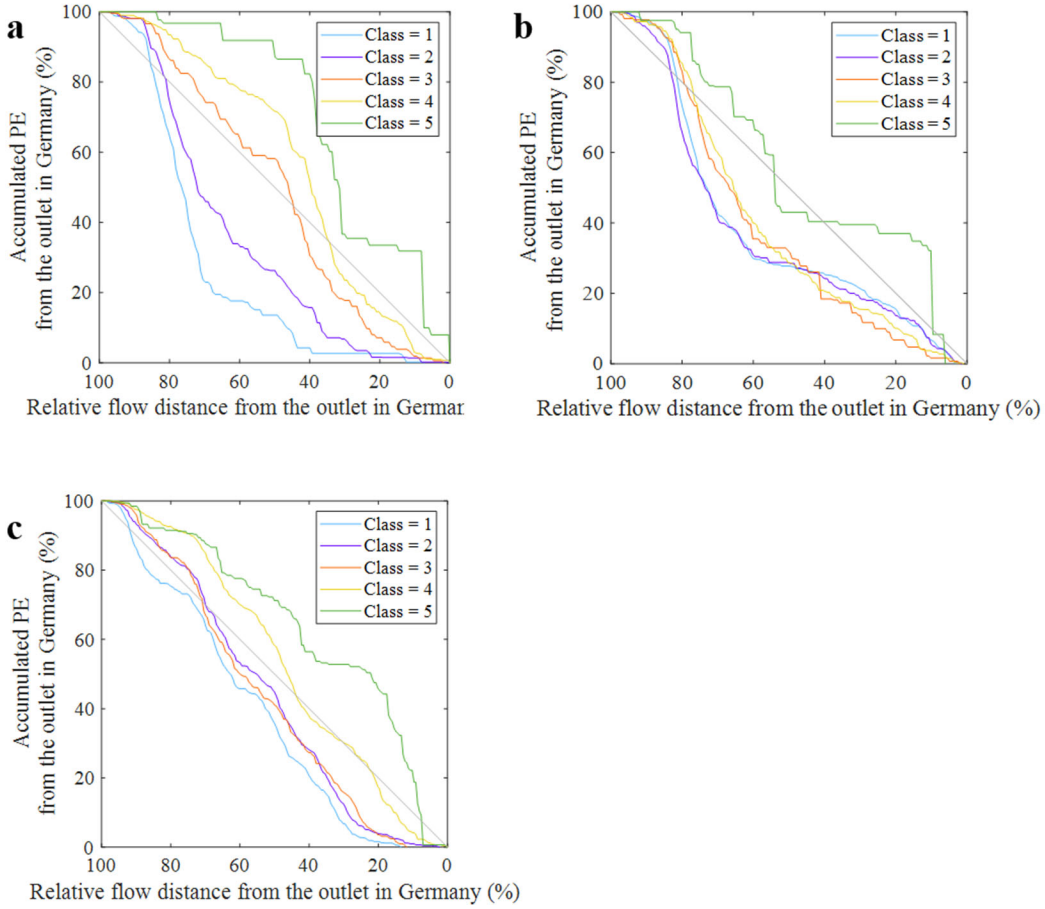

Figure 5.8 (a) For Weser, (b) Elbe, and (c) Rhine River basins, accumulated PE distribution from the basin outlet at a given relative flow distance from the outlet in Germany. Note that the flow direction from the left to the right-had side is toward the outlet in Germany. The five class-sizes of German WWTPs are marked as different colors.

All values of β_k^{PE} indicating the degree of spatial clustering for PE served by class-size k WWTPs were statistically significant at the 99% confidence level ($p < 0.01$), except $\beta_{k=5}^{PE}$ for the Weser and Elbe basins (Table 5.2, Figures 5.9 and 5.10). Significant similarity of the spatial auto-correlation for PE including the largest class-size for the Rhine basin depends on the intervals among populated areas along hydrological flow distances (Table 5.2 and Figure 5.11). Normalized mean separation distance between urban zones ($\bar{\tau}$) for the Rhine basin (0.12) was half of that for the Weser and Elbe basins (0.23 and 0.22), reflecting the larger number and greater sizes of more populated areas in the Rhine basin (Figure 5.2). When the populated areas are closer, the patterns

of WWTPs across the five class-sizes along hydrological flow distances are more similar (Figures 5.5-5.7), decreasing the differences in the degree of PE clustering among the five class-sizes. Therefore, the findings suggest that the degree of spatial clustering for PE served by each class-size reflects unique pattern for the size and location of populated areas in individual river basins. Under an adequate assumption for life-style and water-use of inhabitants, the distinct patterns for the nutrient loads discharged from WWTPs are predictable from those of PE-WFs for class-sizes. For assessing hydrological alteration and water-quality impairment from point-source pressures, I suggest a combined approach employing H-S order hierarchy and the longitudinal perspective, recognizing the key role of receiving river discharge in the evaluations (Ekka et al., 2006; Rice & Westerhoff, 2017).

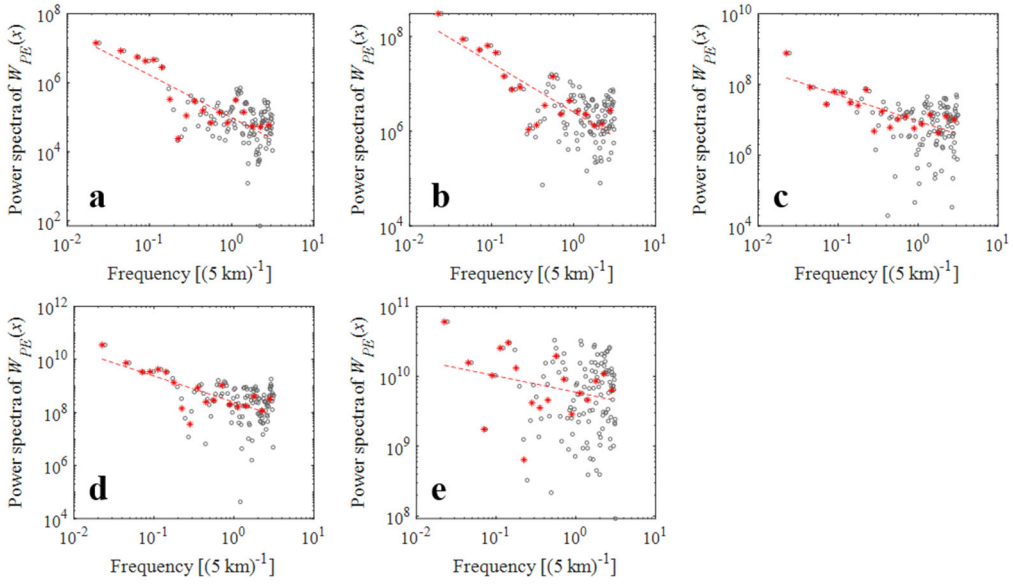

Figure 5.9 For Weser River basin, (a-e) Power spectra for the PE-WFs ($W_{PE}(x)$) on a log-log scale for each class-size k=1-5 in sequence. Red dashed lines identify the power law fitted lines estimated using log-binned data within 0.1 frequency interval (red asterisks) from the original data (gray dots). Significant level for each power law exponent is set as p<0.01 for k=1-4 and p<0.2 for k=5

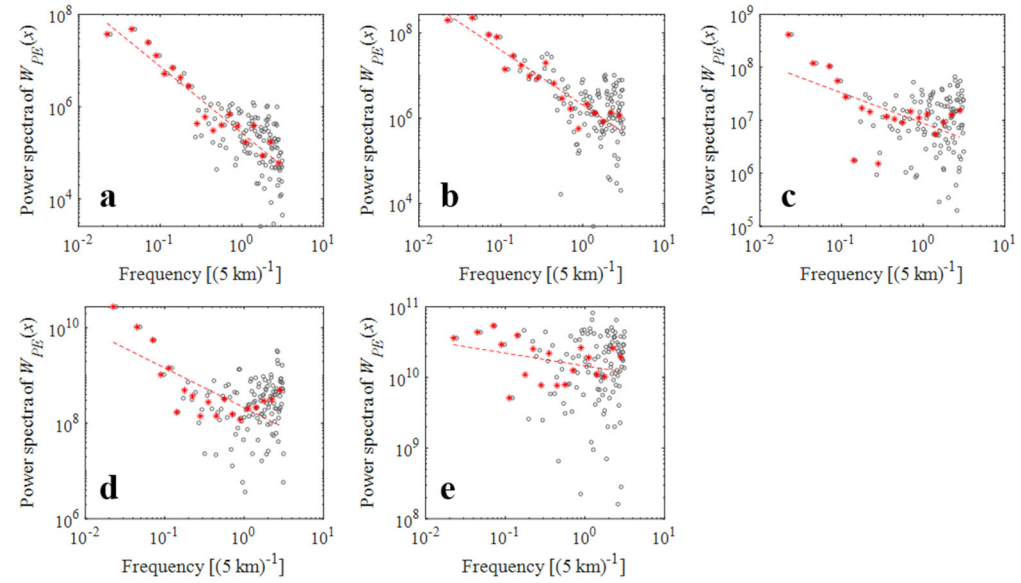

Figure 5.11 For Elbe River basin, (a-e) Power spectra for the PE-WFs ($W_{PE}(x)$) on a log-log scale for each class-size k=1-5 in sequence. Red dashed lines identify the power law fitted lines estimated using log-binned data within 0.1 frequency interval (red asterisks) from the original data (gray dots). Significant level for each power law exponent is set as p<0.01 for k=1-4 and p<0.2 for k=5

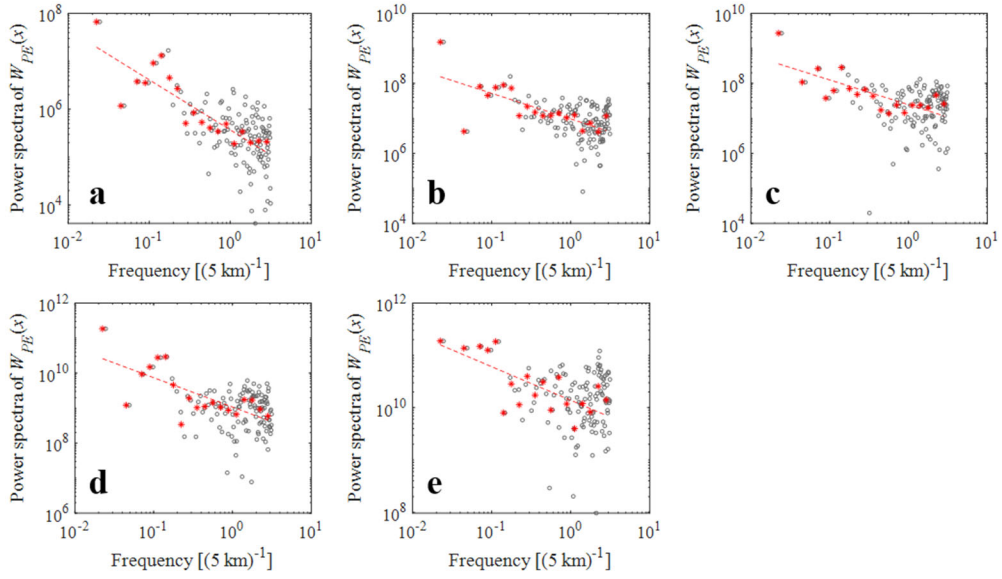

Figure 5.10 Rhine River basin, (a-e) Power spectra for the PE-WFs ($W_{PE}(x)$) on a log-log scale for each class-size k=1-5 in sequence. Red dashed lines identify the power law fitted lines estimated using log-binned data within 0.1 frequency interval (red asterisks) from the original data (gray dots). Significant level for each power law exponent is set as p <0.01 for all class-sizes

6. SPATIAL DISTRIBUTIONS OF POINT-SOURCE IMPACTS AT REACH-SCALE

The contents of this section are based on the results & discussions sections of following published paper: Soohyun Yang, Olaf Buettner, Rohini Kumar, Christoph Jaeger, James W. Jawitz, P. Suresh C. Rao, and Dietrich Borchardt, (2019). Spatial patterns of water quality impairments from point source nutrient loads in Germany's largest national River Basin (Weser River). *Science of the Total Environment.*

6.1 River discharge simulated and WWTP discharge reported

Across the Weser River network, mean of both Q_{R50} and Q_{R90} ($\overline{Q}_{R50}$ and $\overline{Q}_{R90}$) scaled exponentially over seven stream orders, with a scaling exponent of 1.13 and 1.17 (for both, $p <$ 0.01 and $R^2 \sim 1$), respectively (Figure 6.1); these values are on the lower end of reported range (1.1 to 1.8) for drainage area ratios found from natural rivers (Schumm, 1956; Rodríguez-Iturbe & Rinaldo, 2001). For a given stream order, $\overline{Q}_{R50}$ increased about three orders of magnitude from 0.4 m^3/s (ω = 1) to 306 m^3/s (ω = 7) (Table 6.1). Values of $\overline{Q}_{R90}$ were ~2.5 times smaller than $\overline{Q}_{R50}$, on average, over seven stream orders (standard deviation; std, 0.22), and the ratio of $\overline{Q}_{R50}/\overline{Q}_{R90}$ decreased monotonically with increasing stream order (Table 6.1).

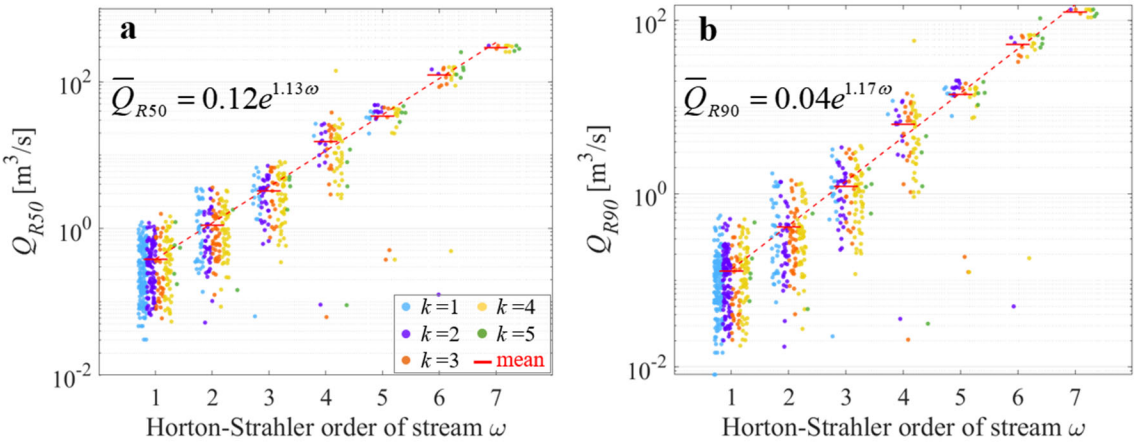

Figure 6.1 Spatial patterns over stream orders for (a) median flow Q_{R50} and (b) base-flow Q_{R90} (both are simulated using mHM). The five class-sizes (k=1-5) of German WWTPs are marked as different colors. Red dashed lines are fitted exponential lines (for both (a) and (b), $p < 0.01$ and $R^2 = 0.99$).

Table 6.1 For Q_{R50} and Q_{R90} [m^3/s], key statistics over stream orders (ω). Values in the parenthesis for ω = 4 were estimated by excluding exceptionally deviated results of the mHM simulation.

H-S order (ω)	Number of data	Median flow condition (Q_{R50} [m^3/s])			Low-flow condition (Q_{R90} [m^3/s])		
		Statistics			Statistics		
		Median [m^3/s]	Mean [m^3/s]	CV	Median [m^3/s]	Mean [m^3/s]	CV
1	401	0.3	0.4	0.8	0.1	0.1	0.8
2	175	0.8	1.1	0.8	0.3	0.4	0.9
3	125	3.0	3.2	0.6	1.1	1.2	0.7
4	69	12.1 (12.7)	15.3 (14.1)	1.1 (0.6)	5.0 (5.9)	6.3 (5.8)	1.2 (0.6)
5	38	38.0	34.0	0.4	15.3	14.0	0.4
6	25	128.2	123.9	0.4	55.1	53.2	0.4
7	12	306.0	291.8	0.1	132.3	125.7	0.1

*Note that five hydrographs deviated from the others (three for ω = 5; two for ω = 6, about 8% of total WWTPs in each H-S order) were excluded for the mean CV_{Q^*} calculation.

Mean WWTP discharge ($\overline{Q}_U$) also scaled exponentially (Figure 6.2) from 0.009 to 0.21 m^3/s with stream order, with a scaling exponent of 0.46 ($p < 0.01$, $R^2 = 0.87$). High CV values for Q_U for all stream orders resulted from the variability of PE among and across different five class-sizes for each given order. (Table 6.2). Given the variability in Q_R and Q_U, combination of class-size (k) and stream order (ω) determines the variability in Urban Wastewater Discharge Fraction (Φ) (see Section 6.3), which in turn is reflected in estimated reach-scale nutrient concentrations (see Section 6.4.1).

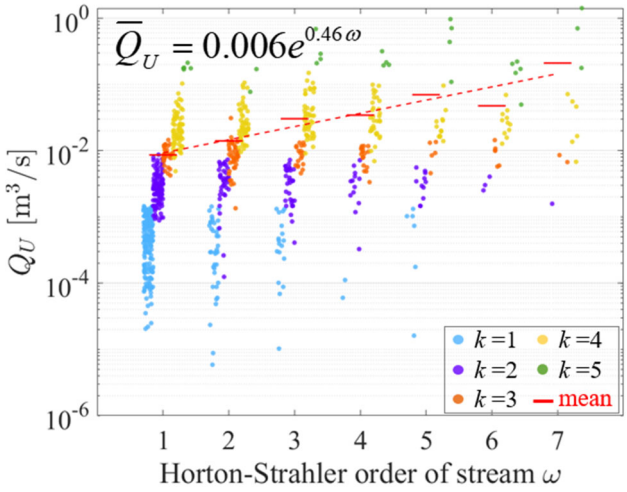

Figure 6.2 Spatial patterns over stream orders for steady-state discharge of treated wastewater from WWTPs Q_U. The five class-sizes (k=1~5) of German WWTPs are marked as different colors. Red dashed lines are fitted exponential lines ($p < 0.01$ and $R^2 = 0.87$).

Table 6.2 For Q_U [m^3/s], key statistics over Horton-Strahler (H-S) stream orders.

H-S order (ω)	**Number of data**	**Statistics**		
		Median [m^3/s]	Mean [m^3/s]	CV
1	386	$1.6\text{x}10^{-3}$	$8.6\text{x}10^{-3}$	2.7
2	172	$6.8\text{x}10^{-3}$	$1.4\text{x}10^{-2}$	1.6
3	123	$9.9\text{x}10^{-3}$	$3.1\text{x}10^{-2}$	2.4
4	69	$1.2\text{x}10^{-2}$	$3.5\text{x}10^{-2}$	1.6
5	38	$8.9\text{x}10^{-3}$	$7.0\text{x}10^{-2}$	2.9
6	25	$2.1\text{x}10^{-2}$	$4.8\text{x}10^{-2}$	1.4
7	12	$3.2\text{x}10^{-2}$	$2.1\text{x}10^{-1}$	2.0

6.2 Point-source pressure

Total N and P loads from all 845 WWTPs in the Weser basin were: 8.6×10^6 kg N/yr and 9.6×10^5 kg P/yr. Mean N and P loads also scaled exponentially with stream order (Figures 6.3a-b), with scaling exponents of 0.37 ($p < 0.01$, $R^2 = 0.87$) for N and 0.26 ($p < 0.01$, $R^2 = 0.84$) for P. Regular patterns in variabilities of N and P loads over stream orders were not evident (Table 6.3), but with a highly consistent pattern in CV of Q_U, which expected from the scaling between Q_U and nutrient loads (Figure 6.4).

Mean molar ratio of N/P estimated from WWTPs nutrient loads was ~16 ($\omega = 1$~5), then increased to ~32 ($\omega = 7$) (Figure 6.3c; Table 6.3). The lower mean N/P value was around the threshold to assess N-limitation (N/P molar ratio = 15); whereas the highest mean N/P value was close to the threshold to evaluate P-limitation (N/P molar ratio = 33) (McDowell et al., 2009). This finding indicates that WWTPs in $\omega \leq 5$ removed less P compared to those in $\omega \geq 6$. Indeed, >50% of WWTPs discharging to $\omega \leq 5$ consisted of lower class-sizes ($k \leq 3$) (Figure 6.3d), which deployed, at best, secondary treatment (physical and biological technologies) with no statutory regulations for P removal (EEC, 1991; DWA, 2018). On the other hand, >60% of WWTPs in $\omega \geq 6$ were larger WWTPs ($k \geq 4$) deploying the tertiary treatment technologies targeting P removal (more stringent for higher k) (EEC, 1991). Thus, the higher N/P values for larger streams ($\omega \geq 6$) reflect the combination of a larger portion of WWTPs with $k \geq 4$ and the use of advanced treatment technologies for P removal.

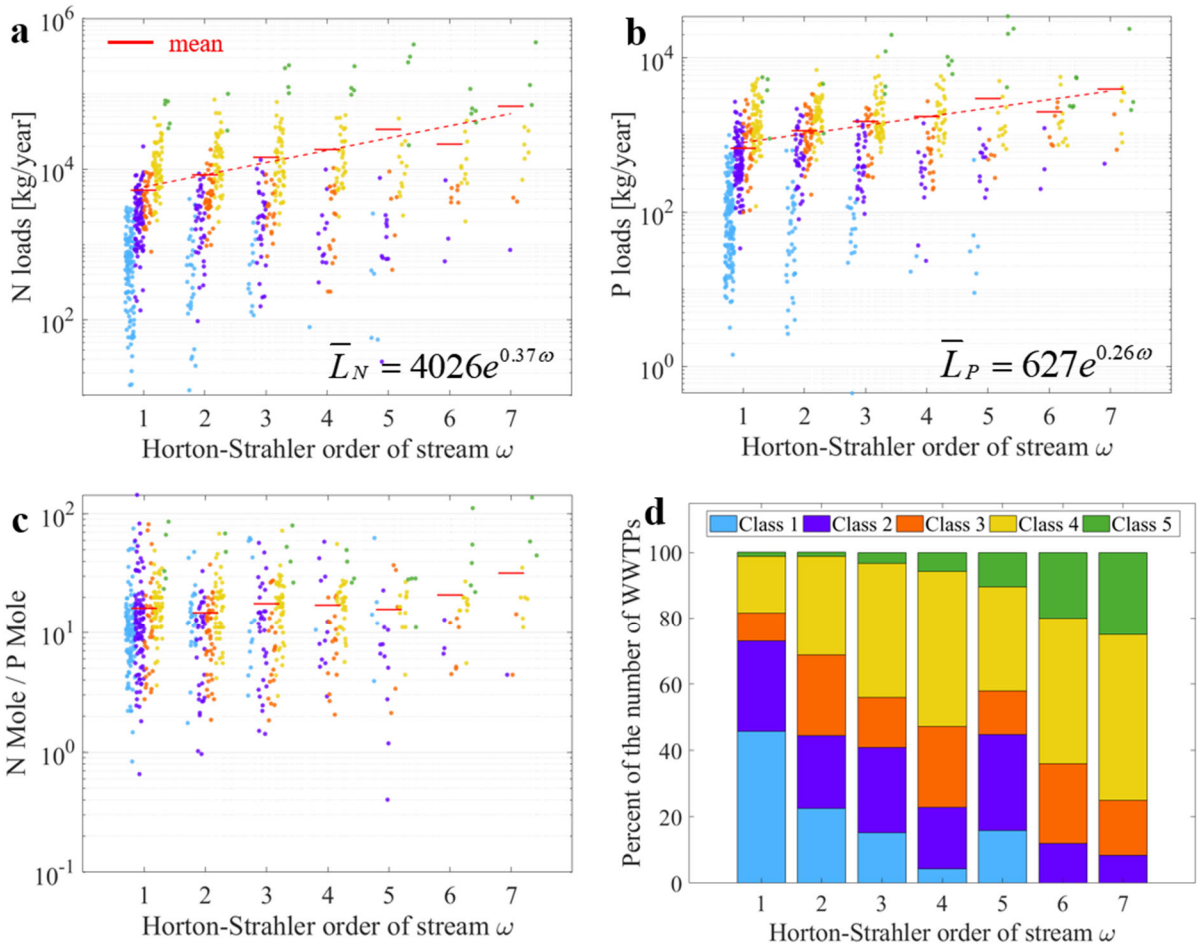

Figure 6.3 Spatial patterns over H-S orders in the Weser River for (a-b) N and P loads [kg/yr] discharged from all WWTPs, and (c) molar ratio of N/P. (d) Relative portion of the number of WWTPs depending on each class-size for a given H-S order. Mean values in (a-c) are given as red bars. Red dashed lines in (a) and (b) are linear fitting lines on a semi-log paper (p<0.01, $0.84 \leq R^2 \leq 0.87$). The five class-sizes of German WWTPs are marked as different colors (light-blue, purple, orange, yellow, and light-green for class 1 to 5, in sequence).

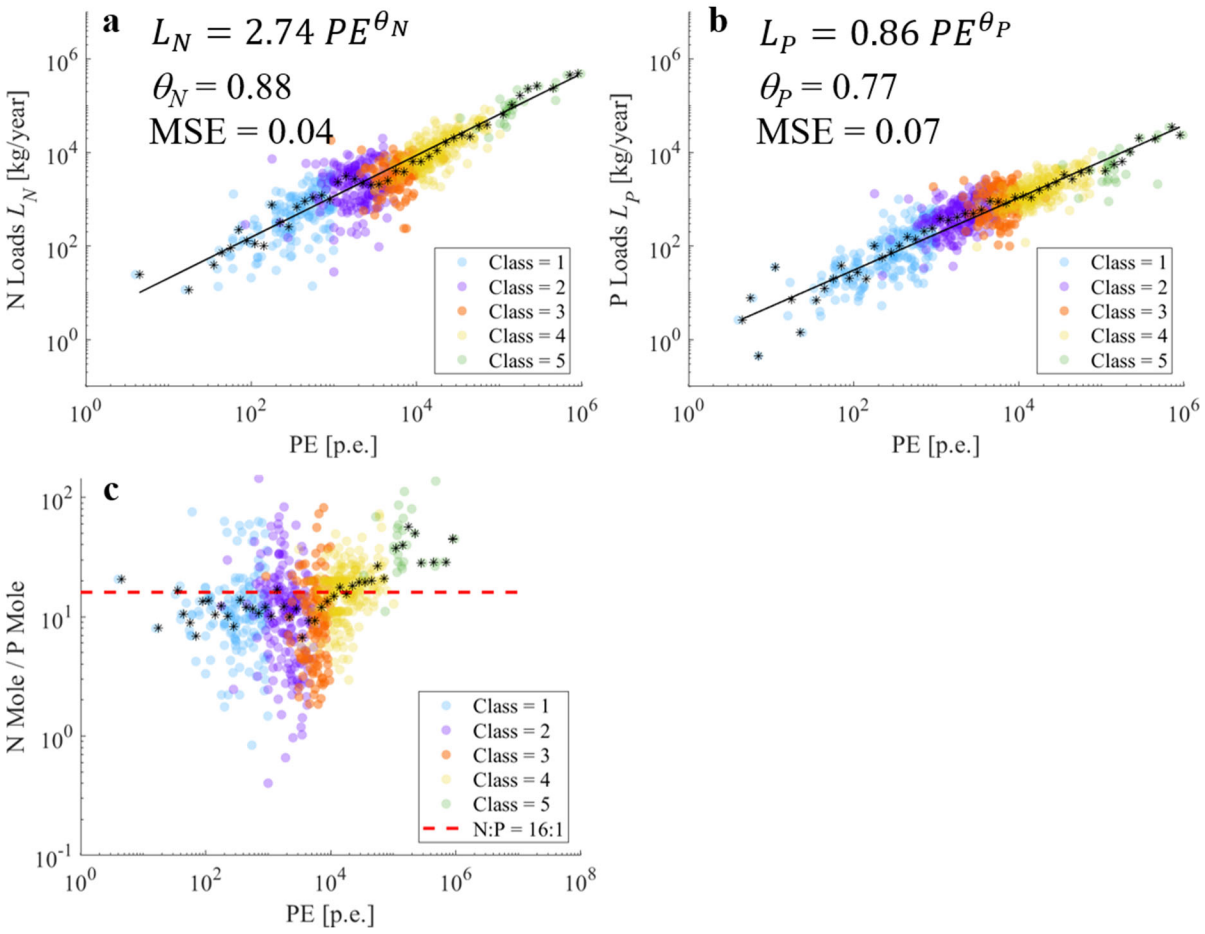

Figure 6.4 Scattered plot using all WWTPs in the Weser River basin. (a, b) Discharged N and P loads [kg/year] VS. PE [p.e.]. (c) N/P molar ratio VS. PE. Fitted θ_N 0.84 with standard error 0.04 for 95% confidence interval; fitted θ_P 0.71 with standard error 0.04 for 95% confidence interval. Mean squared error (MSE) values are given in the figures.

Table 6.3 For N and P loads discharged from available data of WWTPs in the Weser River basin, key statistics over H-S orders

H-S order (ω)	N loads $L_{U(N)}$			P loads $L_{U(P)}$			N/P molar ratio		
	Statistics			Statistics			Statistics		
	Median [kg/yr]	Mean [kg/yr]	CV	Median [kg/yr]	Mean [kg/yr]	CV	Median	Mean	CV
1	$2.2x10^3$	$5.2x10^3$	1.9	$3.3x10^2$	$6.6x10^2$	1.4	12.2	16.4	1.0
2	$4.0x10^3$	$8.4x10^3$	1.6	$8.7x10^2$	$1.1x10^3$	1.0	12.8	14.8	0.7
3	$4.6x10^3$	$1.4x10^4$	2.4	$9.8x10^2$	$1.5x10^3$	1.6	14.5	17.7	0.9
4	$6.0x10^3$	$1.8x10^4$	2.0	$1.0x10^3$	$1.7x10^3$	1.2	15.7	17.1	0.7
5	$4.1x10^3$	$3.4x10^4$	2.8	$6.6x10^2$	$3.0x10^3$	2.4	14.2	15.7	0.8
6	$7.4x10^3$	$2.2x10^4$	1.3	$1.5x10^3$	$2.0x10^3$	0.8	15.5	20.9	1.1
7	$1.9x10^4$	$6.8x10^4$	2.0	$2.4x10^3$	$3.9x10^3$	1.6	19.6	31.9	1.2

*Number of available data for N loads = [333; 161; 118; 66; 37; 25; 12]
**Number of available data for P loads = [376; 170; 124; 69; 38; 25; 12]

6.3 Hydrological impact

At the Weser River basin outlet, the Urban Wastewater Discharge Fraction (Φ) values estimated for median flow and low-flow (Φ_{QR50} and Φ_{QR90}) were 0.06 and 0.12, respectively, suggesting that, on a basin-wide average, contribution of WWTPs discharge is small relative to river discharge. However, spatial variations in reach-scale hydrologic impacts are also important. Mean Φ values for both flow conditions ($\overline{\Phi}_{QR50}$ and $\overline{\Phi}_{QR90}$) decreased exponentially, as stream order increased with exponent 0.56 ($p < 0.01$; R^2=0.85 and 0.89), from 2.9x10^{-2} to 7.6x10^{-4} and from 6.7x10^{-2} to 1.8x10^{-3}. The ratio of exponents for Q_R and Q_U is ~2.5, suggesting that Q_R increases more relative to Q_U with increasing stream orders; thus, dilution effect is greater in larger stream reaches. The average of $\overline{\Phi}_{QR90}/\overline{\Phi}_{QR50}$ across all stream orders was 2.4 (std. = 0.3) similar to $\overline{Q}_{R50}/\overline{Q}_{R90}$, demonstrating that wastewater discharge is more likely to be a significant contribution to total river flow under drier weather condition (Figure 6.5 and Table 6.4).

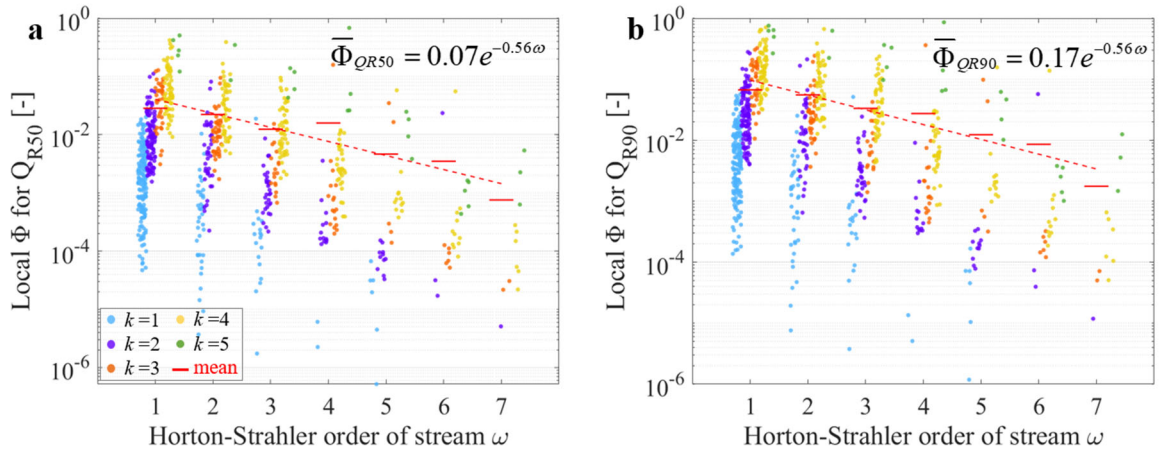

Figure 6.5 Spatial hierarchy of Urban Wastewater Discharge Factor (Φ) over seven stream orders in the Weser from (a) median flow Q_{R50} and (b) base-flow Q_{R90}. Red dashed lines in both (a) and (b) are linear fitting lines on a semi-log paper (p<0.01, R^2=0.9).

Variability in Φ_{QR50} and Φ_{QR90} was large for both median flow and low-flow conditions. *CV* values for Φ_{QR50} and Φ_{QR90} were characterized by three trends: (1) the largest *CV* for $\omega = 4$, (2) relatively smaller *CV*s for streams with $\omega \leq 3$, and (3) relatively larger *CV*s for higher orders (ω = 5~7). Minimum and maximum *CV* values were 2.1 and 5.3 for Φ_{QR50}, and 1.8 and 4.1 for Φ_{QR90}. The strikingly high *CV* for Φ_{QR50} and Φ_{QR90} for $\omega = 4$ resulted from the exceptional peak of CV_Q for $\omega = 4$. Overall higher *CV* values for Φ_{QR50} than for Φ_{QR90} reflect the increasing magnitude of streamflow Q_R ($Q_{R50} > Q_{R90}$) (Table 6.4).

The findings presented above for Φ suggest that WWTPs treated effluents are not likely to generate significant hydrologic alterations to natural stream flows in the Weser River. However, several important exceptions are evident for smaller streams. Among total 825 WWTPs (excluding WWTPs with no data of PE), portions of streams having $\Phi \geq 0.1$ were ~5% for Φ_{QR50} and ~15% for Φ_{QR90}. Among the streams with $\Phi \geq 0.1$, first-order streams accounted for the largest portion (~70% for Φ_{QR50} and ~66% for Φ_{QR90}), followed by second-order streams (~16% for Φ_{QR50} and ~20% for Φ_{QR90}). More than 70 % of the lower-order streams ($\omega<3$) with $\Phi \geq 0.1$ received the treated effluents from larger WWTPs ($k \geq 4$) serving large urban agglomerations. How these hydrologic patterns are manifested in water quality impairments is discussed in the following section, at reach-scale.

Table 6.4 For Urban Wastewater Discharge Factor (Φ) estimated from each of Q_{R50} and Q_{R90}, key statistics over H-S orders

H-S order (ω)	Number of data	Φ estimated from Q_{R50}			Φ estimated from Q_{R90}		
		Statistics			Statistics		
		Median	Mean	CV	Median	Mean	CV
1	386	6.7×10^{-3}	2.9×10^{-2}	2.1	1.8×10^{-2}	6.7×10^{-2}	1.8
2	172	8.8×10^{-3}	2.2×10^{-2}	2.1	2.3×10^{-2}	5.6×10^{-2}	1.7
3	123	4.0×10^{-3}	1.2×10^{-2}	1.8	1.1×10^{-2}	3.3×10^{-2}	1.8
4	69	1.5×10^{-3}	1.6×10^{-2}	5.3	3.6×10^{-3}	2.7×10^{-2}	4.1
5	38	2.6×10^{-4}	4.7×10^{-3}	2.5	6.3×10^{-4}	1.2×10^{-2}	2.6
6	25	1.7×10^{-4}	3.5×10^{-3}	3.4	3.9×10^{-4}	8.6×10^{-3}	3.4
7	12	1.0×10^{-4}	7.6×10^{-4}	2.1	2.3×10^{-4}	1.8×10^{-3}	2.1

6.4 Water quality impact

6.4.1 Pattern in hierarchical structures

I further examined the internal variability of reach-scale water quality impairments from P and N loads discharged from WWTPs, by estimating reach-scale nutrient concentrations using Eq. (3.21) for given nutrient loads discharged to receiving streams. For median flow (Q_{R50}), mean of $C_{reach(P)}$ and $C_{reach(N)}$ decreased from $8.6\text{x}10^{-2}$ to $4.5\text{x}10^{-4}$ mg P/L, and from $6.1\text{x}10^{-1}$ to $7.9\text{x}10^{-3}$ mg N/L for higher-order streams (Tables 6.5 and 6.6). For low-flow (Q_{R90}), the mean of $C_{reach(P)}$ and $C_{reach(N)}$ increased by a factor of 2.5 on average for each stream order, proportional to the ratio of $\overline{Q}_{R50}/\overline{Q}_{R90}$ ~2.5 (see Section 6.1), and suggesting the dominant contribution of Q_R compared to Q_U (see Section 6.3).

I used a threshold of C_P^* = 0.1 mg/L and C_N^* = 2.8 mg/L to evaluate water quality impairments which limit the achievement of at least *Good* ecological status, which is the EU WFD objective. At median flow, <20% of total WWTPs (17% for P, and 2% for N) are likely to have reach-scale nutrient impairment (e.g., $C_{reach(P)} > C_P^*$); of these, lower-order streams ($\omega<3$) accounted for ~93% for P and N (Figures 6.6a-b). About half of these P-impaired low-order streams received nutrient loads from larger class-size ($k\geq4$) WWTPs. At low-flow, the proportion of impaired streams increased by a factor of more than two (37% for P, and 11% for N), with most (~90%) being lower-order streams (Figures 6.6c-d).

Table 6.5 For the reach-scale concentration for P ($C_{reach(P)}$ [mg/L]) estimated from each of Q_{R50} and Q_{R90}, key statistics over H-S orders

H-S order (ω)	Number of data	$C_{reach(P)}$ from Q_{R50}			$C_{reach(P)}$ from Q_{R90}		
		Statistics			Statistics		
		Median [mg/L]	Mean [mg/L]	CV	Median [mg/L]	Mean [mg/L]	CV
1	370	$3.7x10^{-2}$	$8.6x10^{-2}$	1.6	$1.0x10^{-1}$	$2.2x10^{-1}$	1.4
2	169	$3.2x10^{-2}$	$6.1x10^{-2}$	1.8	$9.1x10^{-2}$	$1.6x10^{-1}$	1.7
3	122	$9.1x10^{-3}$	$2.3x10^{-2}$	1.5	$2.5x10^{-2}$	$6.3x10^{-2}$	1.5
4	69	$3.5x10^{-3}$	$2.3x10^{-2}$	4.4	$8.6x10^{-3}$	$4.5x10^{-2}$	3.9
5	38	$7.0x10^{-4}$	$7.3x10^{-3}$	2.7	$1.8x10^{-3}$	$1.9x10^{-2}$	2.8
6	25	$4.1x10^{-4}$	$1.6x10^{-2}$	3.9	$9.6x10^{-4}$	$3.9x10^{-2}$	3.9
7	12	$2.5x10^{-4}$	$4.5x10^{-4}$	1.7	$5.7x10^{-4}$	$1.1x10^{-3}$	1.7

Table 6.6 For the reach-scale concentration for N ($C_{reach(N)}$ [mg/L]) estimated from each of Q_{R50} and Q_{R90}, key statistics over H-S orders

H-S order (ω)	Number of data	$C_{reach(N)}$ from Q_{R50}			$C_{reach(N)}$ from Q_{R90}		
		Statistics			Statistics		
		Median [mg/L]	Mean [mg/L]	CV	Median [mg/L]	Mean [mg/L]	CV
1	329	$2.5x10^{-1}$	$6.1x10^{-1}$	1.7	$7.0x10^{-1}$	1.5	1.4
2	161	$1.6x10^{-1}$	$4.1x10^{-1}$	1.8	$4.3x10^{-1}$	1.0	1.6
3	116	$6.2x10^{-2}$	$2.0x10^{-1}$	2.0	$1.6x10^{-1}$	$5.3x10^{-1}$	1.9
4	66	$1.9x10^{-2}$	$2.8x10^{-1}$	5.5	$4.6x10^{-2}$	$4.6x10^{-1}$	4.3
5	37	$4.7x10^{-3}$	$4.2x10^{-2}$	2.1	$1.2x10^{-2}$	$1.1x10^{-1}$	2.1
6	25	$2.2x10^{-3}$	$1.0x10^{-1}$	3.6	$5.1x10^{-3}$	$2.5x10^{-1}$	3.6
7	12	$2.2x10^{-3}$	$7.9x10^{-3}$	2.1	$5.1x10^{-3}$	$1.8x10^{-2}$	2.1

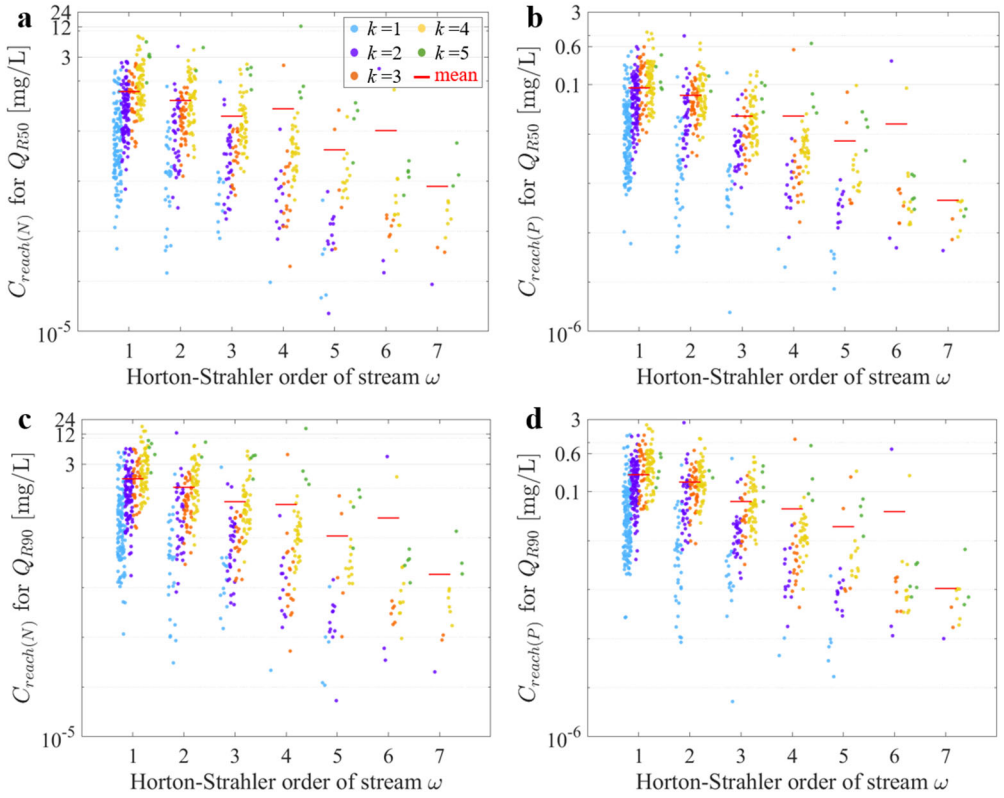

Figure 6.6 Spatial hierarchy over stream orders for nutrients (i = N and P) concentrations at the reach-scale ($C_{reach(i)}$) under each of median flow Q_{R50} and base-flow Q_{R90}, with the condition of zero background concentration (C_o = 0 mg/L). (a and c) Reach-scale N-concentration results for Q_{R50} and Q_{R90}, respectively. (b and d) Reach-scale P-concentration results for Q_{R50} and Q_{R90}, respectively.

6.4.2 Longitudinal distribution patterns

Longitudinal distributions for the estimated, reach-scale, N and P concentrations along hydrologic flow paths with the locations of the impaired lower-order streams are shown (Figure 6.7 for Q_{R50}; Figure 6.8 for Q_{R90}). Two regions are of specific interest. First, at 200-300 km from the outlet, where four of the eight largest cities (Brunswick, Wolfsburg, Salzgitter, and Hildesheim) in Lower Saxony are located and are served by larger WWTP class-sizes. Second, about 500-600 km from the outlet, several smaller urban areas served by lower class-size ($k \leq 2$) WWTPs, but with larger PE discharging to small streams with lower river discharge. Thus, WWTP locations with a combination of large PE (regardless of class-size) and small river discharge (regardless of stream order) are likely to cause water quality impairment of streams.

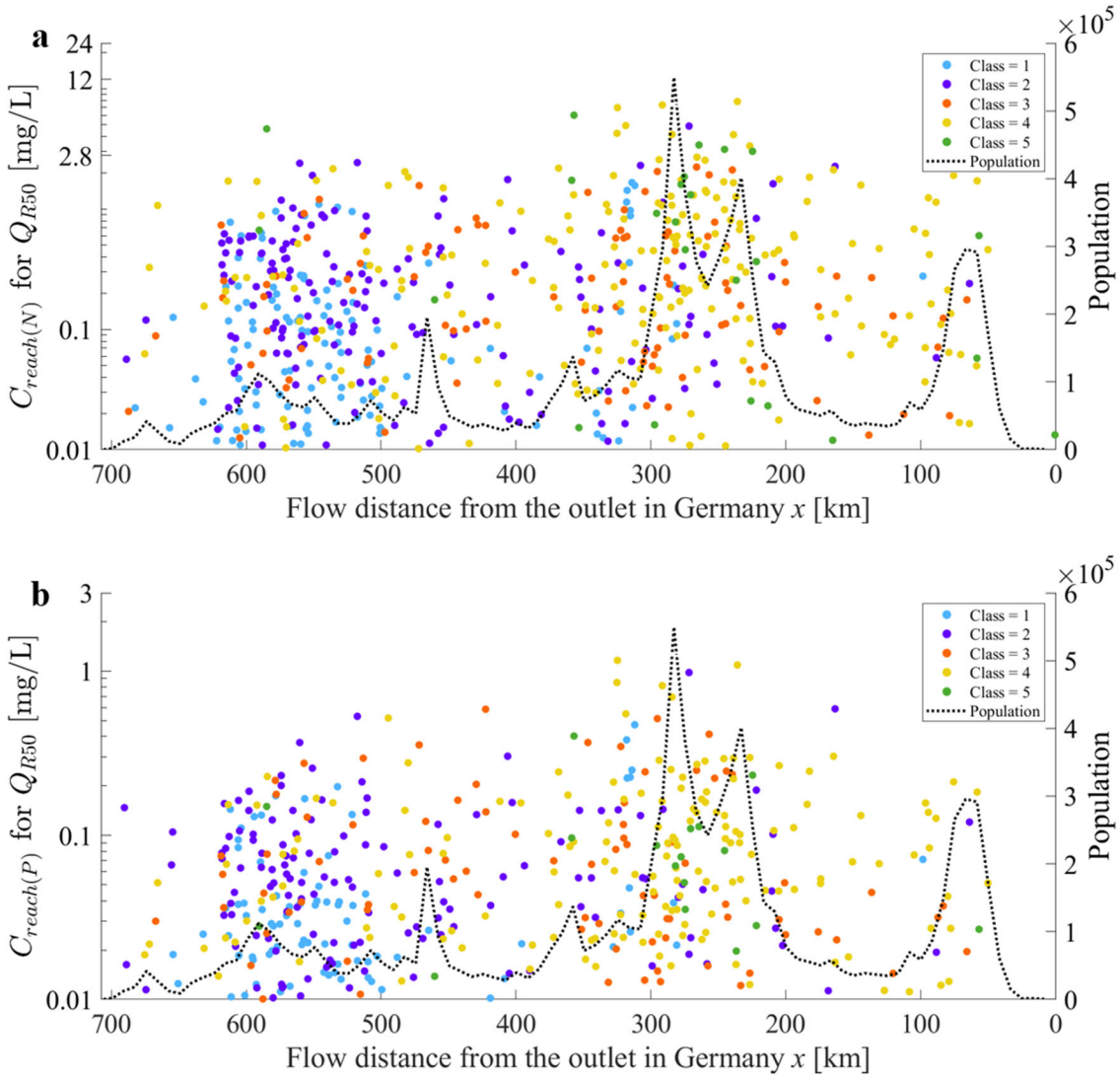

Figure 6.7 For the median flow condition $Q_{R50,}$ longitudinal distribution along the mainstream of the Weser for (a) N concentration ($C_{reach(N)}$, mg/L) and (b) P concentration ($C_{reach(P)}$, mg/L) at the discharge-point of WWTPs (local-scale) (left-hand side y-axis). Each color in circle-markers represents each class-size of WWTPs. Lower limit value on the left y-axis is set as a measurable concentration (USEPA, 1993) for visualization efficiency. Out of total WWTPs, 15% for N and 40% for P result the reach-scale concentration < 0.01 mg/L. Note that the flow direction from the left to the right-hand side is toward the Weser basin outlet. Human population distribution along the mainstream (right-hand side y-axis) is plotted to identify a relevant pattern between populated areas and water quality impaired regions.

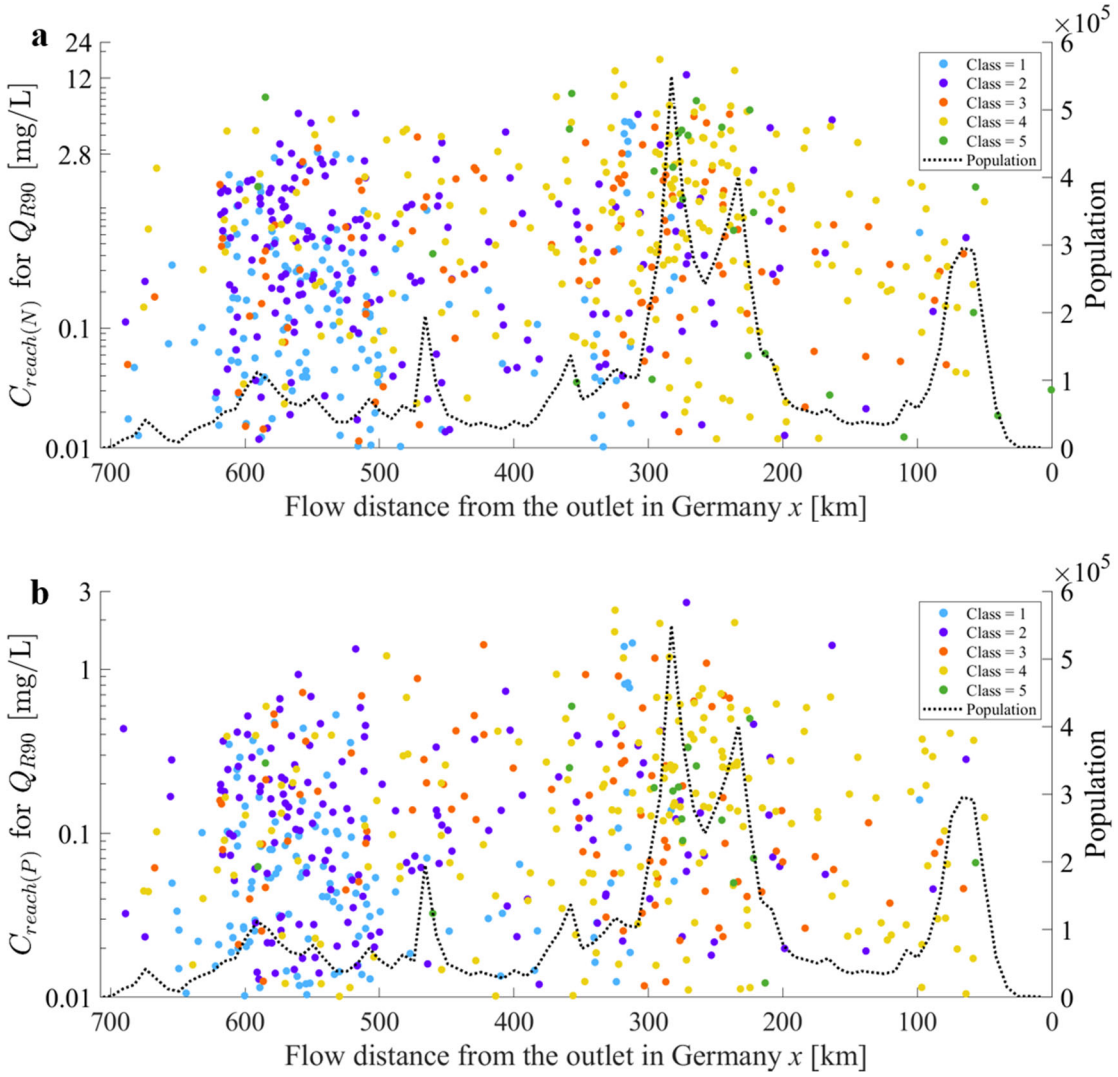

Figure 6.8 For the base-flow condition $Q_{R90,}$ longitudinal distribution along the mainstream of the Weser for (a) N concentration ($C_{reach(N)}$, mg/L) and (b) P concentration ($C_{reach(P)}$, mg/L) at the discharge-point of WWTPs (local-scale) (left-hand side y-axis). Each color in circle-markers represents each class-size of WWTPs. Lower limit value on the left y-axis is set as a measurable concentration (USEPA, 1993) for visualization efficiency. Out of total WWTPs, 9% for N and 26% for P result the reach-scale concentration < 0.01 mg/L. Note that the flow direction from the left to the right-hand side is toward the Weser basin outlet. Human population distribution along the mainstream (right-hand side y-axis) is plotted to identify a relevant pattern between populated areas and water quality impaired regions.

7. BASIN-SCALE WESER RIVER EUTROPHICATION ASSESSMENT

The part of this section is based on the results & discussions sections of following published paper: Soohyun Yang, Olaf Buettner, Rohini Kumar, Christoph Jaeger, James W. Jawitz, P. Suresh C. Rao, and Dietrich Borchardt, (2019). Spatial patterns of water quality impairments from point source nutrient loads in Germany's largest national River Basin (Weser River). *Science of the Total Environment.*

7.1 Sole contribution of point-source pressure

I evaluated the cumulative effects of WWTP nutrient loads at all locations downstream from WWTPs, first by considering only the role of dilution. At median discharge Q_{R50}, compared to reach-scale assessments, the number of impaired streams were around doubled, from 136 to 266 for P, from 15 to 31 for N. This accounts for ~32% (for P) and 4% (for N) of all WWTP locations. Of these, larger streams (ω>3) accounted for ~35% (for P) and ~45% (for N), suggesting the increased effects of cumulative N and P loads along flow paths. Including in-stream nutrient uptake, the impaired streams decreased to ~27% (for P) and 3.8% (for N). Because I estimated the basin-scale $C_{cum(i)}$ at the exact points of WWTP locations (consistent with the reach-scale assessments), the small decline (by ~5% for P and 0.2% for N) mostly resulted from the decrease portion for WWTPs discharging to larger streams. At low-flow Q_{R90}, considering in-stream nutrient uptake, the number of WWTP locations where $C_{cum(i)}$ exceeds the threshold concentrations was 463 for P (~56%) and 112 for N (~14%), around 1.7 (for P) and 3.6 (for N) times larger than that at Q_{R50}. This finding highlights the increased eutrophication risk at low-flow conditions. Larger streams (ω>3) once again represented a disproportionate fraction of these locations (~29% for P, ~23% for N).

Fraction of P and N losses over the entire basin (Ψ) were estimated as $\Psi_P = 0.47$ and $\Psi_N = 0.32$ for Q_{R50}. For P loads, starting from each of the 845 WWTP locations, I estimated the Nutrient Delivery Ratio (NDR_P) along flow paths to the basin outlet (Figures 7.1a-b). In all cases, the NDR profile was convex downward with distance towards the basin outlet, indicating the decline of the nutrient uptake rate constant k_x (see Eq. (3.27)). At low-flow Q_{R90}, fraction of P and N loads removed over the entire basin was larger than for Q_{R50} ($\Psi_P \sim 0.63$; $\Psi_N \sim 0.46$), corresponding to lower NDR and higher k_x (Figures 7.1c-d). However, P and N concentrations at the basin outlet increased ~1.5 times for Q_{R90} compared to Q_{R50}, from 0.05 to 0.07 mg P/L, and from 0.56 to 0.96

mg N/L. Thus, for Q_{R90}, increased in-stream nutrient uptake was countered by a smaller dilution-effect (Q_{R90}/Q_{R50} ~0.4 on average). These findings suggest that in-stream nutrient uptake plays an important role in reducing loads in low-order streams, while dilution is a major determinant for decreasing P and N concentrations in larger streams.

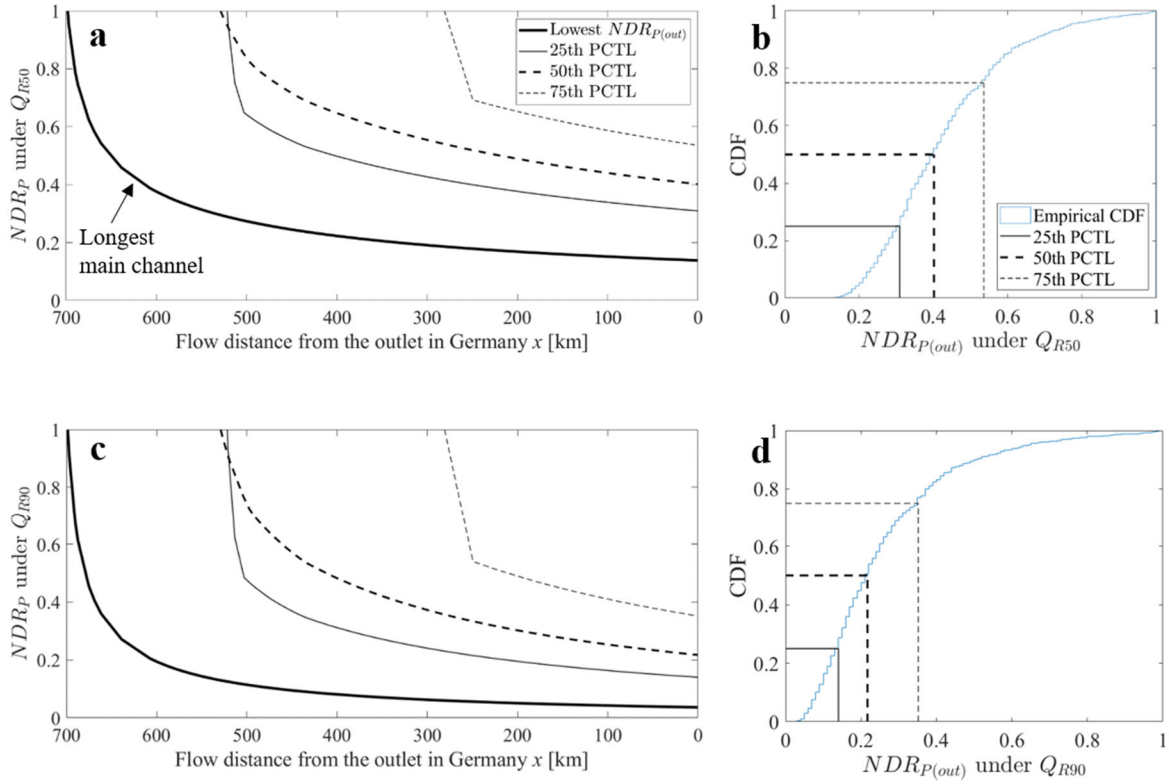

Figure 7.1 (a) Longitudinal profile of the Nutrient Delivery Ratio for P loads (NDR_P) estimated under median flow (Q_{R50}). Among individuals 845 flow paths starting from each WWTP, four representative ones were selected depending on the NDR value at the basin outlet ($NDR_{P(out)}$): (1) the lowest, (2) 25th, (3) 50th, and (4) 75th percentile (PCTL). Each line indicates a flow path from a WWTP location to the basin outlet (towards the right-hand direction). Anchor points on the profile represent confluences of side river streams. (b) Cumulative Distribution Function (CDF) of all estimated values for $NDR_{P(out)}$ under Q_{R50}. (c-d) are illustrated using the estimated results of NDR_P and $NDR_{P(out)}$ under low-flow (Q_{R90}) condition

7.2 Temporal trends of eutrophication from point- and diffuse-sources

Mean P concentration over the entire Weser river basin decreased from 0.37 to 0.19 mgP/L during recent few decades, because of significant reduction of total annual P loads (from 10K ton in 1980s to 3.1K ton in 2010s). Noting the heterogeneous spatial distributions for/within diffuse- and point-sources P loads despite total P loads reduction, it is also important to identify which streams within the Weser basin have been impaired consistently or recovered gradually over time. Thus, I separately examined P concentration estimated from diffuse- and point-source P loads ($C_{DS(P)}$ and $C_{PS(P)}$) and consequent total P concentration ($C_{Total(P)}$) (Figure 7.2). In 1980s, point-source P loads accounting for ~57% of total P loads dominated the spatial pattern of $C_{Total(P)}$. Figure 7.2a shows that most of streams with red-color code (ratio >2.5) are collocated between two maps of $C_{PS(P)}/C_P^*$ and $C_{Total(P)}/C_P^*$, with a similar mean concentration value of ~0.37 mg/L over the entire basin. On the other hand, since 2000s, diffuse-source of P loads played a key determinant to the resulted total P concentration, despite its 45% reduction than 1980s (Figures 7.2b and 7.2c). This is because the significant reduction magnitude of point-source P loads (~87% reduction than 1980s), which affected by the implementation of the EU WFD, increased the relative portion of diffuse-source of P loads.

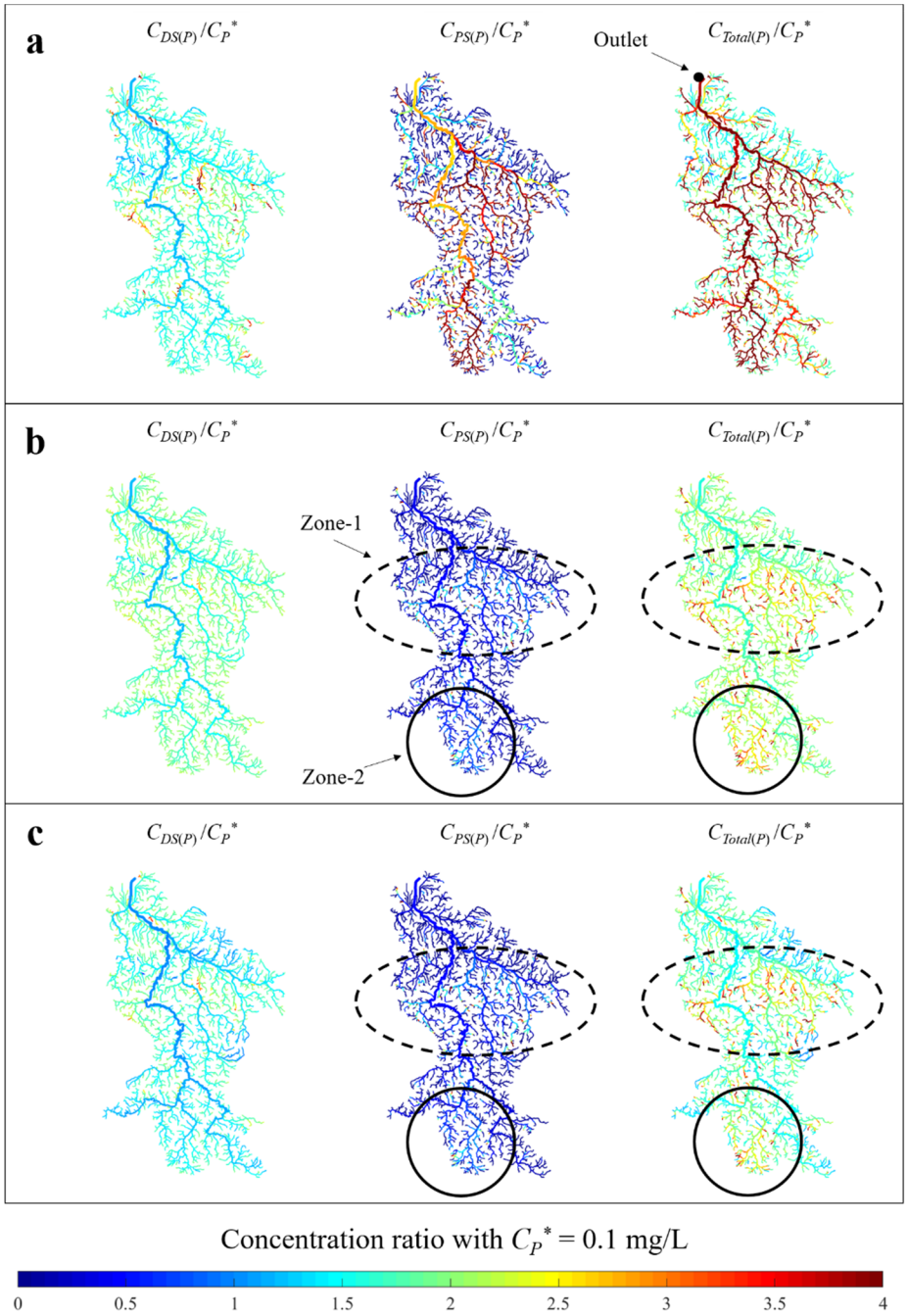

Figure 7.2 For the Weser River basin, basin-scale simulated P concentration from individual inputs of diffuse- and point-sources P loads ($C_{DS(P)}$ and $C_{PS(P)}$), and from both together ($C_{Total(P)}$) for three different periods: (a) 1980s, (b) 2000s, and (c) 2010s. These temporal variability reflected the differences in the pattern of land cover, the total P loads from both diffuse- and point-sources. For better visualization to recognize streams with less than good-status assessment regarding water-quality, absolute magnitudes of the three P concentration were normalized with the threshold of P concentration (C_P^* = 0.1 mg/L). Mean annual river discharge (Q_{Rmean}) was used to estimate the P concentrations.

Moreover, it is noteworthy that the reduced magnitude of diffuse-source P loads is insufficient to improve water-quality status for the recent few decades, implying the necessity of further reduction for diffuse-source P loads. Applying the threshold for P concentration (C_P^* = 0.1 mgP/L), $C_{DS(P)}$ values of almost all streams exceeded C_P^* for all three periods. In contrast, the reduction of point-source P loads facilitated to increase of good-state streams regarding water-quality impairment at least from point-sources (15% in 1980s to 84% from 2000). Remaining streams with $C_{PS(P)} > C_P^*$ were mostly terminal tributaries in midstream (Zone-1) and upstream (Zone-2) regions (Figures 7.2b and 7.2c). These point-source P loads discharged to small streams amplified P concentration within a short downstream range, demonstrating higher nutrient uptake rate upstream as water depth decreases (Figure 7.3).

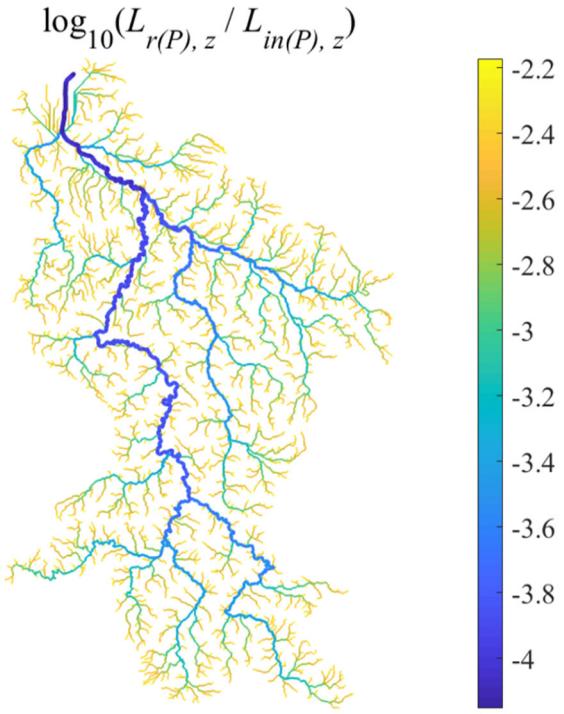

Figure 7.3 The map of the nutrient P removal efficiency for each stream segment z of the Weser River basin. The removal efficiency is indicated as the portion of nutrient removed within a segment z ($L_{r(P),z}$), compared to a given nutrient input ($L_{in(P),z}$). Mean annual river discharge (Q_{Rmean}) was considered to estimate the nutrient uptake rate constant. For visual efficiency, log-scaled values of $L_{r(P),z}$ / $L_{in(P),z}$ are depicted.

7.3 Comparison with water quality monitoring data

Monitoring data (measured concentrations for P and N) for the pre- and post-WFD time periods (T_{pre} = 1979-1999 for the pre-WFD; T_{post} = 2000-2015 for the post-WFD) indicate the significant water quality improvements achieved from significant reductions in diffuse- and point-source nutrient loads (Behrendt et al., 2003; BMUB/UBA, 2014, 2016). For all stream orders, median value for the T_{pre} data ($C_{meas,pre}$) was significantly larger than that for T_{post} data ($C_{meas,post}$) ($p < 0.01$ from Mann-Whitney test), with a factor of 1.6 ± 0.3 (mean ± std.) for P and 1.2 ± 0.2 for N. The variability in both $C_{meas,pre}$ and $C_{meas,post}$ decreased with increasing stream order for both P and N (Tables 7.1 and 7.2).

The findings from the Weser River monitoring data reflect the water quality recovery in other neighboring EU countries which also experienced similar reductions in WWTP nutrient loads. For example, in the Lower Seine River basin in France (~76K km^2; 18 million people), ~80% reduction in P loads from the largest WWTP serving Paris urban agglomeration (~12 million people) since the EU WFD initiation resulted in decrease of maximum P concentration, from ~2 mg/L to ~0.4 mg/L (Aissa-Grouz et al., 2018). These authors also point out the role of advanced P removal technologies (e.g., coagulation, flocculation, and decantation) in increasing P sorption onto suspended colloidal matter, thus altering bioavailable P in river reaches, which need to be accounted in estimating frequency of algal blooms.

Following the findings in Section 7.1, P loads discharged from WWTPs remarkably influenced on water quality impairment for P, whereas N loads from WWTPs hardly contributed to water quality degradation for N which implies much more dominant effect of diffuse-sources driven N loads. Thus, to understand the impact of nutrient loads from point-source WWTP discharges on river water quality, I focus only nutrient P in the following discussion. I compared the measured concentrations during T_{post} ($C_{meas,post(P)}$) and the basin-scale, estimated nutrient concentrations for point-source WWTP discharge loads ($C_{cum(P)}$) from both Q_{R50} and Q_{R90} conditions. I highlight three apparent spatial patterns over stream orders in the comparison (Figure 7.4a): (1) variability in $C_{meas,post(P)}$ was lower than that in $C_{cum(P)}$; (2) median value of $C_{meas,post(P)}$ was twice as large (2.0±0.6; $p < 0.01$ from Mann-Whitney test) than that of $C_{cum(P)}$; and (3) out of total number of each dataset, the portion of $C_{meas,post(P)}$ exceeding the concentration threshold (C_P^*) was >71%, and ~42% for $C_{cum(P)} > C_P^*$.

Several important factors need to be considered in interpreting these trends. First, pooled measured data are based on monitoring over different time periods and sampling intervals (on average, monthly). River discharge at sampling times was variable, while the $C_{cum(P)}$ values estimated for two specific flow conditions ($Q_{R50;}$ Q_{R90}) and were aggregated to cover the two occurrence frequencies in flow conditions. Thus, variabilities in $C_{meas,post(P)}$ and $C_{cum(P)}$ reflect both differences in site-specific conditions among streams of a given order, and variability in river discharge (CV of Q_R~1). Second, their median ratio ($\widehat{C}_{meas,post(P)}/\widehat{C}_{cum(P)}$) is ~1.5 for low-order streams ($\omega \leq 3$), which drain more numerous upstream sub-basins with smaller drainage area, compared to ~2.5 for high-order streams ($\omega > 5$) that represent converging flows and aggregated loads from much larger drainage areas (Figure 7.4b). Third, as ω increased, the portion of $C_{meas,post(P)} > C_P^*$ increased (61% to 100%), while that of $C_{cum(P)} > C_P^*$ decreased (44% to 0%). The last two factors suggest that in-stream P concentration in upstream locations are influenced mostly by WWTPs loads, while that larger nutrient concentrations in the higher-order streams are the result of accumulated diffuse sources nutrient loads from agricultural areas (~60% of total drainage area), resulting in increase of eutrophication risk.

Using the basin-scale network model, I could investigate the aforementioned argument about more increasing influence of diffuse-source P loads on river water quality status for higher-order streams. I estimated the total P concentration ($C_{Total(P)}$) through the basin-scale network model simulation considering both point- and diffuse-sources P loads (with nutrient loads input conditions in 2010s). Seven different frequencies for steady-state river discharges over the entire basin (in Section 3.5.1) were applied to ameliorate the limitation of dealing with two Q_R conditions (Q_{R50}; Q_{R90}) in the $C_{cum(P)}$ calculation.

Compared to $C_{meas,post(P)}$, the estimated $C_{Total(P)}$ showed two distinct trends over stream orders (Figure 7.5a). First, for the highest two orders (ω = 6-7), median value of $C_{Total(P)}$ significantly represented that of $C_{meas,post(P)}$ dataset ($\widehat{C}_{meas,post(P)}/\widehat{C}_{Total(P)} \sim 1$; $p<0.01$ from Mann-Whitney test). This result suggests that the inclusion of diffuse-source P loads filled the largest difference between $C_{meas,post(P)}$ and $C_{PS(P)}$ in ω = 6-7 ($\widehat{C}_{meas,post(P)}/\widehat{C}_{PS(P)} \sim 3.4$; $p<0.01$ from Mann-Whitney test) (Figure 7.5b). Second, for the other lower orders (ω =1-5), the calculated values of $C_{Total(P)}$ were over-estimated than $C_{meas,post(P)}$ dataset ($0.6 \leq \widehat{C}_{meas,post(P)}/\widehat{C}_{Total(P)} \leq 0.9$; $p<0.01$ from

Mann-Whitney test), and further their median ratio decreased for lower-order stream (Figure 7.5b). Seemingly, the discrepancy between $C_{Total(P)}$ and $C_{meas,post(P)}$ in ω =1~5 might indicate less correct input loads estimation (e.g., over-estimation of diffuse-source P loads input), or missing complexity in the model (e.g., under-estimated nutrient attenuation process). However, I interpret those potential factors not as the first-order impact on the discrepancy, because of the well-represented model result for the highest two orders streams receiving more aggregated P loads.

Rather, the discrepant result would be induced by the application of the identical relative proportion for a given Q_R percentile into all river streams, which employed as an alternative simple approach. In fact, smaller streams are in highly heterogeneous environments such as hydro-climatic conditions (larger variabilities in CV_{Q^*} for lower ω; mentioned in Section 2.3.1) and combination of land cover types (shown in Figure 2.7). Thus, I anticipate that employing a certain percentile river discharge derived from unique hydro-climatic factors would be a significant key to straightforwardly demonstrate the consistency between estimated $C_{Total(P)}$ and recorded $C_{meas,post(P)}$ for lower-order streams.

Table 7.1 Key statistics over H-S orders, for the measured concentration for inorganic P ($C_{meas(P)}$ [mg/L]) during the Pre-WFD period (T_{pre} = 1979 – 1999) and the Post-WFD period (T_{post} = 2000 – 2015).

H-S order (ω)	$C_{meas(P)}$ during T_{pre}				$C_{meas(P)}$ during T_{post}			
	Number of data	Statistics			Number of data	Statistics		
		Median [mg/L]	Mean [mg/L]	CV		Median [mg/L]	Mean [mg/L]	CV
1	2905	0.24	0.44	1.3	4863	0.12	0.19	1.4
2	5050	0.21	0.32	1.2	6871	0.13	0.16	0.9
3	6140	0.21	0.33	1.2	7659	0.13	0.16	0.7
4	3855	0.26	0.34	0.8	4543	0.14	0.18	0.8
5	753	0.29	0.39	0.8	1505	0.16	0.18	0.5
6	1119	0.31	0.38	0.8	798	0.18	0.19	0.6
7	265	0.27	0.33	0.6	90	0.17	0.21	1.1

Table 7.2 Key statistics over H-S orders, for the measured concentration for inorganic N ($C_{meas(N)}$ [mg/L]) during the Pre-WFD period (T_{pre} = 1979 – 1999) and the Post-WFD period (T_{post} = 2000 – 2015)

H-S order (ω)	$C_{meas(N)}$ during T_{pre}				$C_{meas(N)}$ during T_{post}			
	Number of data	Statistics			Number of data	Statistics		
		Median [mg/L]	Mean [mg/L]	CV		Median [mg/L]	Mean [mg/L]	CV
1	2641	4.99	5.64	0.7	5632	3.80	4.42	0.6
2	4454	4.31	5.52	0.8	7713	3.64	4.20	0.6
3	7172	4.82	5.56	0.6	8726	3.86	4.37	0.6
4	3695	4.81	5.07	0.5	5035	3.60	3.86	0.5
5	628	5.20	5.17	0.3	1269	3.83	4.02	0.3
6	913	4.61	4.62	0.2	795	3.48	3.54	0.3
7	218	4.92	4.79	0.2	90	3.37	3.55	0.3

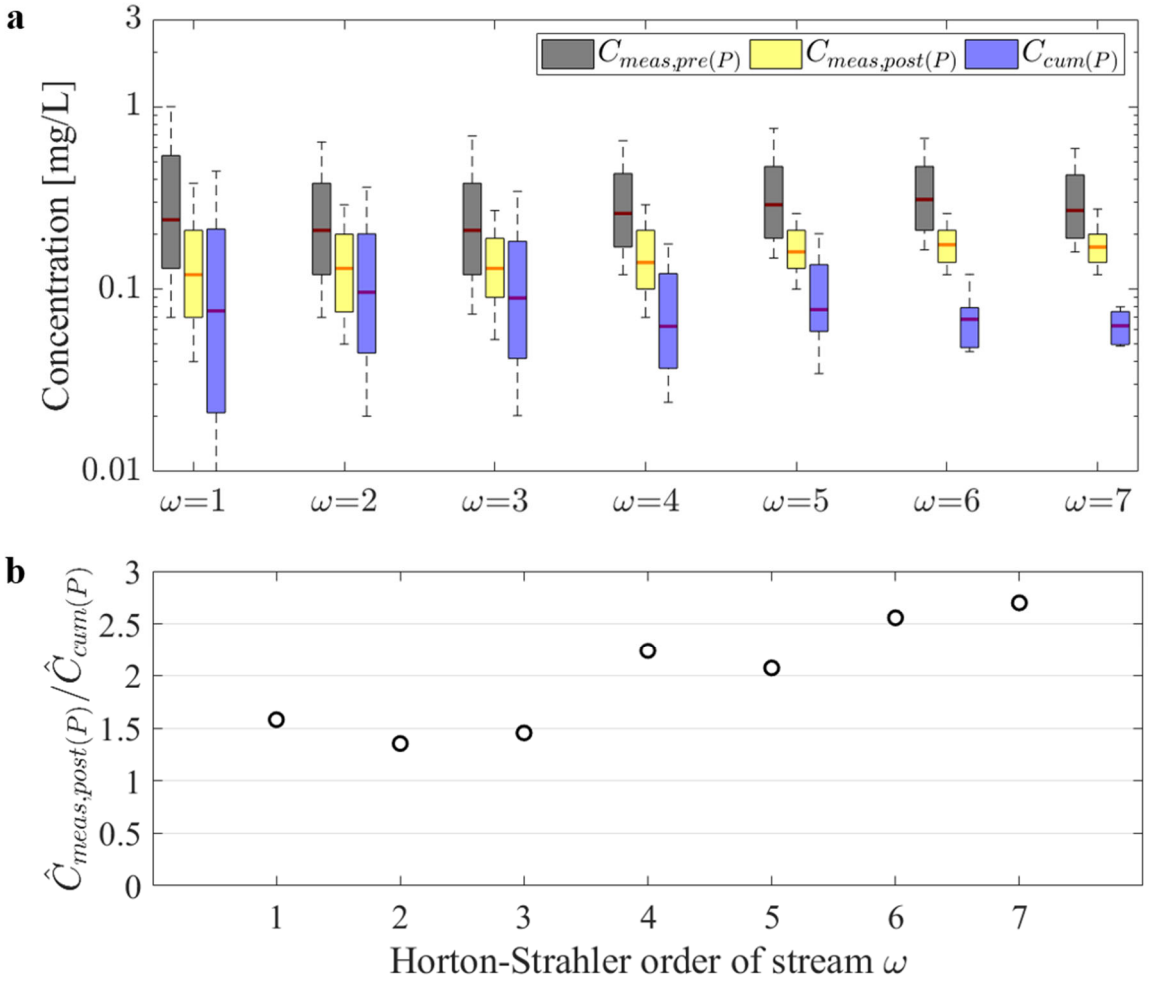

Figure 7.4 Comparisons among inorganic P concentrations over H-S orders. (a) Monitoring data pooled into the two periods ($C_{meas,pre(P)}$ for 1979-1999; $C_{meas,post(P)}$ for 2000-2015), and the basin-scale estimated concentration ($C_{cum(P)}$) under both the median and low-flow conditions. Red line inside each box represents median value. Upper and lower values of each box are 25th and 75th percentile. Upper and lower whiskers for each box are 10th and 90th percentile. (b) Ratio between median values of $C_{meas,post(P)}$ and $C_{cum(P)}$ (i.e., $\widehat{C}_{meas,post(P)}/\widehat{C}_{cum(P)}$).

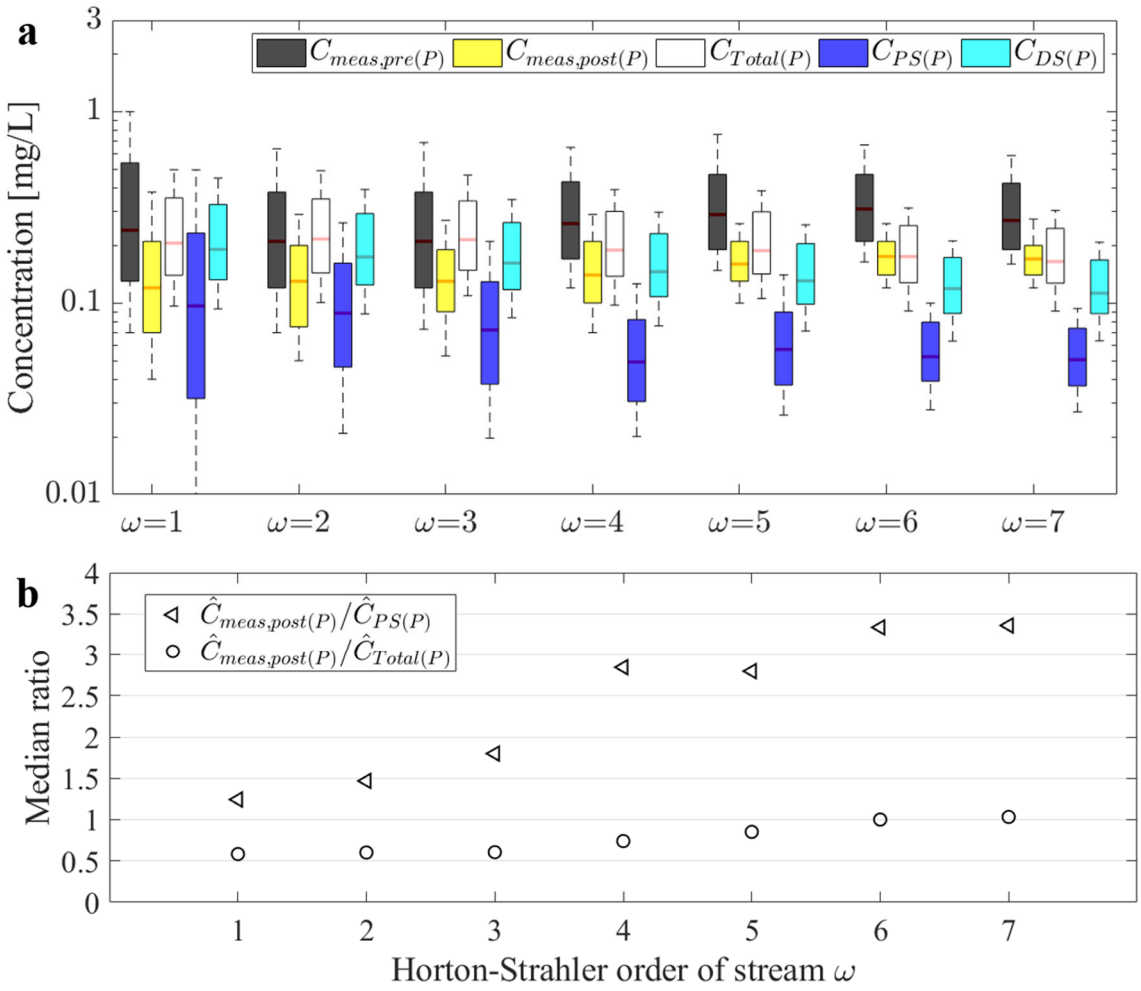

Figure 7.5 Over H-S orders, comparisons of in-stream P concentrations resulted from both point- and diffuse-sources P loads by using the basin-scale network model. (a) Monitoring data pooled into the two periods ($C_{meas,pre(P)}$ for 1979-1999; $C_{meas,post(P)}$ for 2000-2015), and the model estimated P concentration ($C_{PS(P)}$ for only point-source loads; $C_{DS(P)}$ for only diffuse-source loads; $C_{Total(P)}$ for both) under the estimated seven different occurrence frequency for river flow. Red line inside each box represents median value. Upper and lower values of each box are 25th and 75th percentile. Upper and lower whiskers for each box are 10th and 90th percentile. (b) Median ratios for $C_{meas,post(P)}$ compared to $C_{PS(P)}$ and $C_{Total(P)}$. Triangle- and circle-markers show the multiplying factor for the median values of each $C_{PS(P)}$ and $C_{Total(P)}$ to be the median of $C_{meas,post(P)}$.

8. CONCLUSIONS AND IMPLICATIONS

The contents of this section are mainly based on the conclusions & implications sections of following published papers: (1) Soohyun Yang, Kyungrock Paik, Gavan S. McGrath, Christian Urich, Elisabeth Krueger, Praveen Kumar, and P. Suresh C. Rao, (2017). Functional Topology of Evolving Urban Drainage Networks. *Water Resources Research;* **(2)** Soohyun Yang, Olaf Buettner, James W. Jawitz, Rohini Kumar, P. Suresh C. Rao, and Dietrich Borchardt, (2019). Spatial organization of human population and wastewater treatment plants in urbanized river basins. *Water Resources Research;* **(3)** Soohyun Yang, Olaf Buettner, Rohini Kumar, Christoph Jaeger, James W. Jawitz, P. Suresh C. Rao, and Dietrich Borchardt, (2019). Spatial patterns of water quality impairments from point source nutrient loads in Germany's largest national River Basin (Weser River). *Science of the Total Environment.*

8.1 Topology and evolution / UDN

The analyses suggest that as the drainage area of UDNs increases in a growing city, topological features increasingly *resemble* those of river networks, despite differences in the underlying generative processes. Three findings from the analyses of UDN data stand out:

$P(A \geq \delta)$ plots for UDNs exhibit exponential tempering ($c > 0$), while abrupt truncation ($c \sim 0$) is evident in those for rivers. The relationship between main sewer line length and drainage area follows a power-law, like Hack's law in river networks, dissected into two segments: an upstream segment with $h \approx 1$, and a downstream segment with $h \approx 0.6$. I found that with increasing UDN size, UDN topology increasingly resembles that of river networks in two ways: (1) decrease in the constant c with the UDN size which implies the sharper truncation of power-law $P(A \geq \delta)$ resulting from finite-size effects, and (2) extension of the downstream segment with $h \approx 0.6$ in length-area relationship. Nevertheless, the relationship of $\varepsilon+h \approx 1$ for river networks does not necessarily hold for UDNs because the space-filling constraints in river networks are not relevant for UDNs.

The power-law exponent ε for a UDN depends on the network size and can be larger than that reported for river networks. This suggests that these engineered networks have a greater hierarchical density, expected of an imperfect non-random branching tree topology. Analyses of UDN data from multiple cities will help identify the range in ε values, and factors that contribute to variability among diverse UDNs.

Different UDN subnets in a city evolve through both expansion and densification, but at heterogeneous growth rates, reflected in the decreasing rate of the tempering constant c with growth. Observed variability among UDN subnets within a city and among UDNs for different cities is reflective of engineering constraints that generate an imperfect, non-random tree structure.

Adjustments or additions to growing UDN necessitate adaptive design improvements in order to maintain functionality throughout a UDN. Such incremental engineering changes at local- and city-scale have strong parallels to "self-organization," where the city and its infrastructure networks continually evolve, and are adjusted to meet expansion and changing needs. Indeed, several studies have shown that cities evolve to exhibit fractal geometries, with optimal space-filling physical networks and assets (Batty et al., 1989; Batty & Longley, 1994; Shen, 2002).

Lu & Tang (2004) showed that as cities grow to occupy increasingly larger areas, the urban spaces are filled more densely by city roads, which are increasingly more fractal, providing more efficient access to all locations within the city. Geospatial co-location of roads and sewers suggests similar functional topology for UDNs and roads. The importance of "local" engineering optimization evident in small subnets of UDNs diminishes as the "global" optimization becomes more dominant at larger scales. Thus, large UDNs appear to be "self-organized" though differently to rivers. Further analysis of other UDNs from other cities is required to support or contradict these conclusions; such efforts are currently underway.

8.2 Implications of UDN topology analysis to flow modeling

The analyses of UDN topology suggest that the rich literature on flows in river networks can be extended to the prediction of urban water flows in UDNs. Examples include successful efforts to model UDN hydrograph time-series based on geomorphological width functions (Seo & Schmidt, 2012) or deriving instantaneous unit hydrographs (Seo & Schmidt, 2014) based on network topological features. Linking UDN hydrological responses to geochemical and ecological impacts in receiving waters (rivers) can also be fruitful lines of investigation.

8.3 Organization patterns of human population, PE, and WWTPs

For three German river basins (Weser, Elbe, and Rhine), the spatial hierarchies of POP, PE, and the total number of WWTPs over H-S orders follow scale-invariant distributions, as

quantified by extended Horton scaling ratios (R_{POP}, R_{PE}, and R_{WWTP}), analogous to conventional Horton ratios found for river networks. Narrow ranges for the three extended Horton scaling ratios across the three German basins indicate consistent patterns over H-S orders for: (1) degree of scale-invariance of German population distribution; (2) an increasing trend for PE agglomeration; and (3) a decreasing trend for the total number of WWTPs.

The location and degree of PE spatial clustering vary among WWTP class-sizes. The PE-clustering location of higher (lower) class-size WWTPs is relatively further downstream (upstream). The degree of clustering for PE served by lower class-size WWTPs is stronger than that for higher class-size WWTPs. Note that unique patterns of the size and location of urban agglomerations significantly affect the spatial distributions of PE served by each class-size along hydrological flow paths.

Three scaling indices I proposed here capture correlated spatial organization of POP, PE, and WWTPs distributions embedded in the hierarchy of river networks. I find that population distributions reveal neutral or weak preference for settlement in eigen-area of higher H-S orders. I also find that WWTPs discharging to higher H-S orders treat more non-sanitary wastewater, and that WWTPs discharging to higher H-S order streams consist of a smaller number of WWTPs but with higher class-sizes.

8.4 Potential extensions of scaling indices to EU countries and outside Europe

High connectivity (>90%) to urban sanitary infrastructure in Germany (WHO/UNICEF, 2015a) reflects a conscious choice made to improve public health, and the environmental regulations mirror pragmatic choices made to minimize adverse ecological impacts on receiving streams (BMUB/UBA, 2016). However, lack of regulations on nutrient loads discharged from smaller WWTPs (class sizes 1-3), which comprise the vast majority (~77%) of the WWTPs in Germany but serve a small fraction (~10%) of the total PE, may have potential adverse hydrologic and water-quality implications to low-order streams ($\omega \leq 3$).

Even with common environmental regulations across EU, such as the Water Framework Directive 2000/60/EC (European Commission, 2000), the fraction of the national population connected to WWTPs varies widely between member countries (EEA, 2017b). For example, central European countries (Austria, Belgium, Denmark, Netherlands, Germany, Switzerland, Luxembourg) had overall high connectivity (>90%) to WWTPs in 2015. The connection rate was

similar for northern countries (~86%), but was somewhat lower for eastern, southern, and southeastern countries (75% to 78%). Variability in connection to WWTPs that implement tertiary treatment was also surprisingly large. For example, the highest connection rate to WWTPs with tertiary treatment was >77% of total population in central and northern Europe (e.g., ~93% for Germany), while the lowest (~20%) was in southeastern Europe (EEA, 2017b). Socio-economic variability and percentage of population in urban areas are contributing factors to such variability. For example, urban fraction was >80% in central and northern Europe, ~76% in southern, and ~65% in eastern and southeastern Europe, respectively (WHO/UNICEF, 2015a).

Given the aforementioned variabilities within Europe, extension of the findings for the three large urbanized basins in Germany to other river basins within Germany, and diverse basins in other EU countries requires further data analyses. Of the seven other major river basins in Germany, three coastal basins (Eider and Scheli/Trava, both <10K km^2; Warnow/Penne, ~21K km^2) are entirely within the territorial boundaries, similar to the Weser River. The findings should also be applicable to these smaller German basins. Two others are international river basins with larger drainage areas within Central Europe. Drainage within Germany are: for Meuse, ~4K km^2, rest in Belgium, France, Netherlands, and Luxembourg; and for Ems of ~17K km^2, rest in Netherlands. Given similarities in connectivity to WWTPs and socio-economic factors, the findings may be also applicable to these river basins. Upstream drainage area (~56K km^2) for the Danube River basin is within Germany, but large portions (~93%) of the basin are in multiple European countries. A small area of Odra basin (~10K km^2) is within Germany, with large areas (~92%) in Czech Republic and Poland. Differences in the connectivity and treatment technologies among the EU countries are especially important for the analyses of spatial patterns of POP, PE and WWTPs in international river basins, even though all river networks share same fractal geometries. While human settlements have similar globally scale-invariant patterns (Fang et al., 2018), variabilities among smaller sub-basins within large basins also need to be investigated.

Extrapolating the observed patterns to urbanized river basins in OECD (Organization for Economic Co-operation and Development) countries might be possible if I assume that spatially organized patterns of population, PE and WWTPs follow the scaling rules I found here. Additional analyses are required with data for urbanized catchments in other continents. However, extending the findings to urbanized river basins in Asia, Africa, and South/Central America is challenging for two key reasons. First, accessibility to reliable data of WWTPs at country or regional scales is

limited, confounding analyses similar to what I presented here. Second, in many countries I expect low levels of connectivity to sanitary networks and well-managed centralized wastewater treatment systems (WHO/UNICEF, 2015b; WWAP, 2017).

8.5 Spatial pattern of water quality pollution affected from point-source pressure

Treated wastewater effluents discharged from WWTPs can alter hydrologic and geochemical regimes of receiving river networks. I investigated the potential for such alterations at ~845 WWTP discharge locations in the Weser River basin in Germany to identify the reach- and basin-scale impacts based on (1) Urban Wastewater Discharge Fraction (Φ) as a measure of likely dilution, and (2) nutrient concentrations (C_{reach}; C_{cum}) for N and P as a measure of water quality impairments. For the Weser River basin, hydrologic alternations are not likely to be significant, because the volumetric discharge of WWTPs effluents is sufficiently diluted by larger natural river flows. I found Φ to decrease with increasing stream-order, representing smaller dilution capacity of lower-order streams. Also, when larger WWTPs discharge to smaller streams, hydrologic impacts of WWTPs discharge may be large, especially under the low-flow conditions or during persistent drought periods.

I estimated that overall, ~20% of all stream reaches receiving WWTP nutrient loads are likely to have P-impaired water quality at the reach-scale for median flow (~2% for N-impairment). Such alterations are more likely in lower-order streams ($\omega<3$), mostly with discharge from larger class-size WWTPs ($k>3$). However, smaller WWTPs ($k<3$) discharging to the lower-order streams can also impair water quality when the magnitude of WWTPs discharge is close to or larger than the discharge of the receiving stream, even though the WWTP discharge is within the regulated range for the class-size of the WWTP. Dry-weather conditions (i.e., low-flow) exacerbate water quality impairment compared to median flow. Basin-scale analyses suggest that the role of in-stream nutrient uptake diminishes with increasing stream-order, while dilution plays an increasingly important role in reducing nutrient concentrations in larger streams with larger river discharge from converging flows.

The findings for the Weser River align with the European Commission report on the WFD implementation in Germany (European Commission, 2012). For total 1,414 surface water bodies (rivers, lakes, transitional and coastal waters) in the Weser basin, point source pressure is likely to prevent ~21% of them from reaching *Good* status regarding nutrients, while diffuse source nutrient

loads affect ~85% of them. The fact that rivers comprise ~97% of the Weser surface water bodies implies the dominant influence of the diffuse source loads on nutrient enrichment in the Weser River. Indeed, the dominant diffuse sources are exported from agricultural land-use, comprising ~67% of the Weser basin drainage area (IWRM-net, 2010; Hirt et al., 2012; Heidecke et al., 2015). In addition, geomorphic alterations of streams also play a major role in habitat loss and fragmentation, thus threatening biodiversity (BMUB/UBA, 2014; Fuller et al., 2015; Geist & Hawkins, 2016).

8.6 Implications of point- and diffuse-sources on ecological status

The decreased role of WWTPs point-sources compared to diffuse-sources has been evident over the past two decades in Germany (BMUB/UBA, 2016). Total nutrient emissions from diffuse- and point-sources to all German river basins decreased from ~1,088 kton N/yr and ~92 kton P/yr during 1983-87 period to ~688 kton N/yr and ~33 kton P/yr during 1998-2000 period. Contribution of P loads from WWTPs during this period had declined from ~62% to ~25% of total loads, while total N loads from WWTPs decreased from ~28% to ~17% (Behrendt et al., 2003). Since the declaration of the EU WFD in 2000, the total nutrient loads decreased continuously to ~594 kton N/yr and ~26 kton P/yr during 2006-2008 period (~45% and ~72% reduction compared to 1983-1987). Especially, significant reduction in P inputs is mainly attributed to the decrease in WWTPs loads, primarily through the implementation of tertiary treatment technologies of WWTPs and the introduction of phosphorous-free detergents (BMUB/UBA, 2014; Ibisch et al., 2016).

Nutrient loads from WWTPs are likely causing reach-scale water quality impairments at several low-order streams, resulting in eutrophication. Persistent presence of benthic algal mats in smaller streams, sustained by WWTP loads, might serve as chronic (erosion) and episodic (scouring) sources for downstream pelagic algal loads. These algal sources combined with diffuse nutrient loads in larger streams might exacerbate algal blooms in larger streams.

Furthermore, reductions in P loads at the end-of-pipe may not always guarantee the recovery of ecological improvements in river networks (Westphal et al., 2019), similar to the well-known hysteretic impairment-recovery trajectories in lakes and coastal systems shown in recent global analysis (McCrackin et al., 2017). Engineered hydraulic structures (e.g., dams and weirs) constructed in mid- and downstream sections on larger river reaches are likely to play a crucial role in delaying the decline of P loads and extending algal blooms, even though they contribute to

significant removal of sediments and sorption of contaminants by providing longer retention times (Stanley & Doyle, 2002; Maavara et al., 2015; Westphal et al., 2019). For example, Westphal et al. (2019) estimated ~30% P removal from construction of weirs and dams in the Ruhr River basin, a part of the Rhine River basin in Germany (~4500 km^2, ~2 million population; 66 WWTPs; ~220-km long). However, P release from legacy loads accumulated in sediments in impoundments as well as river networks (e.g. desorption; resuspension) contributes to the delayed recovery.

8.7 Implications of climate change on river water quantity/quality

The impacts of climate change on the integrity of diverse water bodies and their ecosystems have been broadly investigated (Moss et al., 2011; Charlton et al., 2018; Trolle et al., 2019). Here, I considered the variation of river flows, median (Q_{R50}) and low-flow (Q_{R90}) for normal and drier climate condition, respectively. Weser River basin is more likely to experience significant alterations to the hydrological regime and geochemical regimes under the low-flow condition. For basins in more arid zones (e.g., central Spain with semi-arid climate), severe adverse impacts from point source nutrient loads would be experienced because of persistent or episodic occurrence of much lower river discharge and large variation in flow conditions (i.e., $CV_{Q^*} > 1$).

Recent prolonged heat wave and dry conditions experienced in Central Europe in 2018 (DWD, 2018). Such extreme hydro-climatic conditions during only one year increased water quality impairments and aquatic ecological disruptions (algal blooms; fish-kills) (JRC-EDO, 2018). Indeed, much lowered river discharge is a primary signal. The measured record of river discharge at the "Hemelingen" gauge, the closest to the Weser basin outlet but not influenced by tide (Hirt et al., 2008), was 112 m^3/s on average during May through November 2018 (BfG, 2018). This discharge corresponds to the 5^{th}-percentile of mHM-simulated Q_R time-series (111 m^3/s) at the Weser outlet for 1956-2015 period. In fact, the extreme hydro-climatic conditions are more likely under climate-change scenarios (EEA, 2017a; Duncombe, 2019). This implies more frequent occurrence for water quality impairments and threats to aquatic ecosystems integrity (Whitehead et al., 2009; Michalak, 2016; Paerl et al., 2016). Thus, inter-disciplinary research across diverse academic fields with integrated management perspectives is required for assessments at multiple spatial and temporal scales (Woznicki et al., 2016; Molina-Navarro et al., 2018; Riley et al., 2018; Le Moal et al., 2019).

9. RESEARCH OUTLOOK: MONITORING, MODELING, AND MANAGEMENT

During my PhD projects, I identified the characteristics of the coupled natural (rivers) – humans – engineered (urban drainage infrastructure) systems, inspired by analogy, coexistence, and causality. Urban sanitary sewer networks in two cities in different countries revealed scale-invariance in their binary and multinary structures like natural rivers. Joint organizations of rivers, human population, and WWTPs were quantified and showed consistent patterns in three large German rivers. Discharges (treated wastewater and nutrient loads) from five different class-sizes (across three orders of magnitude in PE) WWTPs posed hydrological alteration and eutrophication risk on smaller streams, at both reach- and basin scales under steady-state river flow condition. In this last section, my PhD research findings are revisited through the three lenses of monitoring, modeling, and management, synthesizing research findings and guiding future research paths.

Dataset recorded at monitoring stations are valuable for not only understanding the diverse environmental parameters (physicochemical, water quality, ecological etc.), but also testing the system modeling results, and sequentially guiding researchers to revise the model through physical-processes addition or model-parameters range/value modification. Note that the monitoring stations in the Weser River basin were extracted from all monitoring stations where samples were collected across Germany. While analyzing the confidential dataset of Weser monitoring stations in my PhD project, I found that for a given stream order ω, the number of monitoring stations per one stream is lower than that of WWTPs acting as point-source pressures, around 3 times on average over all seven stream orders. For smaller streams, one monitoring station exists per ~12 streams ($\omega = 1$) or ~ 3 streams ($\omega = 2$), whereas other streams with $\omega \geq 3$ are monitored by at least one monitoring station.

Interpreting the findings from comparing the number of monitoring stations, WWTPs, and river stream segments led me to set a hypothesis: *Smaller streams in the Weser River would not be monitored sufficiently although monitoring them is necessary*. The hypothesis posed a question: *How could I identify smaller streams requiring regular monitoring in the near future?* As synthesizing my PhD work, I propose the potential of the data-model synthesis approach to characterize for environmental conditions of sub-basins where the current monitoring stations are in place; and to suggest which additional streams need to be monitored. To do this, basic platform

used is the ternary diagram constructed using the relative proportions of the three main land covers (as shown in Figure 2.7).

Here, the analysis results on the first-order sub-basins are presented by focusing on their importance as provision of diverse habitats and maintenance of species diversity. Examined objects are all sub-basins for a given stream order (Figure 9.1a). To reflect the impacts of point- and diffuse-source loads on each sub-basin, the nutrient concentration estimated with only diffuse-source at the sub-basin outlet through the basin-scale network model (Figure 9.1b), and the presence of WWTPs within a sub-basin (Figure 9.1c) are considered. Then, the data on the existence of monitoring stations within the sub-basin is incorporated (Figure 9.1d). Most of the current monitoring stations are in sub-basins mainly occupied by agricultural area (80 ~ 90%). I applied two significant criteria to prioritize sub-basins to be monitored, one is the existence of WWTPs because their discharges alter water quality and aquatic ecosystems composition (Ortiz & Puig, 2007; Aissa-Grouz et al., 2015; Inostroza et al., 2018), and the other is the estimated $C_{DS(P)}$ under mean river flow ≥ 0.1 mgP/L (C_P^*) of *Good*-status threshold in the EU WFD. Since around 95% of total first-order sub-basins have $C_{DS(P)} \geq 0.1$ mgP/L, the criterion for WWTP-existence played a key role in determining sub-basins where preferentially monitoring plans are required (Figure 9.1e). Then, sub-basins in Zone-U (Figure 9.1b) manifesting the remarkable effect of urban area dominance could be considered as secondary candidates for initiating monitoring programs. Furthermore, on the framework to prioritize monitoring-necessary sub-basins, relevant other criteria (e.g., N to P molar ratio) or more detailed properties (e.g., class-size of WWTPs) can also be incorporated to classify the urgent level for sub-basins to be monitored.

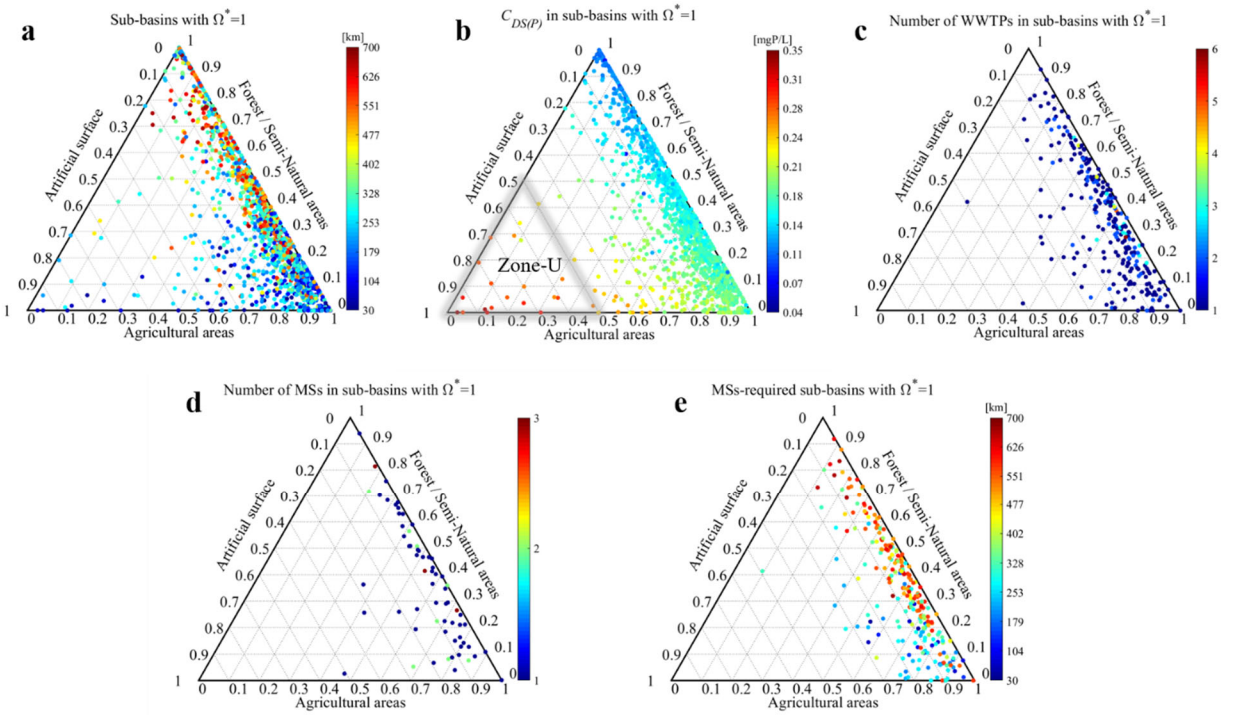

Figure 9.1 For each 1st-order sub-basin in the Weser River, ternary plots representing (a) the proportion of three land cover types, (b) the model-estimated P concentration for diffuse-source loads under mean annual flow, (c) the number of WWTPs, (d) the number of monitoring stations (MSs), and (e) the suggested sub-basins to be monitored. Ternary axes are based on three dominant land cover types (Class 1 = Artificial surface; Class 2 = Agricultural areas; Class 3 = Forest / Semi-natural areas). Each dot represents a sub-basin. Color-bar in (a) and (e) means the distance to the Weser River outlet from the outlet of each sub-basin.

In addition, I point out the necessity of increasing monitoring frequency for biological quality elements (BQEs) (e.g., phytoplankton and macrophytes) or their corresponding properties (e.g., chlorophyll *a* concentration) over larger spatial scale within a river basin. Since the EU WFD implementation in 2010, the BQEs have received more attention because they are the most critical determinants on ecological status assessment result (i.e., 'one-out all-out' principle), and only ~18% of all German river bodies are likely to achieve the WFD objectives by the end of second management cycle in 2021 (BMUB/UBA, 2016). In fact, under regulations of the EU WFD, the EQEs have been monitored at least once per one to three years (surveillance monitoring sites) and at least once every three years (operational monitoring) (Arle et al., 2016). Although the required frequency and interval for monitoring BQEs might be sufficient to assess ecological status of Europe-wide surface water bodies every seven years of WFD management cycle, the monitoring records are too sparse to be used in understanding long-term trajectory of aquatic communities

responses to anthropogenic pressures, and in developing a system dynamic model purposed to establish applicable measures to meet the WFD goal (Aissa-Grouz et al., 2018; Westphal et al., 2019). Meanwhile, long-term high-resolution monitoring data (e.g., weekly records over 30 years) are generally available at the most downstream site or near the basin outlet. That might be attributed to less recognized importance of aquatic ecosystems before the WFD era or limited financial budget to set monitoring sites up.

Since high spatial variability in P concentration over large area of Weser River basin was shown in this thesis, its corresponding heterogeneity in aquatic ecosystems responses (e.g., algae; benthic communities) would be inevitable, necessitating larger spatial coverage to monitor status of water quality and aquatic ecosystems. Compared to traditional in situ monitoring methods, small and low-cost unmanned aerial systems can be the most promising solution in near future to collect temporally and spatially high resolution monitoring data over large surface water bodies (Su & Chou, 2015; Shang et al., 2017; Becker et al., 2019). The high resolution monitoring results will be essential resources for scientists to develop models which assess water quality and aquatic communities, for managers to establish achievable measures for the WFD commitment, and for the public to recognize the current status of the water environmental issues and encourage them to reduce anthropogenic pressures.

The basin-scale network model studied in my PhD works was essentially targeted to estimate in-stream nutrient concentration for a given spatially heterogeneous point- and diffuse-sources, under steady-state river flow condition. Using the model results, river streams at risk of eutrophication could be identified based on the WFD regulatory thresholds for a given nutrient. As a linkage of in-stream trophic status and aquatic ecosystems, incorporating responses of algal communities to a given nutrient into the current model can be one of future research topics. Main idea for generating algae responses is that constant discharges of P loads from WWTP located on small upstream reaches are likely to sustain a persistent mat of benthic algal biomass at each WWTP location. Algal biomass released through steady erosion and episodic disruption of these benthic mats (Biggs, 2000) can be transported to downstream reaches and contribute to growth of pelagic algae, supported by larger P concentrations from diffuse sources and absent competition from benthic algae in larger streams (Jäger & Borchardt, 2018). Thus, for the Weser river basin, low-order streams which mainly dominated by WWTP nutrient loads are expected to be impacted by benthic algae blooms, while larger downstream reaches with persistent algal sources from

diffuse-source nutrient loads can sustain larger pelagic algal biomass. The separation distance between successive WWTPs might play a key role in to mitigate the additional impact of benthic algal source controlled by a carry-over effect.

Indeed, the advanced model concept encompasses River Ecology and River Eutrophication influenced by People, Loads from point- and diffuse-sources pressures, Attenuation by engineered systems such as WWTPs, and Natural attenuation such as nutrient uptake in hyporheic zones. Next paramount procedure for the "RE-PLAN" model improvement is to introduce temporal variabilities in nature. Considering that hydro-climatic forcing fundamentally controls the availability of natural water resources, rainfall pattern variabilities in frequency, and magnitude are priority to be integrated into the model framework. Inevitably, the temporal fluctuations of rainfall induce temporally varying responses of the coupled natural-human-engineered systems in urbanized river basins as following examples. In natural river bodies, river discharge time-series mirror temporal patterns of rainfall (Marengo, 2005; Botter et al., 2007; da Silva et al., 2015). For human societies, daily water use of urban residents increases during dry weather from rainfall deficit (Protopapas et al., 2000; Balling Jr. et al., 2008). For urban drainage systems, the probability, frequency and duration of combined sewer overflows occurrence are strongly determined by rainfall patterns properties (Sandoval et al., 2013; Fortier & Mailhot, 2015; McGrath et al., 2019). Thus, establishing temporal dynamics of rainfall into the model platform is of significance to address interdisciplinary issues across hydrological, biogeochemical, ecological, engineering, and socio-economic factors, and further climate change impact on the coupled natural (river)-human-engineered systems. Scenario-based analysis results of the envisioned model can provide us crucial insights to formulate societal adaptation strategies to the impacts of climate change and integrated watershed management guidelines at national- and international-scales.

REFERENCES

Aban, I. B., Meerschaert, M. M., & Panorska, A. K. (2006). Parameter estimation for the truncated Pareto distribution. *Journal of the American Statistical Association, 101*(473), 270-277. doi: 10.1198/016214505000000411

Aissa-Grouz, N., Garnier, J., & Billen, G. (2018). Long trend reduction of phosphorus wastewater loading in the Seine: determination of phosphorus speciation and sorption for modeling algal growth. *Environmental Science and Pollution Research, 25*(24), 23515-23528. doi: 10.1007/s11356-016-7555-7

Aissa-Grouz, N., Garnier, J., Billen, G., Mercier, B., & Martinez, A. (2015). The response of river nitrification to changes in wastewater treatment (The case of the lower Seine River downstream from Paris). *Ann. Limnol. - Int. J. Lim., 51*(4), 351-364. doi: 10.1051/limn/2015031

Alexander, R. B., Boyer, E. W., Smith, R. A., Schwarz, G. E., & Moore, R. B. (2007). The Role of Headwater Streams in Downstream Water Quality1. *Journal of the American Water Resources Association, 43*(1), 41-59. doi: 10.1111/j.1752-1688.2007.00005.x

Alexander, R. B., Smith, R. A., & Schwarz, G. E. (2000). Effect of stream channel size on the delivery of nitrogen to the Gulf of Mexico. *Nature, 403*, 758. doi: 10.1038/35001562

Altermatt, F. (2013). Diversity in riverine metacommunities: a network perspective. *Aquatic Ecology, 47*(3), 365-377. doi: 10.1007/s10452-013-9450-3

Andres-Domenech, I., Garcia-Bartual, R., Montanari, A., & Marco, J. B. (2015). Climate and hydrological variability: the catchment filtering role. *Hydrology and Earth System Sciences, 19*(1), 379-387. doi: 10.5194/hess-19-379-2015

Arle, J., Mohaupt, V., & Kirst, I. (2016). Monitoring of surface waters in Germany under the Water Framework Directive—A review of approaches, methods and results. *Water, 8*(6), 217. doi: 10.3390/w8060217

Baattrup-Pedersen, A., Larsen, S. E., Andersen, D. K., Jepsen, N., Nielsen, J., & Rasmussen, J. J. (2018). Headwater streams in the EU Water Framework Directive: Evidence-based decision support to select streams for river basin management plans. *Science of the Total Environment, 613-614*, 1048-1054. doi: 10.1016/j.scitotenv.2017.09.199

Balling Jr., R. C., Gober, P., & Jones, N. (2008). Sensitivity of residential water consumption to variations in climate: An intraurban analysis of Phoenix, Arizona. *Water Resources Research, 44*(10). doi: 10.1029/2007wr006722

Band, L. E. (1986). Topographic partition of watersheds with digital elevation models. *Water Resources Research, 22*(1), 15-24. doi: 10.1029/WR022i001p00015

Basu, N. B., Rao, P. S. C., Thompson, S. E., Loukinova, N. V., Donner, S. D., Ye, S., & Sivapalan, M. (2011). Spatiotemporal averaging of in-stream solute removal dynamics. *Water Resources Research, 47*(10). doi: 10.1029/2010WR010196

Batty, M., & Longley, P. A. (1994). *Fractal cities: A geometry of form and function*. San Diego, CA, USA: Academic Press.

Batty, M., Longley, P. A., & Fotheringham, S. (1989). Urban growth and form: Scaling, fractal geometry, and diffusion-limited aggregation. *Environment and Planning A, 21*(11), 1447-1472. doi: 10.1068/a211447

Becker, R. H., Sayers, M., Dehm, D., Shuchman, R., Quintero, K., Bosse, K., & Sawtell, R. (2019). Unmanned aerial system based spectroradiometer for monitoring harmful algal blooms: A new paradigm in water quality monitoring. *Journal of Great Lakes Research, 45*(3), 444-453. doi: 10.1016/j.jglr.2019.03.006

Beer, T., & Borgas, M. (1993). Horton's Laws and the fractal nature of streams. *Water Resources Research, 29*(5), 1475-1487. doi: 10.1029/92WR02731

Behrendt, H. , Bach, M. , Kunkel, R., Opitz, D., Pagenkopf, W.-G., Scholz, G. G., & Wendland, F. (2003). Nutrient emissions into river basins of Germany on the basis of a harmonized procedure. *The German Federal Environmental Agency Research Report*.

Bertuzzo, E., Azaele, S., Maritan, A., Gatto, M., Rodriguez-Iturbe, I., & Rinaldo, A. (2008). On the space-time evolution of a cholera epidemic. *Water Resources Research, 44*(1). doi: 10.1029/2007wr006211

Bertuzzo, E., Casagrandi, R., Gatto, M., Rodriguez-Iturbe, I. , & Rinaldo, A. (2010). On spatially explicit models of cholera epidemics. *Journal of The Royal Society Interface, 7*(43), 321-333. doi: 10.1098/rsif.2009.0204

Bertuzzo, E., Helton, A. M., Hall, R. O., & Battin, T. J. (2017). Scaling of dissolved organic carbon removal in river networks. *Advances in Water Resources, 110*, 136-146. doi: 10.1016/j.advwatres.2017.10.009

Bertuzzo, E., Maritan, A., Gatto, M., Rodriguez-Iturbe, I., & Rinaldo, A. (2007). River networks and ecological corridors: Reactive transport on fractals, migration fronts, hydrochory. *Water Resources Research, 43*(4). doi: 10.1029/2006wr005533

Bertuzzo, E., Rodriguez-Iturbe, I., & Rinaldo, A. (2015). Metapopulation capacity of evolving fluvial landscapes. *Water Resources Research, 51*(4), 2696-2706. doi: 10.1002/2015WR016946

Besemer, K., Singer, G., Quince, C., Bertuzzo, E., Sloan, W., & Battin, T. J. (2013). Headwaters are critical reservoirs of microbial diversity for fluvial networks. *Proceedings of the Royal Society B: Biological Sciences, 280*(1771), 20131760. doi: 10.1098/rspb.2013.1760

BfG. (2018). Water levels – Data from selected gauging stations on German federal waterways. Available from the German Federal Institute of Hydrology (Bundesanstalt für Gewässerkunde) https://www.bafg.de/EN/06_Info_Service/01_WaterLevels/waterlevels.html

Biggs, B. J. F. (2000). Eutrophication of streams and rivers: dissolved nutrient-chlorophyll relationships for benthic algae. *Journal of the North American Benthological Society, 19*(1), 17-31. doi: 10.2307/1468279

Blumensaat, F., Wolfram, M., & Krebs, P. (2012). Sewer model development under minimum data requirements. *Environmental Earth Sciences, 65*(5), 1427-1437. doi: 10.1007/s12665-011-1146-1

BMUB/UBA. (2014). *Water Resource Management in Germany - Part 2: Water quality*. The Environment, Nature Conservation, Building and Nuclear Safety (BMUB) and the German Federal Environmental Agency (UBA). Retrieved from https://www.umweltbundesamt.de/publikationen/water-resource-management-in-germany-part-2.

BMUB/UBA. (2016). *Water Framework Directive – The status of German waters 2015*. The Environment, Nature Conservation, Building and Nuclear Safety (BMUB) and the German Federal Environmental Agency (UBA). Retrieved from https://www.umweltbundesamt.de/publikationen/die-wasserrahmenrichtlinie-deutschlands-gewaesser.

BMUB/UBA. (2018). *Water resource management in Germany- Fundamentals, pressures, measures.*: The Environment, Nature Conservation, Building and Nuclear Safety (BMUB)

and the German Federal Environmental Agency (UBA). Retrieved from https://www.umweltbundesamt.de/en/publikationen/water-resource-management-in-germany.

Bonnet, S. (2009). Shrinking and splitting of drainage basins in orogenic landscapes from the migration of the main drainage divide. *Nature Geoscience, 2*(11), 766-771. doi: 10.1038/ngeo666

Botter, G., Basso, S., Rodriguez-Iturbe, I., & Rinaldo, A. (2013). Resilience of river flow regimes. *Proceedings of the National Academy of Sciences, 110*(32), 12925-12930. doi: 10.1073/pnas.1311920110

Botter, G., Peratoner, F., Porporato, A., Rodriguez-Iturbe, I., & Rinaldo, A. (2007). Signatures of large-scale soil moisture dynamics on streamflow statistics across U.S. climate regimes. *Water Resources Research, 43*(11). doi: 10.1029/2007wr006162

Brown, B. L., & Swan, C. M. (2010). Dendritic network structure constrains metacommunity properties in riverine ecosystems. *Journal of Animal Ecology, 79*(3), 571-580. doi: 10.1111/j.1365-2656.2010.01668.x

Campos, D., Fort, J., & Méndez, V. (2006). Transport on fractal river networks: Application to migration fronts. *Theoretical Population Biology, 69*(1), 88-93. doi: 10.1016/j.tpb.2005.09.001

Cantarella, G. E., & Vitetta, A. (2006). The multi-criteria road network design problem in an urban area. *Transportation, 33*(6), 567-588. doi: 10.1007/s11116-006-7908-z

Cantone, J., & Schmidt, A. R. (2011a). Dispersion mechanisms and the effect of parameter uncertainty on hydrologic response in urban catchments. *Water Resources Research, 47*, W05503. doi: 10.1029/2010WR009331

Cantone, J., & Schmidt, A. R. (2011b). Improved understanding and prediction of the hydrologic response of highly urbanized catchments through development of the Illinois Urban Hydrologic Model. *Water Resources Research, 47*, W08538. doi: 10.1029/2010WR009330

Carrara, F., Altermatt, F., Rodriguez-Iturbe, I., & Rinaldo, A. (2012). Dendritic connectivity controls biodiversity patterns in experimental metacommunities. *Proceedings of the National Academy of Sciences, 109*(15), 5761-5766. doi: 10.1073/pnas.1119651109

Center for International Earth Science Information Network - Columbia University (2017). *Gridded Population of the World, Version 4 (GPWv4): Population Count Adjusted to Match 2015 Revision of UN WPP Country Totals, Revision 10*. Palisades, NY: NASA Socioeconomic Data and Applications Center (SEDAC), doi: 10.7927/H4JQ0XZW, Accessed 12 Feb 2018, http://sedac.ciesin.columbia.edu/data/set/gpw-v4-population-count-adjusted-to-2015-unwpp-country-totals-rev10.

Ceola, S., Laio, F., & Montanari, A. (2015). Human-impacted waters: New perspectives from global high-resolution monitoring. *Water Resources Research, 51*(9), 7064-7079. doi: 10.1002/2015wr017482

Chan, C., & Dueñas-Osorio, L. (2014). Spatial-temporal quantification of interdependencies across infrastructure networks. In G. D'Agostino & A. Scala (Eds.), *Networks of Networks: The Last Frontier of Complexity* (pp. 323-340). Cham: Springer International Publishing.

Charlton, M. B., Bowes, M. J., Hutchins, M. G., Orr, H. G., Soley, R., & Davison, P. (2018). Mapping eutrophication risk from climate change: Future phosphorus concentrations in English rivers. *Science of the Total Environment, 613-614*, 1510-1526. doi: 10.1016/j.scitotenv.2017.07.218

Crave, A., & Davy, P. (1997). Scaling relationships of channel networks at large scales: Examples from two large-magnitude watersheds in Brittany, France. *Tectonophysics, 269*(1–2), 91-111. doi: 10.1016/S0040-1951(96)00142-4

da Silva, R. M., Santos, C. A. G., Moreira, M., Corte-Real, J., Silva, V. C. L., & Medeiros, I. C. (2015). Rainfall and river flow trends using Mann–Kendall and Sen's slope estimator statistical tests in the Cobres River basin. *Natural Hazards, 77*(2), 1205-1221. doi: 10.1007/s11069-015-1644-7

Destatis. (2018). Cities (All municipalities with city law) by area, population and population density. Available from Federal Statistical Office of Germany https://www.destatis.de/DE/Themen/Laender-Regionen/Regionales/Gemeindeverzeichnis/Administrativ/05-staedte.html

Diao, K., Farmani, R., Fu, G., Astaraie-Imani, M., Ward, S., & Butler, D. (2014). Clustering analysis of water distribution systems: Identifying critical components and community impacts. *Water Science and Technology, 70*(11), 1764-1773. doi: 10.2166/wst.2014.268

Duncombe, J. (2019). 2018 is the fourth-hottest year on record. *Eos, 100*. doi: 10.1029/2019EO115671

DWA. (2018). Leaders in mixing and aeration. *International Special Edition*.

DWD. (2018). The weather in Germany in 2018. Available from Deutscher Wetterdienst https://www.dwd.de/EN/press/press_release/press_release_archiv_2018_node.html

EEA. (1999). Environmental indicators: Typology and overview. *European Environment Agency (EEA) Report, 25*.

EEA. (2017a). Climate change, impacts and vulnerability in Europe 2016, An indicator-based report. *European Environment Agency (EEA) Report, 1*.

EEA (2017b). *Urban wast water treatment*. European Environment Agency, Copenhagen, Denmark: https://www.eea.europa.eu/data-and-maps/indicators/urban-waste-water-treatment/urban-waste-water-treatment-assessment-4.

EEC. (1991). *Council Directive of 21 May 1991 Concerning Urban Waste Water Treatment (91/271/EEC)*. Official Journal of the European Communities. Retrieved from http://ec.europa.eu/environment/water/water-urbanwaste/index_en.html.

Ekka, S. A., Hagard, B. E., Matlock, M. D., & Chaubey, I. (2006). Dissolved phosphorus concentrations and sediment interactions in effluent-dominated Ozark streams. *Ecological Engineering, 26*(4), 375-391. doi: 10.1016/j.ecoleng.2006.01.002

Elliott, M., Burdon, D., Atkins, J. P., Borja, A., Cormier, R., de Jonge, V. N., & Turner, R. K. (2017). "And DPSIR begat DAPSI(W)R(M)!" - A unifying framework for marine environmental management. *Marine Pollution Bulletin, 118*(1), 27-40. doi: 10.1016/j.marpolbul.2017.03.049

Ensign, S. H., & Doyle, M. W. (2006). Nutrient spiraling in streams and river networks. *Journal of Geophysical Research: Biogeosciences, 111*(G4). doi: 10.1029/2005JG000114

European Commission. (2000). *Directive 2000/60/EC of the European Parliament and of the Council of 23 October 2000 Establishing a Framework for Community Action in the Field of Water Policy*. Official Journal of the European Communities. Retrieved from http://ec.europa.eu/environment/water/water-framework/index_en.html.

European Commission. (2012). *The 3rd Water Framework Directive implementation report- River Basin Management Plans (Member State : Germany)*. Retrieved from http://ec.europa.eu/environment/water/water-framework/impl_reports.htm.

Eurostat. (2013). Water use by supply category and economical sector. Available from European Statistics https://ec.europa.eu/eurostat/web/environment/water/database# (Online data codes: env_wat_cat and demo_pop)

Fang, Y., Ceola, S., Paik, K., McGrath, G. S., Rao, P. S. C., Montanari, A., & Jawitz, J. W. (2018). Globally universal fractal pattern of human settlements in river networks. *Earth's Future, 6*. doi: 10.1029/2017EF000746

Fang, Y., & Jawitz, J. W. (2019). The evolution of human population distance to water in the USA from 1790 to 2010. *Nature Communications, 10*(1), 430. doi: 10.1038/s41467-019-08366-z

Feder, J. (1988). *Fractals*. New york: Plenum.

Fortier, C., & Mailhot, A. (2015). Climate change impact on combined sewer overflows. *Journal of Water Resources Planning and Management, 141*(5), 04014073. doi: 10.1061/(ASCE)WR.1943-5452.0000468

Froise, S., & Burges, S. J. (1978). Least-cost design of urban-drainage networks. *Journal of Water Resources Planning and Management Division, ASCE, 104*(1), 75-92.

Fuller, M. R., Doyle, M. W., & Strayer, D. L. (2015). Causes and consequences of habitat fragmentation in river networks. *Annals of the New York Academy of Sciences, 1355*(1), 31-51. doi: 10.1111/nyas.12853

Gall, H. E., Park, J., Harman, C. J., Jawitz, J. W., & Rao, P. S. C. (2013). Landscape filtering of hydrologic and biogeochemical responses in managed catchments. *Landscape Ecology, 28*(4), 651-664. doi: 10.1007/s10980-012-9829-x

Garbrecht, J., & Martz, L. W. (1997). The assignment of drainage direction over flat surfaces in raster digital elevation models. *Journal of Hydrology, 193*(1–4), 204-213. doi: 10.1016/S0022-1694(96)03138-1

García-Galán, M. J., Díaz-Cruz, M. S., & Barceló, D. (2011). Occurrence of sulfonamide residues along the Ebro river basin: Removal in wastewater treatment plants and environmental impact assessment. *Environment International, 37*(2), 462-473. doi: 10.1016/j.envint.2010.11.011

Geist, J., & Hawkins, S. J. (2016). Habitat recovery and restoration in aquatic ecosystems: current progress and future challenges. *Aquatic Conservation: Marine and Freshwater Ecosystems, 26*(5), 942-962. doi: 10.1002/aqc.2702

Gudmundsson, A., & Mohajeri, N. (2013). Entropy and order in urban street networks. *Scientific Reports, 3*, 3324. doi: 10.1038/srep03324

Hack, J. T. (1957). Studies of longitudinal stream profiles in Virginia and Maryland. *United States Geological Survey Professional Paper, 294-B*, 45-97.

Haghighi, A. (2013). Loop-by-loop cutting algorithm to generate layouts for urban drainage systems. *Journal of Water Resources Planning and Management, 139*(6), 693-703. doi: 10.1061/(ASCE)WR.1943-5452.0000294

Hall Jr., R. O., Baker, M. A., Rosi-Marshall, E. J., Tank, J. L., & Newbold, J. D. (2013). Solute-specific scaling of inorganic nitrogen and phosphorus uptake in streams. *Biogeosciences, 10*(11), 7323-7331. doi: 10.5194/bg-10-7323-2013

Harremoës, P., & Rauch, W. (1996). Integrated design and analysis of drainage systems, including sewers, treatment plant and receiving waters. *Journal of Hydraulic Research, 34*(6), 815-826. doi: 10.1080/00221689609498453

Heidecke, C. , Hirt, U., Kreins, P., Kuhr, P., Kunkel, R., Mahnkopf, J., Schott, M., Tetzlaff, B., Venohr, M., Wagner, A. , & Wendland, F. (2015). Endbericht zum Forschungsprojekt "Entwicklung eines Instrumentes für ein flussgebietsweites Nährstoffmanagement in der Flussgebietseinheit Weser". *Thünen Report 21*.

Hirt, U., Kreins, P., Kuhn, U., Mahnkopf, J., Venohr, M., & Wendland, F. (2012). Management options to reduce future nitrogen emissions into rivers: A case study of the Weser river basin, Germany. *Agricultural Water Management, 115*, 118-131. doi: 10.1016/j.agwat.2012.08.005

Hirt, U., Venohr, M., Kreins, P., & Behrendt, H. (2008). Modelling nutrient emissions and the impact of nutrient reduction measures in the Weser river basin, Germany. *Water Science and Technology, 58*(11), 2251-2258. doi: 10.2166/wst.2008.833

Horton, R. E. (1945). Erosional development of streams and their drainage basins; hydrophysical approach to quantitative morphology. *Geological Society of America Bulletin, 56*(3), 275-370. doi: 10.1130/0016-7606(1945)56[275:EDOSAT]2.0.CO;2

Ibisch, R., Austnes, K., Borchardt, D. , Boteler, B., Leujak, W., Lukat, E., Rouillard, J., Schmedtje, U., Solheim, A. L., & Westphal, K. (2016). European assessment of eutrophication abatement measures across land-based sources, inland, coastal and marine waters. *ETC/ICM Technical Report 2*.

Inostroza, P. A., Vera-Escalona, I., Wild, R., Norf, H., & Brauns, M. (2018). Tandem action of natural and chemical stressors in stream ecosystems: Insights from a population genetic perspective. *Environmental Science & Technology, 52*(14), 7962-7971. doi: 10.1021/acs.est.8b01259

IWRM-net. (2010). Innovative instruments and institutions in implementing the water framework directive: The German case study. *Research report of Integrated Water Resource Management (IWRM), No. 2.2.*

Jäger, C. G., & Borchardt, D. (2018). Longitudinal patterns and response lengths of algae in riverine ecosystems: a model analysis emphasising benthic-pelagic interactions. *Journal of Theoretical Biology*. doi: 10.1016/j.jtbi.2018.01.009

Johnson, L. R. (2002). *Central Europe: Enemies, Neighbors, Friends*. New York and Oxford: Oxford University Press.

JRC-EDO. (2018). Drought in Central-Northern Europe – August 2018. *Analytical report of Joint Research Centre - European Drought Observatory (JRD-EDO)*.

Kamjunke, N., Buttner, O., Jager, C. G., Marcus, H., von Tumpling, W., Halbedel, S., Norf, H., Brauns, M., Baborowski, M., Wild, R., Borchardt, D., & Weitere, M. (2013). Biogeochemical patterns in a river network along a land use gradient. *Environmental Monitoring and Assessment, 185*(11), 9221-9236. doi: 10.1007/s10661-013-3247-7

Kirchner, J. W. (1993). Statistical inevitability of Horton's laws and the apparent randomness of stream channel networks. *Geology, 21*(7), 591-594. doi: 10.1130/0091-7613(1993)021<0591:siohsl>2.3.co;2

Klinkhamer, C., Krueger, E., Zhan, X., Blumensaat, F., Ukkusuri, S., & Rao, P. S. C. (2017). Topological analyses of functional networks for urban transport and drainage: Geospatial co-location and spatial heterogeneity. *Scientific Reports*, In Review.

Knezevic, A. (2008). StatNews # 73: Overlapping confidence intervals and statistical significance. Cornell University: Cornell Statistical Consulting Unit. https://www.cscu.cornell.edu/news/statnews/stnews73.pdf

Knighton, D. (1998). *Fluvial forms and processes*. London: Edward Arnold.

Krueger, E., Klinkhamer, C., Urich, C., Zhan, X., & Rao, P. S. C. (2017). Generic patterns in the evolution of urban water networks: Evidence from a large Asian city. *Physical Review E, 95*(3), 032312.

Kuemmerlen, M., Reichert, P., Siber, R., & Schuwirth, N. (2019). Ecological assessment of river networks: From reach to catchment scale. *Science of the Total Environment, 650*, 1613-1627. doi: 10.1016/j.scitotenv.2018.09.019

Kumar, R., Samaniego, L., & Attinger, S. (2013). Implications of distributed hydrologic model parameterization on water fluxes at multiple scales and locations. *Water Resources Research, 49*(1), 360-379. doi: 10.1029/2012WR012195

Kummu, M., de Moel, H., Ward, P. J., & Varis, O. (2011). How close do we live to water? A global analysis of population distance to freshwater bodies. *PLOS ONE, 6*(6), e20578. doi: 10.1371/journal.pone.0020578

La Barbera, P., & Rosso, R. (1989). On the fractal dimension of stream networks. *Water Resources Research, 25*(4), 735-741. doi: 10.1029/WR025i004p00735

Le Moal, M., Gascuel-Odoux, C., Ménesguen, A., Souchon, Y., Étrillard, C., Levain, A., Moatar, F., Pannard, A., Souchu, P., Lefebvre, A., & Pinay, G. (2019). Eutrophication: A new wine in an old bottle? *Science of the Total Environment, 651*, 1-11. doi: 10.1016/j.scitotenv.2018.09.139

Loucks, D. P. (1979). Water resources systems. *Reviews of Geophysics, 17*(6), 1335-1351. doi: 10.1029/RG017i006p01335

Lu, Y., & Tang, J. (2004). Fractal dimension of a transportation network and its relationship with urban growth: A study of the Dallas-Fort Worth area. *Environment and Planning B: Planning and Design, 31*(6), 895-911. doi: doi:10.1068/b3163

Ludwig, W., Dumont, E., Meybeck, M., & Heussner, S. (2009). River discharges of water and nutrients to the Mediterranean and Black Sea: Major drivers for ecosystem changes during past and future decades? *Progress in Oceanography, 80*(3), 199-217. doi: 10.1016/j.pocean.2009.02.001

Maavara, T., Parsons, C. T., Ridenour, C., Stojanovic, S., Dürr, H. H., Powley, H. R., & Van Cappellen, P. (2015). Global phosphorus retention by river damming. *Proceedings of the National Academy of Sciences, 112*(51), 15603. doi: 10.1073/pnas.1511797112

Mair, M., Sitzenfrei, R., Möderl, M., & Rauch, W. (2012, May 20-24, 2012). *Identifying multi utility network similarities.* Paper presented at the World Environmental and Water Resources Congress 2012 : Crossing Boundaries, Albuquerque, New Mexico.

Mair, M., Zischg, J., Rauch, W., & Sitzenfrei, R. (2017). Where to find water pipes and sewers?—On the correlation of infrastructure networks in the urban environment. *Water, 9*(2), 146. doi: 10.3390/w9020146

Mandelbrot, B. B. (1983). *The Fractal Geometry of Nature*. New York: W.H. Freeman.

Marani, M., Rinaldo, A., Rigon, R., & Rodriguez-Iturbe, I. (1994). Geomorphological width functions and the random cascade. *Geophysical Research Letters, 21*(19), 2123-2126. doi: 10.1029/94GL01933

Marengo, J. A. (2005). Characteristics and spatio-temporal variability of the Amazon River basin water budget. *Climate Dynamics, 24*(1), 11-22. doi: 10.1007/s00382-004-0461-6

Mari, L. , Bertuzzo, E., Righetto, L., Casagrandi, R., Gatto, M., Rodriguez-Iturbe, I., & Rinaldo, A. (2012). Modelling cholera epidemics: the role of waterways, human mobility and sanitation. *Journal of The Royal Society Interface, 9*(67), 376-388. doi: 10.1098/rsif.2011.0304

Maritan, A., Rinaldo, A., Rigon, R., Giacometti, A., & Rodríguez-Iturbe, I. (1996). Scaling laws for river networks. *Physical Review E, 53*(2), 1510-1515. doi: 10.1103/PhysRevE.53.1510

Masucci, A. P., Stanilov, K., & Batty, M. (2014). Exploring the evolution of London's street network in the information space: A dual approach. *Physical Review E, 89*(1), 012805. doi: 10.1103/PhysRevE.89.012805

Mattas, C., Voudouris, K. S., & Panagopoulos, A. (2014). Integrated groundwater resources management using the DPSIR approach in a GIS environment context: A case study from the Gallikos River basin, North Greece. *Water, 6*(4), 1043-1068. doi: 10.3390/w6041043

McCrackin, M. L., Jones, H. P., Jones, P. C., & Moreno-Mateos, D. (2017). Recovery of lakes and coastal marine ecosystems from eutrophication: A global meta-analysis. *Limnology and Oceanography, 62*(2), 507-518. doi: 10.1002/lno.10441

McDowell, R. W., Larned, S. T., & Houlbrooke, D. J. (2009). Nitrogen and phosphorus in New Zealand streams and rivers: Control and impact of eutrophication and the influence of land management. *New Zealand Journal of Marine and Freshwater Research, 43*(4), 985-995. doi: 10.1080/00288330909510055

McGrath, G. S., Kaeseberg, T., Reyes-Silva, J. D., Jawitz, J. W., Blumensaat, F., Borchardt, D., Mellander, P.-E., Paik, K., Krebs, P., & Rao, P. S. C. (2019). Network topology and rainfall

controls on the variability of combined sewer overflows and loads. *Accepted in Water Resources Research*.

Meybeck, M., Lestel, L., Carré, C., Bouleau, G., Garnier, J., & Mouchel, J. M. (2018). Trajectories of river chemical quality issues over the Longue Durée: the Seine River (1900S–2010). *Environmental Science and Pollution Research, 25*(24), 23468-23484. doi: 10.1007/s11356-016-7124-0

Meyer, J. L., Strayer, D. L., Wallace, J. B., Eggert, S. L., Helfman, G. S., & Leonard, N. E. (2007). The contribution of headwater streams to biodiversity in river networks1. *Journal of the American Water Resources Association, 43*(1), 86-103. doi: 10.1111/j.1752-1688.2007.00008.x

Michalak, A. M. (2016). Study role of climate change in extreme threats to water quality. *Nature, 535*, 349-350. doi: 10.1038/535349a

Mineau, M. M., Wollheim, W. M., & Stewart, R. J. (2015). An index to characterize the spatial distribution of land use within watersheds and implications for river network nutrient removal and export. *Geophysical Research Letters, 42*(16), 6688-6695. doi: 10.1002/2015gl064965

Miyamoto, H., Hashimoto, T., & Michioku, K. (2011). Basin-wide distribution of land use and human population: Stream order modeling and river basin classification in Japan. *Environmental Management, 47*(5), 885-898. doi: 10.1007/s00267-011-9653-0

Mohajeri, N., Gudmundsson, A., & Scartezzini, J. L. (2015, 9-11 September). *Expansion and densification of cities: Linking urban form to urban ecology.* Paper presented at the International Conference on Future Buildings & Districts Sustainability from Nano to Urban Scale, Lausanne, Switzerland.

Molina-Navarro, E., Andersen, H. E., Nielsen, A., Thodsen, H., & Trolle, D. (2018). Quantifying the combined effects of land use and climate changes on stream flow and nutrient loads: A modelling approach in the Odense Fjord catchment (Denmark). *Science of the Total Environment, 621*, 253-264. doi: 10.1016/j.scitotenv.2017.11.251

Montgomery, D. R., & Dietrich, W. E. (1988). Where do channels begin? *Nature, 336*(6196), 232-234. doi: 10.1038/336232a0

Morris, R. G., & Barthelemy, M. (2014). Spatial effects: Transport on interdependent networks. In G. D'Agostino & A. Scala (Eds.), *Networks of Networks: The Last Frontier of Complexity* (pp. 145-161). Cham: Springer International Publishing.

Moss, B., Kosten, S., Meerhoff, M., Battarbee, R. W., Jeppesen, E., Mazzeo, N., Havens, K., Lacerot, G., Liu, Z., De Meester, Luc, Paerl, H., & Scheffer, M. (2011). Allied attack: Climate change and eutrophication. *Inland Waters, 1*(2), 101-105. doi: 10.5268/IW-1.2.359

Muneepeerakul, R., Bertuzzo, E., Lynch, H. J., Fagan, W. F., Rinaldo, A., & Rodriguez-Iturbe, I. (2008). Neutral metacommunity models predict fish diversity patterns in Mississippi–Missouri basin. *Nature, 453*, 220. doi: 10.1038/nature06813

Musolff, A., Fleckenstein, J. H., Rao, P. S. C., & Jawitz, J. W. (2017). Emergent archetype patterns of coupled hydrologic and biogeochemical responses in catchments. *Geophysical Research Letters, 44*(9), 4143-4151. doi: 10.1002/2017GL072630

OECD. (1993). *Environmental Indicators: OECD Core Set*. Organisation for Economic Co-operation and Development, Paris.

Oh, J. (2010). *Topological characteristics of urban storm sewer networks.* (Master thesis), Korea University.

Ortiz, J. D., & Puig, M. A. (2007). Point source effects on density, biomass and diversity of benthic macroinvertebrates in a mediterranean stream. *River Research and Applications, 23*(2), 155-170. doi: 10.1002/rra.971

Owens, M. (2010). *Wastewater 101: A Primer to Our Wastewater System Treatment Process : Beyond 100 Years of Sustainability* (C. a. C. o. H. Department of Environmental Services, State of Hawaii Ed.): Department of Environmental Services, City and Council of Honolulu, State of Hawaii.

Paerl, H. W., Gardner, W. S., Havens, K. E., Joyner, A. R., McCarthy, M. J., Newell, S. E., Qin, B., & Scott, J. T. (2016). Mitigating cyanobacterial harmful algal blooms in aquatic ecosystems impacted by climate change and anthropogenic nutrients. *Harmful Algae, 54*, 213-222. doi: 10.1016/j.hal.2015.09.009

Paik, K., & Kumar, P. (2007). Inevitable self-similar topology of binary trees and their diverse hierarchical density. *The European Physical Journal B, 60*(2), 247-258. doi: 10.1140/epjb/e2007-00332-y

Paik, K., & Kumar, P. (2010). Optimality approaches to describe characteristic fluvial patterns on landscapes. *Philosophical Transactions of the Royal Society B: Biological Sciences, 365*(1545), 1387-1395. doi: 10.1098/rstb.2009.0303

Paik, K., & Kumar, P. (2011). Power-law behavior in geometric characteristics of full binary trees. *Journal of Statistical Physics, 142*(4), 862-878. doi: 10.1007/s10955-011-0125-y

Parker, R. S. (1977). Experimental study of drainage basin evolution and its hydrologic implications. *Colorado State University, Fort Collins, Colorado, Hydrology Papers, 90*.

Passy, P., Gypens, N., Billen, G., Garnier, J., Thieu, V., Rousseau, V., Callens, J., Parent, J. Y., & Lancelot, C. (2013). A model reconstruction of riverine nutrient fluxes and eutrophication in the Belgian Coastal Zone since 1984. *Journal of Marine Systems, 128*, 106-122. doi: 10.1016/j.jmarsys.2013.05.005

Peterson, E. E., Ver Hoef, J. M., Isaak, D. J., Falke, J. A., Fortin, M-J., Jordan, C. E., McNyset, K., Monestiez, P., Ruesch, A. S., Sengupta, A., Som, N., Steel, E. A., Theobald, D. M., Torgersen, C. E., & Wenger, S. J. (2013). Modelling dendritic ecological networks in space: an integrated network perspective. *Ecology Letters, 16*(5), 707-719. doi: 10.1111/ele.12084

Platts, W. S. (1979). Relationships among stream order, fish populations, and aquatic geomorphology in an Idaho river drainage. *Fisheries, 4*(2), 5-9. doi: 10.1577/1548-8446(1979)004<0005:rasofp>2.0.co;2

Porse, E., & Lund, J. (2015). Network structure, complexity, and adaptation in water resource systems. *Civil Engineering and Environmental Systems, 32*(1-2), 143-156. doi: 10.1080/10286608.2015.1022726

Porta, S., Crucitti, P., & Latora, V. (2006). The network analysis of urban streets: a dual approach. *Physica A: Statistical Mechanics and its Applications, 369*(2), 853-866. doi: 10.1016/j.physa.2005.12.063

Protopapas, A. L., Katchamart, S., & Platonova, A. (2000). Weather effects on daily water use in New York City. *Journal of Hydrologic Engineering, 5*(3), 332-338. doi: 10.1061/(ASCE)1084-0699(2000)5:3(332)

Rice, J., & Westerhoff, P. (2015). Spatial and temporal bariation in De Facto wastewater reuse in drinking water systems across the U.S.A. *Environmental Science & Technology, 49*(2), 982-989. doi: 10.1021/es5048057

Rice, J., & Westerhoff, P. (2017). High levels of endocrine pollutants in US streams during low flow due to insufficient wastewater dilution. *Nature Geoscience, 10*, 587. doi: 10.1038/ngeo2984

Rigon, R., Rodriguez-Iturbe, I., Maritan, A., Giacometti, A., Tarboton, D. G., & Rinaldo, A. (1996). On Hack's Law. *Water Resources Research, 32*(11), 3367-3374. doi: 10.1029/96WR02397

Riley, W. D., Potter, E. C. E., Biggs, J., Collins, A. L., Jarvie, H. P., Jones, J. I., Kelly-Quinn, M., Ormerod, S. J., Sear, D. A., Wilby, R. L., Broadmeadow, S., Brown, C. D., Chanin, P., Copp, G. H., Cowx, I. G., Grogan, A., Hornby, D. D., Huggett, D., Kelly, M. G., Naura, M., Newman, J. R., & Siriwardena, G. M. (2018). Small Water Bodies in Great Britain and Ireland: Ecosystem function, human-generated degradation, and options for restorative action. *Science of the Total Environment, 645*, 1598-1616. doi: 10.1016/j.scitotenv.2018.07.243

Rinaldo, A., Gatto, M., & Rodriguez-Iturbe, I. (2018). River networks as ecological corridors: A coherent ecohydrological perspective. *Advances in Water Resources, 112*, 27-58. doi: 10.1016/j.advwatres.2017.10.005

Rinaldo, A., Rigon, R., Banavar, J. R., Maritan, A., & Rodriguez-Iturbe, I. (2014). Evolution and selection of river networks: Statics, dynamics, and complexity. *Proceedings of the National Academy of Sciences, 111*(7), 2417-2424. doi: 10.1073/pnas.1322700111

Robert, A., & Roy, A. G. (1990). On the fractal interpretation of the mainstream length-drainage area relationship. *Water Resources Research, 26*(5), 839-842. doi: 10.1029/WR026i005p00839

Rodríguez-Iturbe, I., Ijjász-Vásquez, E. J., Bras, R. L., & Tarboton, D. G. (1992). Power law distributions of discharge mass and energy in river basins. *Water Resources Research, 28*(4), 1089-1093. doi: 10.1029/91WR03033

Rodríguez-Iturbe, I., & Rinaldo, A. (2001). *Fractal River Basins: Chance and Self-Organization*. Cambridge, UK: Cambridge University Press.

Rodríguez-Iturbe, I., Rinaldo, A., Rigon, R., Bras, R. L., Marani, A., & Ijjász-Vásquez, E. J. (1992). Energy dissipation, runoff production, and the three-dimensional structure of river basins. *Water Resources Research, 28*(4), 1095-1103. doi: 10.1029/91WR03034

Rosvall, M., Trusina, A., Minnhagen, P., & Sneppen, K. (2005). Networks and cities: An information perspective. *Physical Review Letters, 94*(2), 028701. doi: 10.1103/PhysRevLett.94.028701

Samaniego, L., Kumar, R., & Attinger, S. (2010). Multiscale parameter regionalization of a grid-based hydrologic model at the mesoscale. *Water Resources Research, 46*(5). doi: 10.1029/2008wr007327

Sandoval, S., Torres, A., Pawlowsky-Reusing, E., Riechel, M., & Caradot, N. (2013). The evaluation of rainfall influence on combined sewer overflows characteristics: the Berlin case study. *Water Science and Technology, 68*(12), 2683-2690. doi: 10.2166/wst.2013.524

Schumm, S. A. (1956). Evolution of drainage systems and slopes in badlands at Perth Amboy, New Jersey. *Geological Society of America Bulletin, 67*(5), 597-646.

Seeger, H. (1999). The history of German waste water treatment. *European Water Management, 2*, 51-56.

Seo, Y., & Schmidt, A. R. (2012). The effect of rainstorm movement on urban drainage network runoff hydrographs. *Hydrological Processes, 26*(25), 3830-3841. doi: 10.1002/hyp.8412

Seo, Y., & Schmidt, A. R. (2014). Application of Gibbs' model to urban drainage networks: A case study in southwestern Chicago, USA. *Hydrological Processes, 28*(3), 1148-1158. doi: 10.1002/hyp.9657

Shang, S., Lee, Z., Lin, G., Hu, C., Shi, L., Zhang, Y., Li, X., Wu, J., & Yan, J. (2017). Sensing an intense phytoplankton bloom in the western Taiwan Strait from radiometric measurements on a UAV. *Remote Sensing of Environment, 198*, 85-94. doi: 10.1016/j.rse.2017.05.036

Shen, G. (2002). Fractal dimension and fractal growth of urbanized areas. *International Journal of Geographical Information Science, 16*(5), 419-437. doi: 10.1080/13658810210137013

Shuster, W. D., Bonta, J., Thurston, H., Warnemuende, E., & Smith, D. R. (2005). Impacts of impervious surface on watershed hydrology: A review. *Urban Water Journal, 2*(4), 263-275. doi: 10.1080/15730620500386529

Siksna, A. (1997). The effects of block size and form in North American and Australian city centres. *Urban Morphology, 1*(1), 19-33.

Sitzenfrei, R., Urich, C., Möderl, M., & Rauch, W. (2013). Assessing the efficiency of different CSO positions based on network graph characteristics. *Water Science and Technology, 67*(7), 1574-1580. doi: 10.2166/wst.2013.029

Smart, J. S. (1972). Channel networks. In V. T. Chow (Ed.), *Advances in Hydroscience* (Vol. 8, pp. 305-346). New York and London: Academic Press.

Stanley, E. H., & Doyle, M. W. (2002). A geomorphic perspective on nutrient retention following dam removal: Geomorphic models provide a means of predicting ecosystem responses to dam removal. *BioScience, 52*(8), 693-701. doi: 10.1641/0006-3568(2002)052[0693:agponr]2.0.co;2

Strahler, A. N. (1957). Quantitative analysis of watershed geomorphology. *Eos Transactions American Geophysical Union, 38*(6), 913-920. doi: 10.1029/TR038i006p00913

Su, T.-C., & Chou, H.-T. (2015). Application of multispectral sensors carried on Unmanned Aerial Vehicle (UAV) to trophic state mapping of small reservoirs: A case study of Tain-Pu reservoir in Kinmen, Taiwan. *Remote Sensing, 7*(8), 10078-10097. doi: 10.3390/rs70810078

Türker, U. (2011). Alternative sewerage solution: Condominial method and its application. *Physics and Chemistry of the Earth, 36*(5–6), 179-186. doi: 10.1016/j.pce.2010.03.038

Tarboton, D. G., Bras, R. L., & Rodriguez-Iturbe, I. (1988). The fractal nature of river networks. *Water Resources Research, 24*(8), 1317-1322. doi: 10.1029/WR024i008p01317

Tarboton, D. G., Bras, R. L., & Rodriguez-Iturbe, I. (1991). On the extraction of channel networks from digital elevation data. *Hydrological Processes, 5*(1), 81-100. doi: 10.1002/hyp.3360050107

Thorp, J. H., Thoms, M. C., & Delong, M. D. (2006). The riverine ecosystem synthesis: biocomplexity in river networks across space and time. *River Research and Applications, 22*(2), 123-147. doi: 10.1002/rra.901

Tokunaga, E. (1978). Consideration on the composition of drainage networks and their evolution. *Geographical Rep., 13*, 1-27, Tokyo Metrop. Univ.

Trolle, D., Nielsen, A., Andersen, H. E., Thodsen, H., Olesen, J. E., Børgesen, C. D., Refsgaard, J. C., Sonnenborg, T. O., Karlsson, I. B., Christensen, J. P., Markager, S., & Jeppesen, E. (2019). Effects of changes in land use and climate on aquatic ecosystems: Coupling of

models and decomposition of uncertainties. *Science of the Total Environment, 657*, 627-633. doi: 10.1016/j.scitotenv.2018.12.055

Ukkusuri, S. V., Mathew, T. V., & Waller, S. T. (2007). Robust transportation network design under demand uncertainty. *Computer-Aided Civil and Infrastructure Engineering, 22*(1), 6-18. doi: 10.1111/j.1467-8667.2006.00465.x

United Nations. (2016). *The World's Cities in 2016*, Department of Economic and Social Affairs.

Urich, C., Burger, G., Mair, M., & Rauch, W. (2012). *DynaMind–A softwaretool for integrated modelling of urban environments and their infrastructure.* Paper presented at the 10th International Conference on Hydroinformatics.

Urich, C., Sitzenfrei, R., Möderl, M., & Rauch, W. (2010). An agent-based approach for generating virtual sewer systems. *Water Science and Technology, 62*(5), 1090-1097. doi: 10.2166/wst.2010.364

USEPA. (1993). Method 365.1, Revision 2.0: Determination of Phosphorus by Semi-Automated Colorimetry.

USEPA. (2001). Report to congress: Implementation and enforcement of the combined sewer overflow control policy. Appendix C.

Vannote, R. L., Minshall, G. W., Cummins, K. W., Sedell, J. R., & Cushing, C. E. (1980). The River Continuum Concept. *Canadian Journal of Fisheries and Aquatic Sciences, 37*(1), 130-137. doi: 10.1139/f80-017

Walsh, C. J., Fletcher, T. D., & Burns, M. J. (2012). Urban stormwater runoff: A new class of environmental flow problem. *PLoS ONE, 7*(9), e45814. doi: 10.1371/journal.pone.0045814

Wang, D., & Wu, L. (2013). Similarity of climate control on base flow and perennial stream density in the Budyko framework. *Hydrology and Earth System Sciences, 17*(1), 315-324. doi: 10.5194/hess-17-315-2013

Westphal, K., Graeber, D., Musolff, A., Fang, Y., Jawitz, J. W., & Borchardt, D. (2019). Multi-decadal trajectories of phosphorus loading, export, and instream retention along a catchment gradient. *Science of The Total Environment, 667*, 769-779. doi: 10.1016/j.scitotenv.2019.02.428

Whitall, D., Bricker, S., Ferreira, J., Nobre, A. M., Simas, T., & Silva, M. (2007). Assessment of eutrophication in estuaries: Pressure–State–Response and nitrogen source apportionment. *Environmental Management, 40*(4), 678-690. doi: 10.1007/s00267-005-0344-6

Whitehead, P. G., Wilby, R. L., Battarbee, R. W., Kernan, M., & Wade, A. J. (2009). A review of the potential impacts of climate change on surface water quality. *Hydrological Sciences Journal, 54*(1), 101-123. doi: 10.1623/hysj.54.1.101

WHO/UNICEF (2015a). *Joint Monitoring Program Global Dataset for Water Supply, Sanitation and Hygiene (JMP).* https://washdata.org/data.

WHO/UNICEF. (2015b). *Progress on sanitation and drinking water - 2016 update and MDG assessment*. WHO Press, World Health Organization, Geneva, Switzerland.

Widder, S., Besemer, K., Singer, G. A., Ceola, S., Bertuzzo, E., Quince, C., Sloan, W. T., Rinaldo, A., & Battin, T. J. (2014). Fluvial network organization imprints on microbial co-occurrence networks. *Proceedings of the National Academy of Sciences of the United States of America, 111*(35), 12799-12804. doi: 10.1073/pnas.1411723111

Willett, S. D., McCoy, S. W., Perron, J. T., Goren, L., & Chen, Chia-Yu. (2014). Dynamic reorganization of river basins. *Science, 343*(6175), 1248765. doi: 10.1126/science.1248765

Withers, P. J. A., & Jarvie, H. P. (2008). Delivery and cycling of phosphorus in rivers: A review. *Science of the Total Environment, 400*(1), 379-395. doi: 10.1016/j.scitotenv.2008.08.002

Wollheim, W. M., Vörösmarty, C. J., Peterson, B. J., Seitzinger, S. P., & Hopkinson, C. S. (2006). Relationship between river size and nutrient removal. *Geophysical Research Letters, 33*(6). doi: 10.1029/2006GL025845

Woznicki, S. A., Nejadhashemi, A. P., Tang, Y., & Wang, L. (2016). Large-scale climate change vulnerability assessment of stream health. *Ecological Indicators, 69*, 578-594. doi: 10.1016/j.ecolind.2016.04.002

WWAP. (2017). *The United Nations World Water Development Report 2017: Wastewater, The Untapped Resource*. United Nations World Water Assessment Programme: Paris, UNESCO.

Yang, S., & Paik, K. (2017). New findings on river network organization: Law of eigenarea and relationships among hortonian scaling ratios. *Fractals, 25*(03), 1750029. doi: 10.1142/s0218348x17500293

Yang, S., Paik, K., McGrath, G. S., Urich, C., Krueger, E., Kumar, P., & Rao, P. S. C. (2017). Functional Topology of Evolving Urban Drainage Networks. *Water Resources Research, 53*(11), 8966-8979. doi: 10.1002/2017WR021555

Yao, L., Wei, W., & Chen, L. (2016). How does imperviousness impact the urban rainfall-runoff process under various storm cases? *Ecological Indicators, 60*, 893-905. doi: 10.1016/j.ecolind.2015.08.041

Yazdani, A., & Jeffrey, P. (2011). Complex network analysis of water distribution systems. *Chaos, 21*(1), 016111. doi: 10.1063/1.3540339

Yazdani, A., & Jeffrey, P. (2012). Water distribution system vulnerability analysis using weighted and directed network models. *Water Resources Research, 48*(6), W06517. doi: 10.1029/2012WR011897

Zink, M., Kumar, R., Cuntz, M., & Samaniego, L. (2017). A high-resolution dataset of water fluxes and states for Germany accounting for parametric uncertainty. *Hydrol. Earth Syst. Sci., 21*(3), 1769-1790. doi: 10.5194/hess-21-1769-2017

Zischg, J. , Klinkhamer, C., Zhan, X., Krueger, E., Ukkusuri, S., Rao, P. S. C., Rauch, W., & Sitzenfrei, R. (2017). Evolution of complex network topologies in urban water infrastructure. *In World Environmental and Water Resources Congress 2017*, 648-659.

VITA

Soohyun Yang received B.S. and M.S. degree in Department of Civil, Environmental and Architectural Engineering from Korea University, South Korea. She has published in *Water Resources Research*, and *Science of the Total Environment*. Her research interests include the spatial organizations and emergent patterns of coupled human-engineered-natural systems formed in urbanized river basins, the adverse impacts of anthropogenic pressures on river water quality and aquatic ecosystems integrity, the river basin management at national- and international-scales. She applied the concepts of fractal river network, hydrology, and biogeochemistry in different case studies to provide a better understanding in the interlinked relationships across people, loading of anthropogenic pressures, attenuation processes in nature and technology, and further to assess their comprehensive impacts on river water quality impairments, through data-modeling synthesis approaches

PUBLICATIONS

1. Yang, S., Buettner, O., Kumar, R., Jaeger, C., Jawitz, J. W., Rao, P. S. C., and Borchardt, D. (2019). Spatial patterns of water quality impairments from point source nutrient loads in Germany's largest national River Basin (Weser River). *Science of the Total Environment, 697*, 134145. doi: 10.1016/j.scitotenv.2019.134145.

2. Yang, S., Buettner, O., Jawitz, J. W., Kumar, R., Rao, P. S. C., and Borchardt, D. (2019). Spatial organization of human population and wastewater treatment plants in urbanized river basins. *Water Resources Research*, *55*(7), 6138-6152. doi: 10.1029/2018WR024614.

3. Yang, S., Paik, K., McGrath, G., Urich, C., Kruger, E., Kumar P., and Rao, P. S. C. (2017) Functional topology of evolving urban drainage networks. *Water Resources Research*, *53*(11), 8966-8979, doi: 10.1002/2017WR021555.

4. Yang, S., Bertuzzo, E., Buettner, O., Borchardt, D., and Rao, P. S. C. Scaling patterns of point and diffuse source nutrient loads and response of algal communities in a fractal river network perspective. *In preparation*.